

***Ex vivo* activated human T lymphocytes as living drug
delivery vehicles for cancer therapy**

In vitro studies with nanoparticulate idarubicin and complexed mTHPP
as payload

Dissertation

zur Erlangung des Grades
des Doktors der Naturwissenschaften
der Naturwissenschaftlich-Technischen Fakultät III
Chemie, Pharmazie, Bio- und Werkstoffwissenschaften
der Universität des Saarlandes

von

Diplom-Biochemiker
André-René Blaudszun

Saarbrücken

2015

Tag des Kolloquiums: 26.04.16
Dekan: Prof. Dr.-Ing. Dirk Bähre
Berichterstatter: Prof. Dr. Gerhard Wenz
Prof. Dr. Claus-Michael Lehr
Vorsitz: Prof. Dr. Marc Schneider
Akad. Mitarbeiter: Dr. Björn Becker

Für meine Tochter Levke Marie

Table of Contents

I. Summary	1
II. Zusammenfassung	2
1. Introduction	3
1.1 Envisioned T cell-mediated drug delivery concept for cancer therapy	3
1.2 Cell-mediated drug delivery	7
1.2.1 T lymphocyte-mediated drug delivery for cancer treatment	9
1.3 T lymphocytes	12
1.4 Drugs used as payload for T cells and their mechanisms of actions	16
1.4.1 Anthracycline based chemotherapy	17
1.4.2 Photodynamic therapy	21
1.5 Aim of this thesis	29
1.6 Statement of contributions	31
2. Interactions of statistical glycosylated copolypeptides with human T lymphocytes	33
2.1 Abstract	33
2.2 Introduction	34
2.3 Materials and methods	37
2.3.1 Synthesis and handling of glycosylated peptides by <i>N</i> -carboxyanhydride polymerization	37
2.3.2 Fluorescence spectrometry of polymers	37
2.3.3 Isolation and activation of human T lymphocytes	38
2.3.4 <i>In vitro</i> toxicology assay	38
2.3.5 Flow cytometric analysis of polypeptide uptake by T lymphocytes	39
2.3.6 Fluorescence microscopy of polypeptide treated T cells	40
2.4 Results	42
2.4.1 Fluorescence spectrometry of polypeptides	42
2.4.2 Analysis of T cell survival	43
2.4.3 Flow cytometric analysis of polylysine polymer uptake by T cells	43
2.4.4 Fluorescence microscopy of polypeptide treated T lymphocytes	47
2.5 Discussion	48
2.6 Conclusions	52
2.7 Supplementary Information	52
2.7.1 Size of non-activated and activated T lymphocytes	52
2.7.2 Reduction of XTT tetrazolium salt by T lymphocytes	53

3. Interactions of polyester-idarubicin nanoparticles and polymer-photosensitizer complexes with human T lymphocytes	54
3.1 Abstract.....	54
3.2 Introduction	55
3.3 Materials and methods.....	56
3.3.1 Synthesis of poly(diethylene glycol-maleate- <i>co</i> -sebacate)ester (MPE).....	56
3.3.2 Synthesis of PLGA-IDA, MPE-IDA, and AuSh-IDA nanoparticles.....	57
3.3.3 Determination of colloidal characteristics, drug encapsulation efficiency, nanoparticle morphology and drug release kinetics	57
3.3.4 Preparation and handling of PSS/mTHPP.....	58
3.3.5 Cell culture	58
3.3.6 Loading of T lymphocytes with nanoparticles and PSS/mTHPP	59
3.3.7 Analysis of particle and photosensitizer uptake by flow cytometry.....	59
3.3.8 Fluorescence microscopy (FM) and confocal laser scanning microscopy (CLSM).....	60
3.3.9 Analysis of cell survival	61
3.4 Results	62
3.4.1 Synthesis and characterization of MPE-IDA and PLGA-IDA nanoparticles	62
3.4.2 Uptake of PLGA- and MPE-encapsulated idarubicin by <i>ex vivo</i> activated human T lymphocytes	64
3.4.3 Survival of PLGA-IDA and MPE-IDA NP-loaded T lymphocytes	65
3.4.4 Uptake and cytotoxicity of gold-coated MPE-IDA nanoparticles	66
3.4.5 Intracellular uptake of the polymer-photosensitizer complex PSS/mTHPP.....	68
3.4.6 Viability of PSS/mTHPP-loaded T cells before and after illumination	69
3.4.7 Transfer and phototoxic effect of T cell-delivered mTHPP	70
3.5 Discussion.....	72
3.6 Conclusions	75
3.7 Supplementary Information.....	76
3.7.1 Analysis of PS-transfer from T cells to cancer cells by flow cytometry	76
3.7.2 Phototoxic effect of T cell-delivered mTHPP on cancer cells	77
3.7.3 Characterization of poly(diethylene glycol-maleate- <i>co</i> -sebacate)ester (MPE).....	77
4. Detailed analysis of interactions of PSS/mTHPP with human T lymphocytes and bispecific antibody mediated redirection of PSS/mTHPP-loaded T cells to carcinoma cells	78
4.1 Abstract.....	78
4.2 Introduction	79
4.3 Materials and methods.....	81
4.3.1 T cell isolation, activation and expansion	81

4.3.2 Tumor cell lines	82
4.3.3 Fluorimetric calibration of complexed mTHPP	82
4.3.4 Preparation and handling of PSS/mTHPP-complex	83
4.3.5 Loading of peripheral blood CD3+, CD4+ and CD8+ T lymphocytes	84
4.3.6 Fluorimetric quantitative determination of mTHPP mass in CD3+ T lymphocytes	84
4.3.7 Flow cytometric analysis of mTHPP uptake by CD3+ T lymphocytes	85
4.3.8 Fluorescence microscopy of loaded CD3+ T cells.....	85
4.3.9 Bispecific antibody EpCAM×CD3	86
4.3.10 Flow cytometric analysis of drug transfer	86
4.3.11 Fluorescence microscopic analysis of drug transfer	86
4.3.12 Viability assay	87
4.3.13 Cytotoxicity assay	87
4.3.14 Cytotoxicity assay after light irradiation.....	88
4.3.15 Viability assay after incubation with supernatants obtained from loaded CD3+ T cells.....	88
4.3.16 Fluorimetric detection of mTHPP	89
4.3.17 Statistical analysis	89
4.4 Results	89
4.4.1 Qualitative and quantitative analysis of mTHPP uptake	89
4.4.2 Viability and cytotoxic function of loaded peripheral blood CD3+ T lymphocytes	91
4.4.3 Photosensitizer transfer from loaded peripheral blood CD3+ T lymphocytes to co-cultivated carcinoma cells.....	93
4.4.4 Enhanced cytotoxicity of bsAb-redirectioned, photosensitizer-loaded CD3+ T lymphocytes	95
4.4.5 Cytotoxicity of supernatants obtained from loaded CD3+ T lymphocyte cultures.....	96
4.4.6 Boosted cytotoxicity of bsAb-redirectioned, photosensitizer-loaded CD4+ and CD8+ T lymphocytes	97
4.5 Discussion.....	99
4.6 Conclusions	102
4.7 Supplementary Information.....	103
4.7.1 Purity of isolated, activated and expanded CD4+ or CD8+ T lymphocytes.....	103
4.7.2 Calibration of PSS/mTHPP preparations.....	104
4.7.3 UV/Vis spectra of PSS/mTHPP.....	104
4.7.4 Contribution of mTHPP to absorbance in WST-1 assays	105
4.7.5 Qualitative analysis of mTHPP uptake by fluorescence microscopy	105
4.7.6 Viability of T cells after loading with free or complexed mTHPP	106
4.7.7 Qualitative analysis of mTHPP uptake by flow cytometry	106
5. Overall Conclusion and Outlook	107

6. List of Abbreviations	111
7. References	114
8. Publication List	133
Scientific Publications	133
Patent	133
Contribution to Scientific Conferences	134

I. Summary

Studies have shown that T cells can serve as carriers to deliver cytotoxic drugs to tumors. However, these drugs also impair physiological T cell functions.

The subject of this thesis was to identify therapeutics for T cell-mediated drug delivery, which do not affect natural cytotoxicity and viability after uptake in order to synergize the tumoricidal properties of T cells with the drug effect. By redirecting drug-loaded human T cells to cancer cells via bispecific antibodies, the feasibility of this approach was tested.

Assuming that encapsulation of cytotoxic drugs would protect carrier cells, various polyester nanoparticles, containing the chemotherapeutic idarubicin (IDA-NPs), were examined. Moreover, differently glycosylated polylysine derivatives were tested as a potential drug encapsulation material. Photosensitizers (PS) exhibit cytotoxicity only upon light irradiation. Hence, the suitability of the PS 5,10,15,20-tetrakis(3-hydroxyphenyl)porphyrin (mTHPP) as payload was studied.

Polylysine derivatives were non-toxic and interacted to different extent with T cells. IDA-NPs failed to preserve the viability of carrier cells. In contrast, mTHPP was delivered to target cells and did not impair carrier cell functions when kept in the dark. Upon illumination, retargeted mTHPP-loaded T cells were more efficient in killing cancer cells than unloaded cells. Hence, the use of light-sensitive drugs provides new perspectives for cell-mediated drug delivery.

II. Zusammenfassung

Studien haben gezeigt, daß T-Zellen (TZ) als Träger von Zytostatika (ZS) dienen können, um diese zu Tumoren zu transportieren. Dadurch werden jedoch auch physiologische TZ-Funktionen beeinträchtigt.

Ziel dieser Arbeit war es, Therapeutika für die TZ-vermittelte Medikamentenabgabe zu finden, die diese Funktionen nicht beeinträchtigen, um die tumoriziden Eigenschaften von TZ mit der Wirkung der ZS synergistisch kombinieren zu können. Indem mit ZS beladene humane TZ mittels bispezifischer Antikörper zu Krebszellen dirigiert wurden, wurde die Machbarkeit des Konzepts überprüft.

Unter der Annahme, daß eine Verkapselung von ZS die Trägerzellen schützt, wurden verschiedene Polyester-Nanopartikel, die alle das ZS Idarubicin enthielten (IDA-NP), untersucht. Ferner wurde evaluiert, ob glykosylierte Polylysinderivate (PD) als Verkapselungsmaterial geeignet sein könnten. Photosensibilisatoren (PS) sind nur zytotoxisch, wenn sie mit Licht bestrahlt werden. Daher wurde überprüft, ob der PS mTHPP als Medikamentenfracht geeignet ist.

PD waren nicht toxisch und interagierten unterschiedlich spezifisch mit TZ. IDA-NP reduzierten die TZ-Vitalität signifikant. Im Gegensatz dazu wurde mTHPP an Zielzellen abgegeben. Unter Lichtausschluß beeinträchtigte es zudem nicht die Funktionen von TZ. Nach der Bestrahlung konnten beladene TZ Krebszellen effizienter abtöten als nicht beladene TZ. Somit eröffnet die Verwendung von lichtaktivierbaren ZS neue Perspektiven für die zell-vermittelte Arzneimittelabgabe.

1. Introduction

1.1 Envisioned T cell-mediated drug delivery concept for cancer therapy

The motivation of the presented thesis was to explore the feasibility of using living human T lymphocytes (see section 1.3) as vehicles to deliver cytotoxic drugs (section 1.4) to tumor cells. The purpose of this targeted delivery concept is to improve the selectivity and efficacy of cancer treatment and to reduce adverse effects normally provoked by systemically applied chemotherapeutics. The natural cytotoxicity of tumor-specific effector T lymphocytes has been exploited in adoptive cell transfer (ACT) to treat neoplasms. Clinical studies have demonstrated the curative potential of ACT ^[1]. However, durable complete responses are often limited to a fraction of patients ^[2]. Therefore, the T cell-based drug delivery approach aims to combine the cytotoxicity of cell-delivered pharmaceuticals with the cell-mediated cytotoxicity to improve the curative potential of ACT.

The first step of the envisioned therapy concept is the isolation of polyclonal peripheral blood T lymphocytes of patients. Here, polyclonal means that each cell possess a different target antigen specificity. Most of these lymphocytes are “dormant”, because they have not yet encountered their particular antigen (naïve cells) or are antigen-experienced but inactive memory cells ^[3]. Naïve and memory T cells exhibit no immediate effector function such as cytotoxicity. Therefore, the next step is *ex vivo* activation of T lymphocytes. Consequently, T cells proliferate, expand and acquire effector functions (see section 1.3). Due to expansion, a sufficient number of carriers for treatment is gained ^[4]. Furthermore, the cell size within the non-activated population of T lymphocytes is smaller than that within the population of activated T cells (see chapter 2, Figure S2.1). Hence, it is likely that activated T lymphocytes have a greater capacity for drug uptake. In order to investigate the proposed immunotherapy approach, T cells isolated from blood of healthy donors and targets of defined cancer cell lines were used in the presented work. In contrast to naturally activated and clonally expanded T lymphocytes, *in vitro* stimulated polyclonal T cells are not specific for particular tumor cells. An option to recruit unspecific T lymphocytes to cancers cells is the use of bispecific antibodies (bsAbs) ^[5]. It should be pointed out that Mandruzzato et al. already suggested the use of bsAbs in the context of cell-mediated drug delivery ^[6]. However, the group never published any related results.

Bispecific antibodies (bsAb) are engineered molecules, which in contrast to normal antibodies (monospecific but bivalent) possess dual specificity for two different antigens (bispecific but monovalent). One antigen-binding site of bsAb recognizes a surface marker, such as a tumor-associated antigen (TAA), on the target cell. In T lymphocyte-based therapies, the other moiety binds specifically to a component of CD3, a signaling complex associated to T cells receptors (TCRs) located on the plasma membrane. Normally, effector functions of activated T lymphocytes are initiated after TCRs recognize their antigen-ligands presented by major histocompatibility complex (MHC) molecules expressed on the surface of target cells ^[3]. However, bsAbs induce the cytolytic activity of T lymphocytes in a non-MHC-restricted manner ^[7]. Therefore, by bypassing TCRs using bsAbs, polyclonal T cells become specific just for one TAA. Theoretically, all CD3-positive subsets of T cells (see section 1.3) present in the peripheral blood of cancer patients can be exploited as carrier cells. The bsAb HEA125×OKT3 used in the presented work (kindly provided by Gerhard Moldenhauer, Department of Translational Immunology, German Cancer Research Center, Heidelberg, Germany), redirects T lymphocytes to EpCAM (Epithelial Cell Adhesion Molecule, CD326) over-expressing epithelial tumor cells derived from human carcinomas (Figure 1.1). The therapeutic potential of HEA125×OKT3 was already demonstrated in cell culture and animal experiments as well as in a clinical trial involving ovarian carcinoma patients ^[8-10].

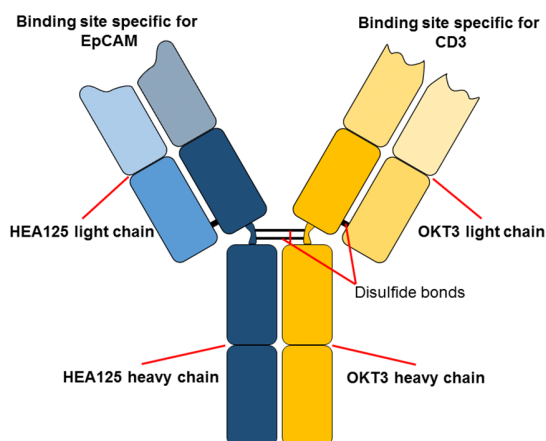


Figure 1.1. Schematic of the bispecific antibody HEA125×OKT3. Cells of the murine hybridoma cell lines OKT3, specific for human CD3, and HEA125, specific for human CD326 (EpCAM), were fused using the hybrid-hybridoma technique ^[10]. While OKT3 cells express type G2a immunoglobulins (IgG2a), HEA125 cells produce IgG1 molecules.

After activation and expansion, T cells are loaded with an anticancer drug-formulation transforming them into drug carriers aptly termed as “pharmacytes” by Huang and colleagues ^[11]. Before commencing the cancer treatment, residual free drug is removed. Then, loaded T cells are mixed with bispecific antibodies. Upon arriving at cancer sites, bsAbs bind T lymphocytes to target cells

and trigger effector functions (T cell effect). At the same time, carrier cells release the drug, ideally in a continuous manner at the tumor site ^[12]. Here, the payload can exert its cytotoxic function (drug effect). The process is schematically illustrated in Figure 1.2.

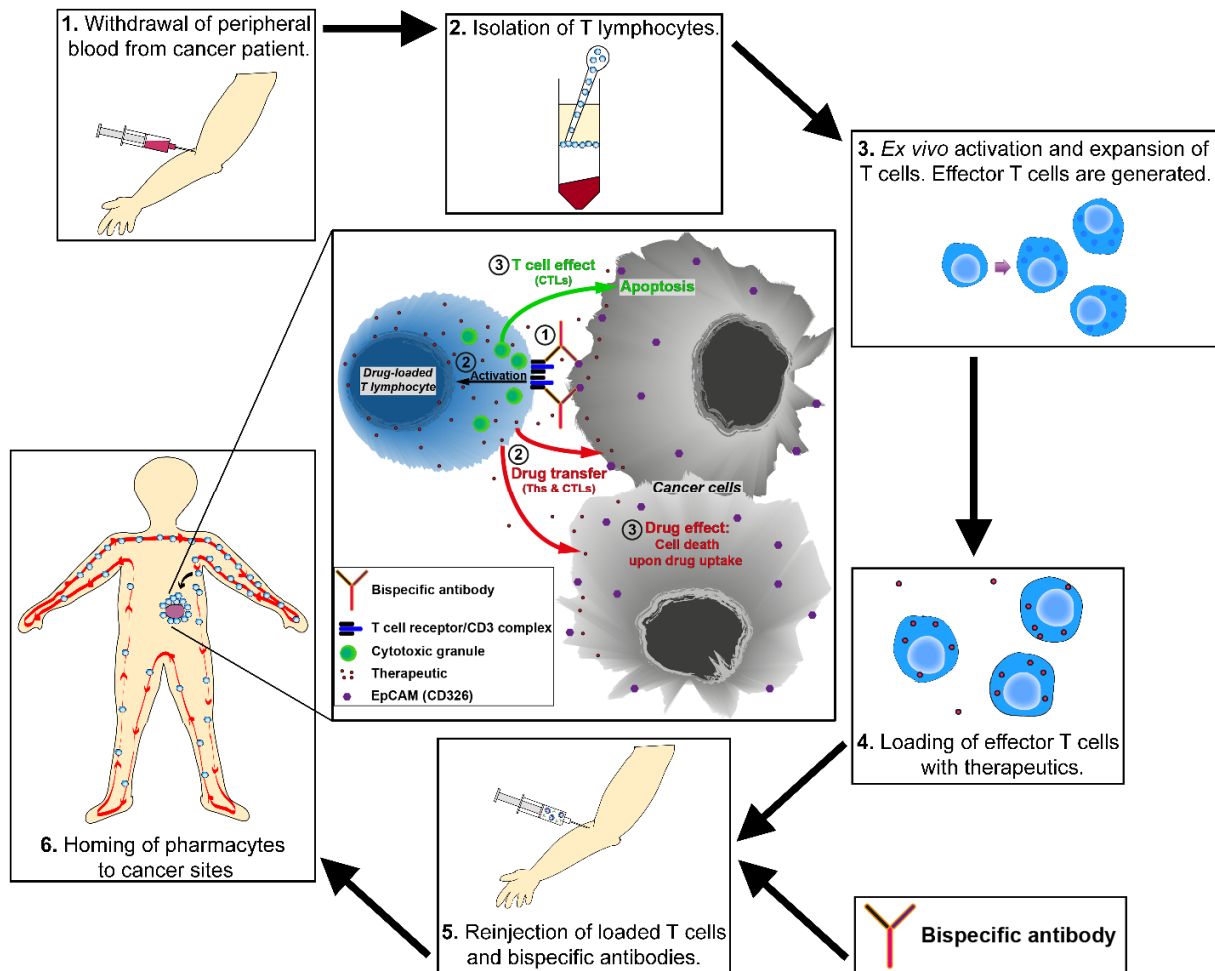


Fig. 1.2. Illustration of the envisioned T cell-mediated drug delivery concept (see text). In this thesis, the approach was pursued until step 4. Then pharocytes and bsAb were applied to cancer target cells cultivated *in vitro*. In the center, the proposed mode of action is shown: ① T lymphocytes are cross-linked through bsAbs to cancer cells. ② After reactivation T cells exert effector functions. In addition, while bound to cancer cells the therapeutic is transferred by pharocytes. ③ T cells with cytotoxic effector function (CTLs) will kill target cells by inducing apoptosis, while T cells with helper function (Ths) can also serve as carrier cells. *All drawings except the center and the bsAb schema were kindly provided by Alice Borth.*

It was proposed that ideal carrier cells should meet the following requirements: 1) Access to patients' cell population should be simple and preferably non-invasive. 2) Sufficient amounts of

cells should be easily generated by *ex vivo* expansion and the respective procedure should not be deleterious for cell properties. 3) Re-implantation of modified cells should be effortless. 4) Cells should possess tropism for (diseased) sites of interest ^[13]. T lymphocytes meet those requirements, because they can easily be isolated from peripheral blood of patients. Moreover, commercial available T cell expansion kits facilitate the generation of large cell numbers. Possible minor reduction of cell viability at the beginning of expansion phase is manageable by removing dead cells from the culture. Reinfusion of manipulated T lymphocytes into patients' blood stream poses no obstacle. Furthermore, T cells are recruited to and infiltrate solid tumors ^[14], which is also reflected by the fact that tumors can evolve multiple strategies to evade T lymphocyte-mediated immune responses ^[15].

Usually, the immune system is able to specifically recognize and destroy cancer cells ^[16]. This process is termed "immune surveillance" and was first suggested in the 1950s by Sir Frank MacFarlane Burnet and Lewis Thomas ^[3, 17]. As already indicated, in tumor-bearing patients this surveillance has failed and natural host defenses are curbed, because cancers have developed immune evasion strategies (reviewed in ^[18, 19]). Nevertheless, the main natural process for detection and eradication of cancers remains the cellular mediated immunity ^[13]. Consequently, adoptive cell therapies have emerged, in which patient-derived immune cells such as T lymphocytes ^[1] or natural killer (NK) cells ^[20] are isolated, manipulated to (re)-gain anticancer functions and transferred back into hosts. As compared to NK cells, T lymphocytes exhibit a greater capacity for proliferation, survival, and elimination of large neoplastic masses ^[20]. Accordingly, T cells have been a major focus of research. Using these lymphocytes in ACT has been proven to be effective in clinical trials involving hematological malignancies ^[21, 22], metastatic melanoma ^[2] and other types of neoplastic diseases ^[23]. In these trials, tumor-reactive autologous (the donor is also the recipient) tumor-infiltrating lymphocytes (TILs) or patient-derived genetically engineered T cells were used for ACT. Transduced T lymphocytes have been redirected towards tumor-associated antigens through genetic modification with T cell receptor or chimeric antigen receptor (CAR) genes ^[24]. As mentioned before, the utilization of bispecific antibodies is another option to target T lymphocytes to sites of malignancies. In addition to fulfilling the aforementioned requirements, the curative potential of T cells in ACT is another reason for choosing them as cellular drug vehicle in this thesis. Several studies have also attempted to use this type of cells as drug vehicle (see section 1.2.1). However, cell-mediated drug delivery is not restricted to T lymphocytes as described in the subsequent section.

1.2 Cell-mediated drug delivery

In recent years, drug delivery systems (DDS) have been comprehensively investigated as an option to enhance the therapeutic efficacy of drugs by improving pharmacokinetics (drug absorption, distribution, metabolism, and excretion (ADME)) and pharmacodynamics (drug efficacy and toxicity). Extensive research efforts have been made to design carriers for therapeutics with improved drug solubility, prolonged circulating time, limited biodistribution, specific targeting, controlled drug release, and reduced toxicity and immunogenicity [25]. A plethora of drug delivery devices such as antibodies [26], fibers [27], films [28], hydrogels [29], liposomes [30], nanoparticles [31, 32], micelles [33], polymers [34, 35], and several modifications thereof have been studied. However, only few DDS such as liposomal formulations of the anticancer drugs doxorubicin (Caelyx[®], Doxil[®], and Myocet[®]), daunorubicin (DaunoXome[®]) and vincristine (Marqibo[®]), an albumin conjugated nanoparticle formulation of the antineoplastic drug paclitaxel (Abraxane[®]), and antibody-drug conjugates for cancer treatment (Kadcyla[®] and Adcetris[®]) have reached the market [36-38]. The major problems of most drug delivery systems are low clinical efficacy due to rapid clearance from patients' blood stream by phagocytic cells of the reticuloendothelial system (RES) [39] and still insufficient targeting to the diseased site. For instance, over 95% of the systematically administered dose of a nanoparticulate system accumulates not at the target site but in the liver, lungs, spleen and kidneys [40]. As reported in several review articles, cell-mediated drug delivery has emerged to overcome these obstacles and to serve as an alternative for the treatment of severe diseases such as cancer, infectious diseases, and inflammatory and neurological disorders [12, 13, 25, 37, 41-43].

In contrast to the relatively simple structural organization of vehicles for drugs, cells are complex biological systems, which can exhibit unique natural properties such as the ability to actively home to pathological sites, a quality even "active targeted" DDS do not possess [40]. In addition, homing includes crossing barriers such as the blood-brain or blood-tumor barrier. Furthermore, autologous cells are generally not immunogenic and some immune cells show natural killing or phagocytic functions, which can additionally be exploited to fight diseases like cancer. By conjugating drugs with cells, thereby transforming them into "Trojan Horses", therapeutics are protected from the hepatic metabolism and the RES, which prolongs the drug half-life. Local drug delivery, slowed drug release, and decreased drug toxicity are further advantages of a cell-based approach. Therefore, phagocytes are considered as a novel class of therapeutics and drug carriers [12, 25, 37, 41, 42].

In principle, three options are available to “upgrade” carrier cells with therapeutics: conjugations of therapeutics to carriers via membrane surface engineering, loading of therapeutics into cells, and transfection of carrier cells with nucleic acids, the translated products of which have therapeutic properties. Chemical processes such as covalent conjugation, biotinylation, and click chemistry (e.g. azide-alkyne Huisgen cycloaddition [44]) are possible options to bind therapeutics to cell membranes. Hypotonic hemolysis (of erythrocytes) and electroporation are physical methods, which facilitate uptake of therapeutics by cells. In addition, adsorption via electrostatic or hydrophobic interactions is used to attach therapeutics to cell membranes. Biological pathways such as endocytosis and ligand-receptor interactions can mediate cellular uptake and binding of therapeutics. Furthermore, gene modification enables carrier cells to express therapeutic proteins (Fig. 1.3) [25, 41].

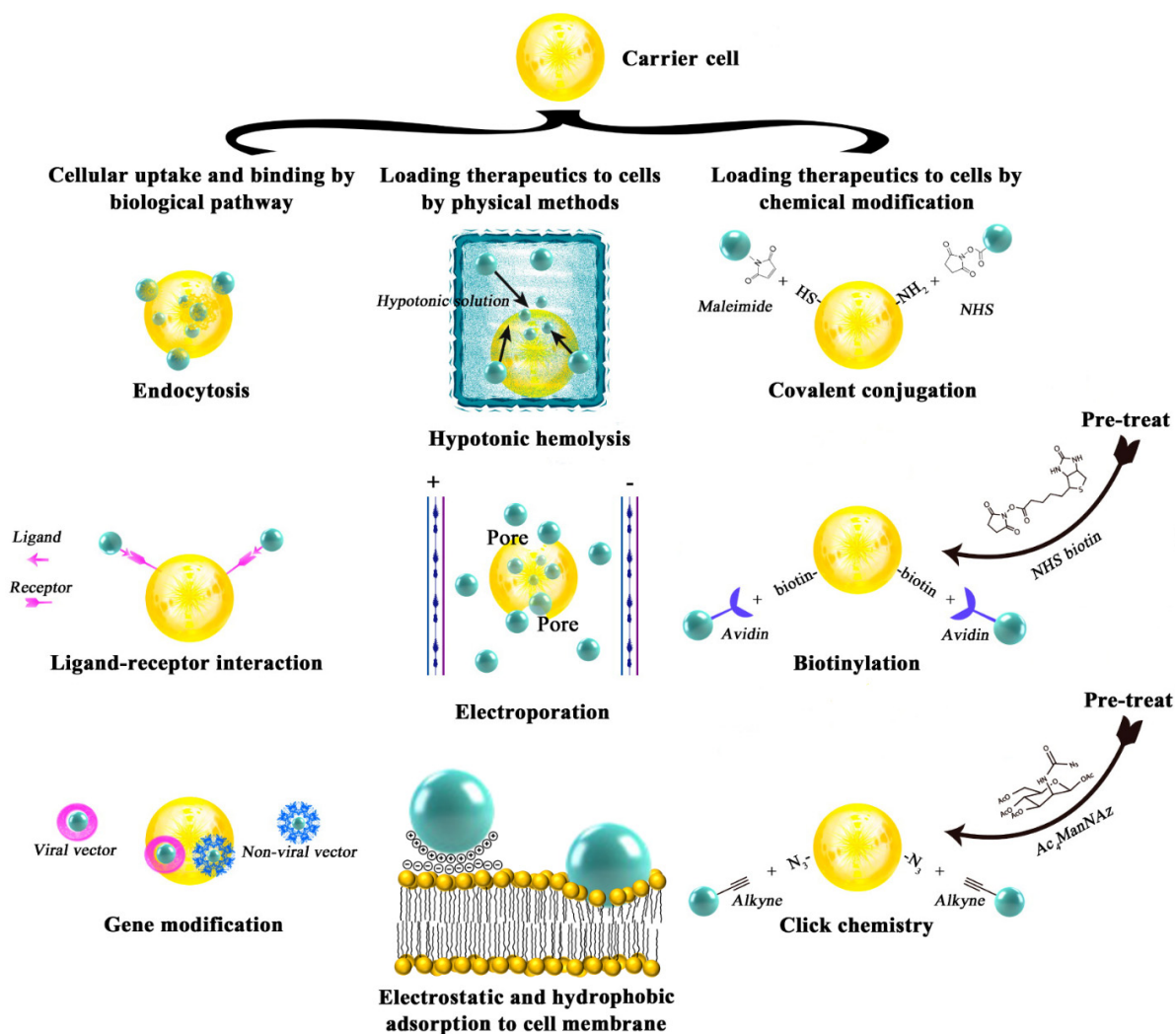


Fig. 1.3. Approaches used in cell-mediated drug delivery for encapsulation/conjugation of therapeutics into/to carrier cells. Adapted with permission from [25]. Copyright 2015 American Chemical Society.

So far, the cell-mediated drug delivery concept has been evaluated in the context of cancer, infectious diseases, and inflammatory and neurological disorders. Subsequent studies have demonstrated positive therapeutic effects by using cellular drug vehicles such as erythrocytes [45-54], fibroblasts [55, 56], encapsulated or inactivated cancer cells [57-59], mesenchymal [60-62] and neural [63-68] progenitor/stem cells, myoblasts [69], Sertoli cells [70] and leukocytes such as dendritic cells [71], monocytes/macrophages [72-79], lymphocytes [80], lymphokine-activated killer (LAK) cells [6, 81, 82], NK cells [83], and T lymphocytes [11, 84-91]. Members of following therapeutic classes were used as payloads for the aforementioned cellular carriers: derivatives of alkaloids [11], anthracyclines [6, 46, 57, 58, 74, 76, 81, 83], antimetabolites [45, 47, 72], antimicrobials [48, 51, 79], cytokines [90], enzymes [52-54, 77], immunomodulators [91], immunosuppressors [49, 50, 70, 71], nanoparticulate gold [75] and iron/iron oxide [73], photosensitizers [47], plant toxins [82, 84], radioactive isotopes [80], and viruses [62, 68, 89]. Expressed therapeutic proteins have included angiogenic growth factors [56, 67], antibodies [59], cytokines [60, 61], enzymes [55, 65, 78], immunotoxins [85-88], and neurotrophic factors [63, 64, 66, 69].

The use of vectors to produce gene-modified carrier cells raises safety concerns. The integration of newly introduced DNA into the genome could transform genetically engineered cells into aberrant cells, because of dysregulation of proto-oncogenes. This could give rise to new malignancies [24]. In addition, therapeutic-producing cells could be hazardous if they remain active in the patient after the cure of the disease [92]. Moreover, clinical gene therapy implicates considerable regulatory and cost barriers [90]. Therefore, a non-genetic engineering approach using endocytic pathways of T lymphocytes was preferred and pursued in this thesis.

1.2.1 T lymphocyte-mediated drug delivery for cancer treatment

The National Cancer Institute at the National Institutes of Health (USA) lists more than 100 different types of cancer [93], which illustrates the complexity of neoplastic diseases. However, Hanahan and Weinberg proposed a number of following *hallmarks* [94], which define an organizing principle underlying the multistep development of malignant tumors. According to the somatic mutation theory (SMT), cancer is initiated by DNA mutations caused by inherited predisposition, genotoxic carcinogens or spontaneous mutations occurring during stem cell divisions [95]. By accumulating of these mutations, normal cells evolve and acquire traits that enable them to become malignant. In normal tissues, proliferation of cells is strictly regulated by growth-promoting signals. Aberrant cells are able to deregulate these mitogenic signals and *sustain proliferative signaling* to multiply uncontrolled. In addition, abnormal cells have acquired the capability to

evade growth suppressors, which negatively regulate normal cell proliferation. Furthermore, those cells are able to *resist cell death*. Growing neoplastic tissue needs nutrients and oxygen. Moreover, metabolic waste and CO₂ have to be removed. Therefore, during tumorigenesis, cells need to acquire the trait to *induce angiogenesis* for blood supply. The ability to *invade* into neighboring tissues and *metastasize* via lymphatics and blood stream to distant locations, distinguishes benign from malignant tumors. Hanahan and Weinberg have additionally proposed two emerging *hallmarks*. Apparently, to fuel uncontrolled cell growth and division, adjustments of energy metabolism are required. Therefore, a *reprogrammed energy metabolism* is another quality of cancer cells. As mentioned before, according to the immune surveillance theory ^[16], the immune system keeps neoplasms in check. However, permanent selection of cell variants resistant to immune effectors (immunoediting) and an immune suppressive tumor-environment ^[18] gives rise to cells, which are able to *evade immune destruction* ^[94].

Despite the many advances in surgery, chemo- and radiation therapy, cancer is still a leading cause of death. All types of malignant neoplasms combined (excluding non-melanoma skin cancer) were responsible for 8.2 million deaths worldwide in 2012 ^[96]. Therefore, other modalities of cancer treatment are the subject of intensive research. Feasibility studies of lymphocyte-based drug delivery were commenced 31 years ago. A paper published in 1984 reports that murine spleen cells, a mixture of cell types also containing T lymphocytes, could serve as donor cells in order to transfer the plant toxin ricin to murine recipient spleen cells *in vitro* ^[97]. Those transfer studies were conducted in the presence of phytohaemagglutinin (PHA), a polyclonal mitogen that only activates T cells ^[3, 98]. Although not stated, McIntosh et al. started to explore a potential cancer therapy modality, which was pursued in a subsequent biodistribution study ^[99]. Therein, the group clearly aimed at exploiting the ability of ricin-loaded lymphocytes to home to lymphatic tissues in order to target associated malignancies. To this end, Sparshott *et al.* used ricin-loaded thoracic duct lymphocytes (TDLs, including T cells) to deliver the toxin to the spleen, lymph nodes and Peyer's patches of healthy rats. TLDs were also used to deposit a radioactive isotope of indium (In-114m) to spleen and lymph nodes of rats to fight tumors of lymphoid origin ^[80]. Repeated injections of In-114m loaded TDL delayed the lethal onset of lymphocytic leukemia. However, this treatment did not lead to permanent remission and after injections were stopped the rats died. Likewise, ricin-loaded Moloney-murine sarcoma virus specific T cells exerted a temporary therapeutic effect in tumor-bearing mice. However, the tumor started to proliferate again after 6 days. In order to prolong the period of tumor growth inhibition, the number of adoptively

transferred ricin-loaded cytotoxic T cells was increased. As consequence, the recipient animals died very quickly, because of ricin toxicity ^[84]. A second study reports that ricin-loaded lymphokine-activated killer cells were more successful in reducing lung metastases in mice than unloaded LAK cells ^[82]. The LAK cell phenomenon is mediated mainly by NK cells but also by T cells ^[100]. The selection of ricin as payload for carrier cells had several drawbacks. First, after adoptive transfer of ricin-loaded lymphocytes, cells became stuck in the tissues and were not able to re-enter the blood stream in same way as normal recirculating lymphocytes. In addition, they also failed to migrate from blood to lymph. Second, the difference between therapeutic and toxic concentration of ricin was very narrow. Most importantly, as early as 3 hours after ricin loading the cytolytic activity of lymphocytes against target cells was seriously impaired ^[82, 84, 99]. Due to the high systemic toxicity, Mandruzzato *et al.* substituted ricin for an antineoplastic anthracycline ^[6]. The authors achieved a striking reduction of lung metastases in mice using adoptively transferred and 4'-deoxy-4'-iododoxorubicin (IDX) loaded LAK cells. However, cytotoxic activity of carrier cells was again gravely inhibited. Furthermore, since LAK cells had redistributed to liver and spleen considerable levels of IDX were found in these organs of the mice. Other investigators have also pursued similar strategies: Steinfeld and colleagues encapsulated the anticancer drug doxorubicin, reversibly attached to nanoparticles, into human T cells to synergize chemotherapy and adoptive T cell immunotherapy ^[101]. Mortensen *et al.* aimed at delivering boron carbide nanoparticles via loaded human T cells to render tumor tissue susceptible for boron neutron capture therapy ^[102]. Iida and colleagues proposed a magnetically mediated immunotherapy using human T cells loaded with magnetite (Fe₃O₄) nanoparticles ^[103]. Kennedy *et al.* tested whether human T lymphocytes are able to deliver gold nanoparticles into murine tumors for photothermal therapy ^[104]. However, none of these studies demonstrated any therapeutic effects *in vitro* as well as *in vivo*.

In the aforementioned studies, therapeutics were loaded into carrier cells. Stephan and colleagues used a cell membrane-modification approach. By covalent coupling of cytokine or small-molecule drug containing nanoparticles onto the plasma membrane surface, they provided a sustained "pseudoautocrine" stimulation to carrier cells, which caused an increased T cell expansion, longevity and an enhanced tumor elimination after *in vivo* transfer. The authors were able to augment the therapeutic potential of T cells without impairing cell functions ^[90, 91]. However, the strategy applied by Stephan and colleagues differs from the one pursued in this thesis in that the payload is attached to the outside of carrier cells. Furthermore, in those studies non-cytotoxic

drugs were used, which acted on carrier cells and not directly on target cells. Recently, the group has substituted these non-toxic payloads for the cytotoxic topoisomerase I poison SN-38 ^[11], which is the active metabolite of the anticancer drug irinotecan (a semisynthetic analog of the alkaloid camptothecin). In this study by Huang et al., SN-38-loaded lipid nanocapsules were attached to the surface of *ex vivo* expanded polyclonal T lymphocytes. Within a therapeutic window, T cells were resistant to SN-38 while lymphoma target cells were not. In contrast to control mice, animals treated with SN-38 nanocapsules bound to T cells showed a significant reduction of tumor burden. However, the intrinsic cytolytic activity of T cells was not exploited in this study, which is part of the approach pursued in this thesis.

As already noted, most of the previously mentioned studies revealed major drawbacks of the cell-based drug delivery strategy that probably hampered clinical trials until now. When carrier cells were loaded with toxic pharmaceuticals, a rapid loss of physiological functions and a decline of cell viability were observed. In the work presented here, formulations of two different types of polymer-encapsulated therapeutics were investigated to overcome the obstacle of cell function loss. The first approach pursued the idea of incorporation of an “active” drug, an anthracycline (see section 1.4.1), into nanoparticulate systems in order to protect the living vehicles (chapter 3). For the second approach, a “stimulus-sensitive” drug represented by a photosensitizer (see section 1.4.2), the mode of action of which is only triggered by light irradiation (chapter 3 and 4), was used. The immunological and physiological functions of T cells meant to be preserved are summarized in the next section.

1.3 T lymphocytes

T lymphocytes (or T cells) play a central role in the acquired (adaptive) immune response against pathogens such as bacteria, fungi, parasites and viruses. In addition, T cells have the potential to kill abnormal cells. They belong to the group of white blood cells also known as leukocytes, which originate in the bone marrow, a central (primary) lymphoid organ. Leukocytes are further divided into two main categories, the lymphoid and myeloid lineages. B cells, natural killer cells and T cells arise from common lymphoid progenitor cells and are therefore classified as lymphocytes. In contrast to other lymphocytes, T cells mature in the thymus, the other primary lymphoid organ located in the upper chest. Here, each thymocyte (a precursor T lymphocyte) generates a

unique T cell receptor, a heterodimer consisting of an α and a β polypeptide chain, through the rearrangement of TCR genes. Afterwards, TCRs are positively selected for the affinity to self-peptide:MHC complexes (major histocompatibility complex restriction). MHC molecules are glycoproteins that present peptide antigens on cell-surfaces. T cells that recognize antigenic self-peptides too strongly are negatively selected and deleted by apoptosis. After maturation, three subsets of T lymphocytes can be distinguished: conventional $\alpha\beta$ T cells that express either CD4 or CD8 co-receptor molecules on the cell membrane surface and CD4⁺ T cells that also express high levels of CD25. The latter population represents a thymic subset of regulatory T cells (natural Tregs). Conventional T cells leave the thymus and recirculate between blood and peripheral (secondary) lymphoid tissues such as lymph nodes and the spleen searching for their specific antigen (Ag) of pathogenic origin. They are also termed “naïve”, as long as they have not encountered their cognate antigen. The repertoire of unique TCRs enable mature T cells to recognize a very broad range of peptides derived from non-self antigens. Upon recognition of their specific non-self-peptide:MHC complexes presented by antigen-presenting cells (APCs) such as dendritic cells (DCs) located in peripheral lymphoid tissues, naïve T cells are activated (primed). DCs are “sentinels”, which traffic from the blood into tissues. Here, while in an immature state they take up Ags and process them to peptides. Pathogenic antigens captured in the context of an inflammatory reaction provoked by infections or cancers drive DCs to leave the tissues and migrate to draining lymphoid organs. Here, they mature to APCs and start to express specialized membrane surface molecules that enable them to prime T lymphocytes [3]. While the TCRs of CD4⁺ T cells bind to peptide:MHC class II complexes present on DCs, TCRs of CD8⁺ T cells are stimulated by peptide:MHC class I complexes. TCR ligation represents the first signal needed to activate naïve T cells. Via further receptor-ligand interactions within the “immunological synapse”, for instance between CD28 expressed by the T cell and CD80/CD86 located on the dendritic cell, the same DC delivers a second “co-stimulatory” signal. This signal induces the secretion of the cytokine interleukin-2 (IL-2) by the activated T lymphocyte to ensure its own survival by autocrine stimulation. Following a defined combination of cytokines expressed by the antigen-presenting cell, the activated T cells are polarized. The combination of cytokines is determined by the type of inflammation (viral, microbial etc.) and represents the third signal (Fig.1.4) [105-107]. Because of their destructive nature (see below), CD8⁺ T cells require a stronger co-stimulation than CD4⁺ T cells. Although this requirement can be met by sufficiently activated DCs, often CD4⁺ T cells provide additional help to fully activate CTLs [108].

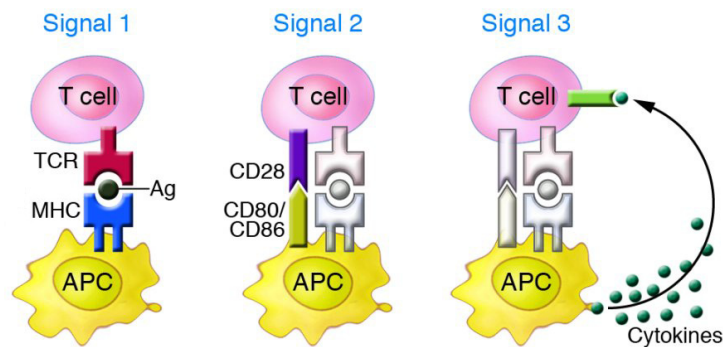


Fig. 1.4. Full activation of T lymphocytes requires three signals. The first signal needed for activation is the recognition of antigenic peptides (Ag) bound to MHC molecules by TCRs of a naïve T cell and presented by an APC. Interactions of co-stimulatory ligand-receptor complexes generate the second signal. The third signal is provided by cytokines secreted by the APC. This process polarizes T lymphocytes to specialized effector cells. *Adapted with permission from [105]. Copyright 2015 American Society for Clinical Investigation.*

Polarization by APC derived cytokines leads to differentiation into different cell lineages, such as the Th1, Th2, and Th17 subsets of CD4⁺ helper (h) or follicular helper (fh) lymphocytes, as well as induced regulatory CD4⁺ T cells (iTregs), type 1 regulatory cells (Tr1), and Th3 cells. Less defined subsets are Th9 and Th22 cells [109]. All subsets exhibit specialized effector functions. For instance, Th1 cells induce macrophage activation and the production of complement-fixing and opsonizing antibodies by B cells. Accordingly, they are involved in the clearance of intracellular bacteria, fungi, protozoal parasites and viruses. Th2 cells fight extracellular pathogens and worms (helminthes and nematodes) by inducing antibody class-switching in B cells and the recruitment of eosinophils to sites of infection. Th9 cells are considered to contribute to the eradication of parasitic infections. Th17 lymphocytes provide protection against extracellular bacteria and fungi by recruiting neutrophils. Tfh cells assist antibody production by secreting B cell-promoting cytokines. Regulatory T cells are generally involved in maintaining self-tolerance and immune homeostasis. The CD4⁺ T cell compartment seems to show plasticity. An established subset is not necessarily committed to its effector function. For instance, Th17 cells can acquire a Th1 or Th2 phenotype. Such flexibility could be beneficial for the host, because it allows an efficient way to fight the same pathogen under different conditions [3, 109-112]. Another example for plasticity are CD4⁺ T lymphocytes, which are post-thymically reprogrammed to gain a cytolytic capacity upon chronic antigen stimulation [113]. CD8⁺ T cells are largely pre-committed to differentiate into cytotoxic T lymphocytes (CTLs) upon activation. The most important ability of CTLs is to detect and kill infected or neoplastic cells by inducing apoptosis, mainly via the granule-dependent exo-

cytotoxic pathway (Fig.1.5) ^[114]. The underlying mechanism is also responsible for the previously described T cell effect. Of note, there is growing evidence that CD8+ T lymphocytes also exhibit heterogeneity in differentiation and function ^[115].

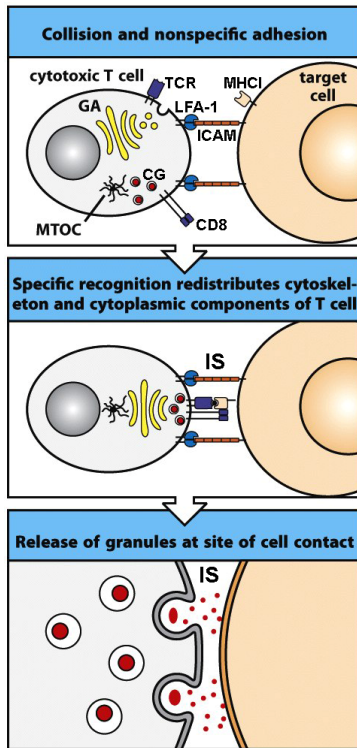


Fig. 1.5. Granule-dependent exocytosis pathway. While screening cells, cytotoxic CD8+ T lymphocytes initially bind to cells through nonspecific adhesion molecules such as LFA-1 and ICAM. Upon recognition of non-self antigens presented by tumor or infected cells, the CTL becomes polarized. It directs components of the killing machinery towards the immunological synapse (IS) formed between CTL and target cell. The microtubule-organizing center (MTOC) is reoriented by the cortical actin cytoskeleton located at the contact site. MTOC in turn aligns the Golgi apparatus (GA), which provides cytotoxic proteins encapsulated into specialized lysosomes termed cytotoxic granules (CG). These granules migrate along microtubules in the direction of the plasma membrane. Their content consists of perforin, granzymes and granulysin. Upon release into the IS, the cytotoxic proteins act in concert to induce apoptosis within the target cell. *Adapted with permission from ^[3]. Copyright 2012 Garland Science/Taylor & Francis Group.*

Upon activation, one T cell can generate a large number of progeny (clonal expansion), that all bear the same specificity for one particular antigen. Notably, effector T cells do not require co-stimulation anymore to mount an immunological attack ^[3]. Following antigen clearance, over 95% of effector cells die by apoptosis (contraction). However, a small pool of T cells survives and differentiates into long-lived immunological memory cells, which also show heterogeneity ^[116]. Memory T lymphocytes provide a protective immunity based on a faster and stronger immune response upon the re-exposure to a pathogenic antigen compared to naïve T cells ^[3, 117]. In addition to $\alpha\beta$ T lymphocytes, other unconventional populations such as $\gamma\delta$ T cells ^[118], mucosa-associated invariant T (MAIT) cells ^[119], and natural killer T cells ^[120] responsible for different aspects of the immune response are described.

Since T lymphocytes constitute an important part in the defense from pathogens, it is no surprise that they also affect tumors. Aberrant cells exhibit gene alterations, which in turn can give rise to altered self-antigens. These “neoantigens” can be presented bound to MHC class I molecules on the surface of tumor cells, which can be then recognized as non-self and killed by CTLs ^[121]. This

process is analogous to the events occurring after immunogenic cell death upon insult with therapeutics shown in Figure 1.10B (section 1.4.2.2). Here however, the first step of this “cancer-immunity cycle” [121], namely the capturing of neoantigens by DCs and subsequent activation of CTLs is initiated by the spontaneous death of cancer cells, for instance induced by hypoxic conditions in the tumor core. Because of their antitumor properties, it is obvious to use CTLs as drug carriers. However, in this thesis all peripheral blood T cells were converted into phagocytes. The rationale behind this approach is the specificity of the bispecific antibody, which cross-links CD3+ T cells to target cells. Since all mature CD4+ and CD8+ T lymphocytes express CD3 [3], all these cells could be exploited as drug carrier cells. This includes also those CD4+ T cells, which exert a cytotoxic phenotype in combination with bsAb [10]. Furthermore, there is evidence that CD4+ T cells could augment the response to adoptive T cell transfer when co-administered with CD8+ T cells *in vivo* [122, 123]. However, the role of the CD4+ T cell compartment in tumor immunity is complex and it is a key modulator of the anticancer immune response. CD4+ T lymphocytes can contribute either to tumor regression or to progression. The presence of Th1 cells in the tumor correlates generally with a good prognosis for the patient. Depending on the cancer type, the infiltration of Th2 cells, Th17 cells or Tregs can comprise a good or poor prognosis or can have no influence at all [14]. Furthermore, Th9 cells can contribute to an anti-cancer immune response via cytokine secretion [124].

1.4 Drugs used as payload for T cells and their mechanisms of actions

In this thesis, formulations of two different kinds of drugs were used as payload for human T lymphocytes. While the anthracycline idarubicin (IDA) was encapsulated into polymeric nanoparticulate systems, the model photosensitizer 5,10,15,20-tetrakis(3-hydroxyphenyl)porphyrin (mTHPP) was applied complexed with the polyelectrolyte poly(styrene sulfonate) sodium salt (PSS). IDA exhibits direct cytotoxicity of its own and is therefore considered as an active pharmaceutical. In contrast, mTHPP exemplifies a passive or inducible therapeutic, because light (and molecular oxygen) are needed to trigger the cytotoxic activity of this photosensitizer.

1.4.1 Anthracycline based chemotherapy

Anthracyclines, a class of antibiotic-based compounds with similar chemical structures, such as daunorubicin, doxorubicin, epirubicin, and idarubicin (Fig. 1.6), belong to the most effective anticancer drugs in current clinical practice [125, 126]. As noted previously, this class of therapeutics has already been used in cell-mediated drug delivery (see section 1.2).

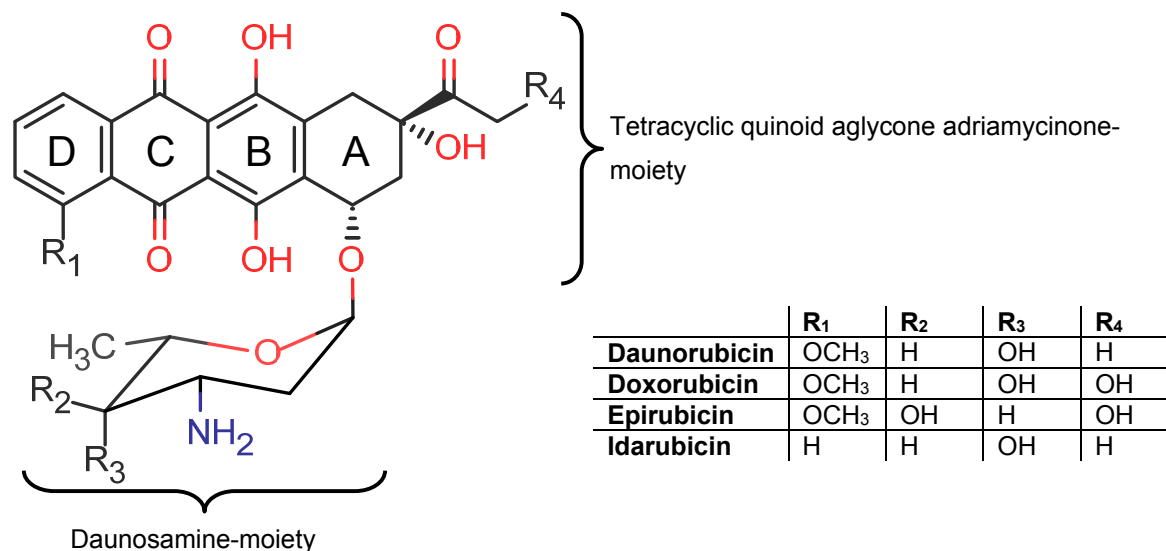


Fig. 1.6. Chemical structures of selected anthracyclines.

Daunorubicin (daunomycin, DAU) and doxorubicin (adriamycin, DOX) were the first anthracyclines isolated from the bacterium *Streptomyces peucetius* [127, 128] and the variant *Streptomyces peucetius* var. *caesius*, respectively, in the 1960s [129]. The range of the antineoplastic activity of anthracyclines is very broad. Solid tumors and leukemia such as acute myelogenous leukemia, breast cancer, hepatocellular carcinoma, Hodgkins' disease, non-Hodgkins' lymphoma, multiple myeloma, sarcoma, and small cell lung cancer, among others are treated with these agents [130].

1.4.1.1 Mechanisms of anthracycline-based tumor destruction

The molecular mechanisms responsible for antitumor activity of anthracyclines are not yet completely elucidated. Several mechanisms of action have been proposed and are controversially debated: 1) production of free radicals causing DNA damage and lipid peroxidation; 2) direct effects on cell membranes; 3) DNA binding and alkylation; 4) DNA cross-linking; 5) interference with DNA unwinding or strand separation and helicase activity; 6) intercalation into DNA leading to inhibition of DNA, RNA and protein synthesis; 7) inhibition of type IIA topoisomerase

(Top) mediated DNA religation generating and accumulating DNA double-strand breaks that consequently cause apoptosis. However, poisoning of Topo is considered a crucial part of the cell-killing activity of anthracyclines at clinically relevant concentrations [125, 131, 132]. Many cellular processes involving the genetic material such as transcription, replication, recombination, mitotic segregation and genomic compaction, affect and stress the topology of DNA. Topoisomerases are enzymes that break and join DNA strands to manage and control the topological state of mitochondrial [133] and genomic DNA [134]. All vertebrates express two isoforms, Top2 α and β , of type IIA topoisomerase. Human neoplastic tissues overexpress Top2 α ; therefore, this enzyme is an ideal target for chemotherapeutics [135]. Anthracyclines act by stabilizing the enzyme-DNA adduct in which DNA chains are cleaved and covalently linked to tyrosine residues of topoisomerase II [136]. Figure 1.7 illustrates the proposed catalytic cycle of type IIA topoisomerases [135] and the poisoning of this cycle by doxorubicin as an example for anthracyclines. In addition, the shown docking models present two calculated configurations of Top2-DNA-DOX ternary complexes, in which the broken DNA ends are kept physically apart so that strand resealing is blocked [137, 138].

Tumors form complex tissues encompassing tumor microenvironment and neovasculature, consisting of non-aberrant multiple distinct cell types such as bone marrow-derived vascular progenitor cells, endothelial cells, fibroblasts, myofibroblasts, mesenchymal stem cells, pericytes, and various types of immune cells [194]. The latter cells are often not able to induce a potent antitumor immune response, due to the presence of immunosuppression signals and the lack of suitable immunostimulatory signals. However, anthracyclines such as DOX and IDA can cause an immunogenic apoptosis of cancer cells. In contrast to physiological apoptosis, which is considered a non-immunogenic or even tolerogenic cell death pathway [139], this so-called immunogenic cell death (ICD) is accompanied by the emission of immunostimulatory damage-associated molecular patterns (DAMPs) [140]. Hence, the clinical efficacy of those anthracyclines is related not only to their intrinsic toxicity but also to their ability to induce ICD, which evokes a robust antitumor immune response [141].

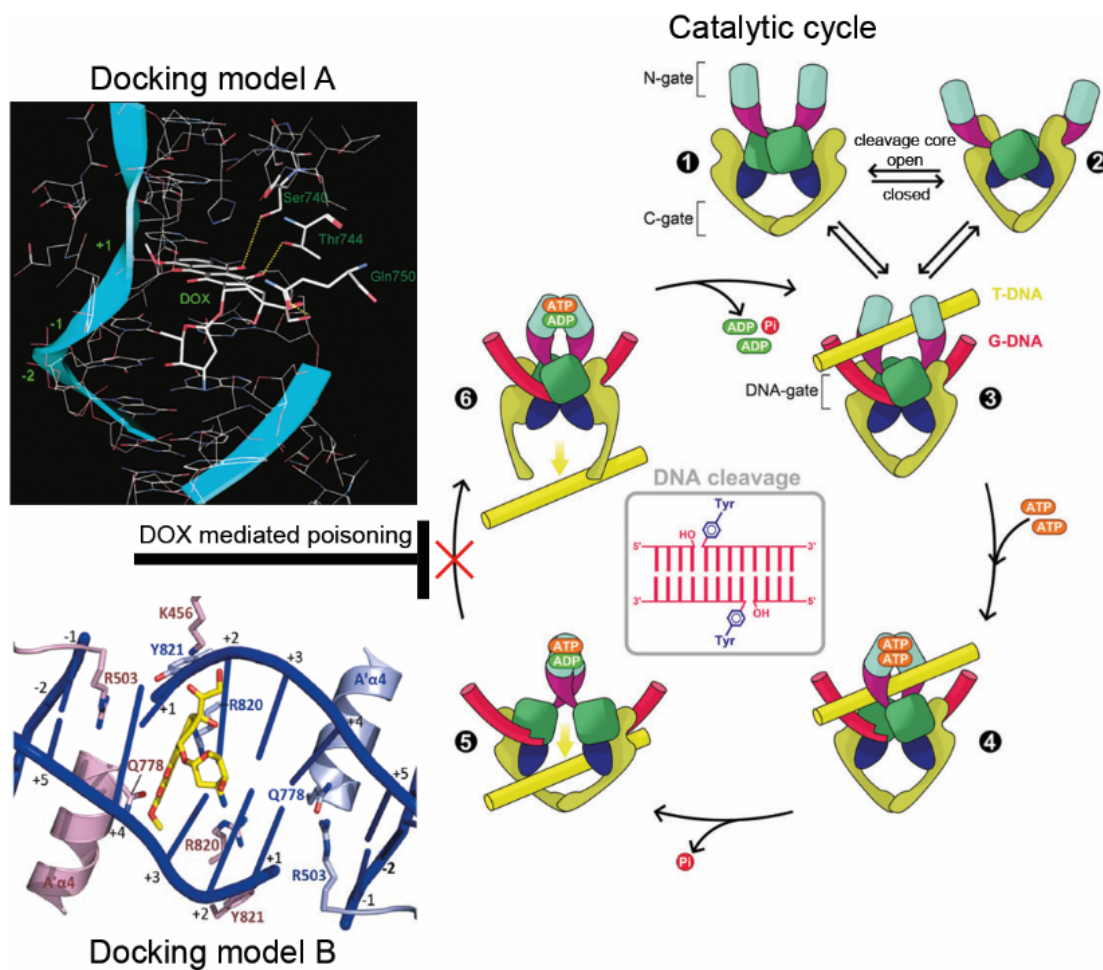


Fig. 1.7. Proposed catalytic cycle and poisoning of type IIA topoisomerases. Top2 enzymes are homodimers forming a molecular clamp at the N-terminal region (N-gate) that also contains ATPase domains. In addition, a DNA cleavage core is sandwiched between the N-terminal domains and a C-gate at the C-terminal region. **State 1 and 2:** N-gate is open and the DNA cleavage core (blue and green domains) is in equilibrium between open and closed form. **State 3:** Upon binding of a duplex DNA G-segment (gate) by the cleavage core, the two ATPase domains undergo a conformational change that partly closes the N-gate. In this state, the N-gate is enabled to capture a duplex DNA T-segment (transport). **State 4:** Upon binding of two ATP-molecules, the N-gate closes, thereby entrapping the T-segment and triggering the unlocking of the DNA-gate by generating a double-strand break with 4-base pair overhangs within the G-segment (center figure and docking model B). Each strand end is covalently bound to the active site tyrosine residue located within a WHD domain (green). **State 5:** Transport of T-segment from N-gate through opened DNA-gate to the C-gate is facilitated by hydrolysis of one of the bound ATP-molecules. **State 6:** Upon closure of the DNA-gate, the cleaved G-segment is religated again. This induces the opening of the C-gate, the release of the T-segment and resetting of the enzyme.

Progression to state 6 is inhibited by intercalation of anthracyclines into the DNA of the already cut G-segment. Docking model A (yeast Top2) and B (human Top2 β) show two possible intercalation sites for a doxorubicin molecule. Docking model A: Blue ribbons highlight the backbones of DNA strands. The DNA break is located between +1 and -1 nucleotide. Yellow lines indicate hydrogen bonds between DOX and amino acid residues of one WHD domain. Adopted with permission from ^[137]. Copyright 2004 American Chemical Society. Docking model B: Only one DOX molecule is located within the cleavage core. Adopted with permission from ^[138]. Copyright 2013 Nucleic Acids Research. Catalytic cycle: Adopted with permission from ^[135]. Copyright 2013 Annual Reviews.

In addition to adverse effects that are usually common to all chemotherapeutics such as gastrointestinal toxicity, myelosuppression, and alopecia, cumulative dose-dependent chronic cardiomyopathy occasionally followed by congestive heart failure also limits the clinical use of anthracyclines^[132]. Recently, Zhang *et al.* suggested that type IIA topoisomerase Top2 β is the key mediator for doxorubicin-induced cardiotoxicity^[142]. The search for novel anthracyclines with improved therapeutic indexes, particularly with regard to cardiotoxicity, resulted in a vast number of analogs. However, only few of them have attained clinical approval. Among them, epirubicin and idarubicin are useful alternatives to doxorubicin or daunorubicin, respectively^[125].

1.4.1.2 Idarubicin

In this thesis, the second-generation semisynthetic anthracycline idarubicin (IDA) was used as drug payload for carrier cells, because of its improved therapeutic index and high lipophilicity. Mandruzzato and colleagues compared doxorubicin and 4'-deoxy-4'-iododoxorubicin (IDX) in the context of LAK cell-mediated drug delivery^[81]. DOX-loaded LAK cells did not affect the growth of lung metastases compared to untreated mice. However, treatment with IDX-loaded LAK cells lead to a significant reduction of metastases. The authors attributed the difference in treatment outcome to the higher lipophilicity of IDX compared to DOX, which could have facilitated a more effective drug transfer from carrier cells to tumor cells. IDA was first purified in 1976^[143] and is a structural analog of daunorubicin but lacks the 4-methoxy group in ring D (Fig. 1.6). This modification alters IDA to a much more lipophilic compound compared to doxorubicin, epirubicin (EPI) and daunorubicin^[144]. Thus, like IDX the use of IDA could be advantageous for cell-mediated drug transfer.

In contrast to DAU, which is mainly used for the treatment of acute lymphoblastic or myeloblastic leukemia, IDA is given to patients suffering from acute myelogenous leukemia, multiple myeloma, non-Hodgkin's lymphoma, and breast cancer^[125, 145]. The wider antineoplastic activity of IDA is probably also due to the increased lipophilicity leading to enhanced cellular internalization and improved stabilization of the ternary topoisomerase II α -DNA-IDA complex^[125]. Furthermore, idarubicin exhibits greater cytotoxicity than DAU, DOX, and EPI against tumor cells *in vitro*^[146]. In addition, IDA is more effective than DOX and DAU in killing tumor cells showing a multidrug resistance phenotype. This is important to note, because the clinical utility of anthracyclines can be limited due to evolving chemoresistant tumor cell populations^[147]. Conversion of keto-anthracyclines, such as DAU, DOX, and EPI to their 13-hydroxy metabolites via

carbonyl-reducing enzymes is regarded as a drug-inactivation pathway. Indeed, the corresponding alcohol metabolites daunorubicinol, doxorubicinol, and epirubicinol exhibit relatively lower anticancer activity. However, even after carbonyl-reducing the principal circulating metabolite of IDA, idarubicinol (IDOL), is still as cytotoxic as the parent drug. Furthermore, IDOL shows a high plasma concentration and a long *in vivo* half-life. Therefore, in contrast to alcohol metabolites of other anthracycline, IDOL contributes to the clinical efficacy of the parent drug ^[146-148]. Idarubicin is more hematotoxic than doxorubicin ^[149]. However, it is considered less cardiotoxic than other anthracyclines ^[150].

Encapsulation of anthracyclines into liposomes has been proven to be a successful strategy to reduce the cardiotoxicity of these compounds due to altered tissue distribution and pharmacokinetics ^[151]. Another option to minimize adverse effects is a targeted approach in which the drug is selectively transported to the disease site. T cell-based drug delivery could be such an approach.

1.4.2 Photodynamic therapy

Photodynamic therapy (PDT) is typically a minimally invasive therapeutic modality ^[152], although intraoperative PDT can have a heavy impact on patients ^[153]. PDT requires the simultaneous presence of three components at the disease site: molecular oxygen, an either topically or systemically administered photosensitizer (PS), and light of a specific wavelength matched to an absorbance peak of the respective PS ^[152]. It is important to note, that none of these components are in general cytotoxic.

As referenced by several reviews ^[152, 154, 155], German medical student Oscar Raab discovered PDT in 1900 by demonstrating the cytotoxic effect of the combination of light and the PS acridine orange on infusoria, a mixture of aquatic microorganisms ^[156]. Since then, PDT has been applied in areas as diverse as cardiology ^[157, 158], cosmetics ^[159], dentistry ^[160], dermatology ^[161], and ophthalmology ^[162, 163]. Moreover, PDT shows potential for antibacterial, antifungal, antiprotozoal, and antiviral medical treatments ^[164]. Notably, PDT is a clinically approved therapeutic modality successfully used for the treatment of neoplastic diseases ^[165]. For the first time, photodynamic therapy was approved by the Canadian health agency for the prophylactic treatment of bladder cancer, using porfimer sodium (Photofrin) as a PS in 1993 ^[166]. Subsequently, worldwide approval for PDT was obtained to treat several types of neoplasm such as bile duct, bladder, brain, esophagus, lung, pancreatic, ophthalmic, ovarian, and skin cancer ^[165]. In addition, palliative photodynamic therapy of head and neck cancer was approved in Europe in 2001 ^[155].

Several advantages render photodynamic therapy as an attractive alternative for cancer treatment. PDT shows intrinsic dual selectivity based on the localization of the photosensitizer in the tumor tissue and on the light, which is directly focused on the malignant lesion. The required spatio-temporal presence of PS and light facilitates highly localized tissue damage and reduced off-target toxicities [167]. In addition, PDT does not lead to cumulative toxicity in patients like anthracyclines (see section 1.4.1.1), and in contrast to chemotherapy and radiation, there is no known maximum cumulative dose [168]. Therefore, PDT could be a modality to contain neoplastic diseases even if a complete cure is not achievable. However, tumor selectivity after systemic application of classical photosensitizers is limited and healthy tissues also accumulate PS [169]. The general distribution of PS leads to adverse effects, like prolonged eye and skin photosensitivity. To circumvent these obstacles, several tumor-targeting PDT strategies are under investigation [170]. The use of cellular vehicles to transport PS molecules directly to the target site, as evaluated in chapter 3 and 4 of this work, could be an option to reduce these adverse effects. As noted previously, oxygen is a major component of PDT. However, tumors often contain hypoxic regions. In addition, oxygen deficits can also arise if oxygen consumption during PDT occurs at a faster rate than oxygen replenishment. An option to counteract the lack of oxygen in tumors is the administration of carbogen and nicotinamide to patients, which can improve PDT-tumor response [171].

1.4.2.1 Basic Photochemistry

The cytotoxicity exhibited by photodynamic therapy is based on a photosensitizing process commencing with the absorption of a photon by the photosensitizer. Most organic molecules have an electronic singlet ground state, which is characterized by paired electrons being in an energetically most favorable molecular orbital (highest occupied molecular orbital, HOMO). Absorption promotes the PS from its electronic ground singlet state S_0 (1PS) to an excited electronic singlet state S_1 ($^1PS^*$) by transferring one of the paired electrons to an orbital of higher energy (lowest unoccupied molecular orbital, LUMO) (Fig. 1.8). The short-lived (nanoseconds) activated species usually relaxes back to the ground state. This deactivation process can occur by photon radiation and/or radiationless transformation of excitation energy into heat (internal conversion). De-excitation via a radiation pathway involving transitions of an electron between states of the same spin multiplicity (singlet-to-singlet or triplet-to-triplet transitions) is referred to as fluorescence. The excited singlet PS can also relax radiationlessly, accompanied by an electron spin con-

version, to a more stable excited electronic triplet state T_1 ($^3PS^*$) by the process known as intersystem crossing. In the triplet state, the PS has a lower energy, because the two electrons are now unpaired and have parallel spins. The triplet state of the excited photosensitizer is longer-lived ($>$ microseconds), because relaxation to the electronic ground state S_0 requires another spin conversion to be consistent with the Pauli exclusion principle. However, spin conversion is less probable and therefore electronic energy is “trapped” in the triplet state. As consequence of this, de-excitation from T_1 to S_0 by light emission, known as phosphorescence, is rather slow. Furthermore, the lifetime of this species is long enough to initiate photoreactions of type I (see next section). In addition, the excited triplet PS can decay radiationlessly via intersystem crossing. In the presence of molecular oxygen, transfer of electronic energy to an oxygen molecule mediated by bimolecular collision can accompany this transition. While the PS molecule is relaxing back to its electronic ground singlet state, the oxygen molecule is elevated from its ground triplet state T_0 (3O_2) to the first excited singlet state S_1 (1O_2). This species is known as singlet oxygen and its formation is referred to as a type II process [165, 172-175].

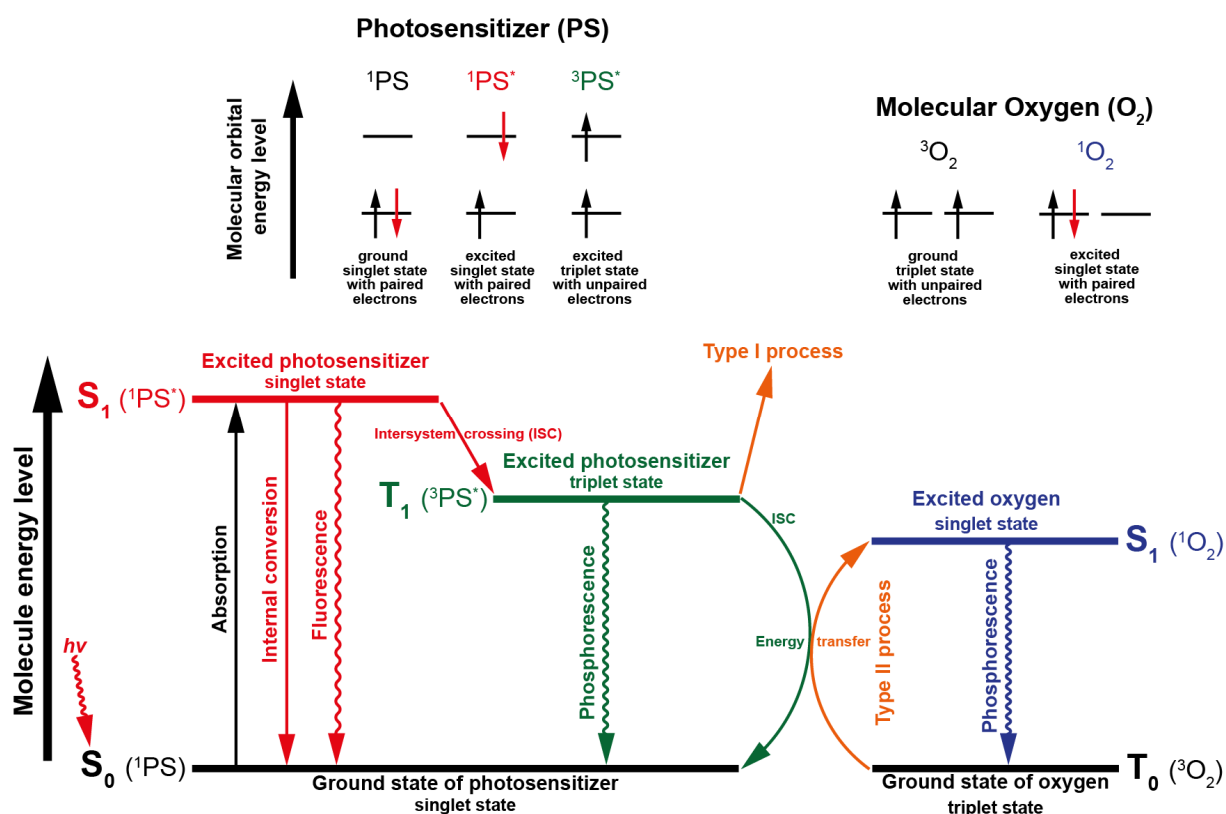


Fig. 1.8. Relevant valence electrons in molecular orbitals (upper panel) participating in electronic transitions illustrated in the simplified Jablonski diagram (lower panel) are shown. Vibrational and rotational energy levels of electronic states were omitted. Electronic transitions are described in the text.

1.4.2.2 Mechanisms of PDT-mediated cytotoxicity and tumor destruction

In biological systems like cells, type I processes are characterized by electron and hydrogen abstraction from biomolecules, located in the cellular microenvironment, by the excited triplet photosensitizer (Fig. 1.9) [165, 176]. Biomolecules usually participating in those reactions are NADPH, guanine in nucleic acids, and tryptophan and tyrosine in proteins [173]. Furthermore, type I processes generate reactive oxygen species (ROS) such as superoxide anion radicals ($O_2^{\cdot-}$), hydroxyl radicals (OH^{\cdot}), hydroperoxyl radicals (HO_2^{\cdot}), and hydrogen peroxide (H_2O_2) (Fig. 1.9), which in turn directly attack other biomolecules. Although singlet oxygen (1O_2), produced via the type II mechanism, is believed to be mainly responsible for the cytotoxic effects elicited by PDT, photosensitizers often induce reactions of both photochemical types [173].

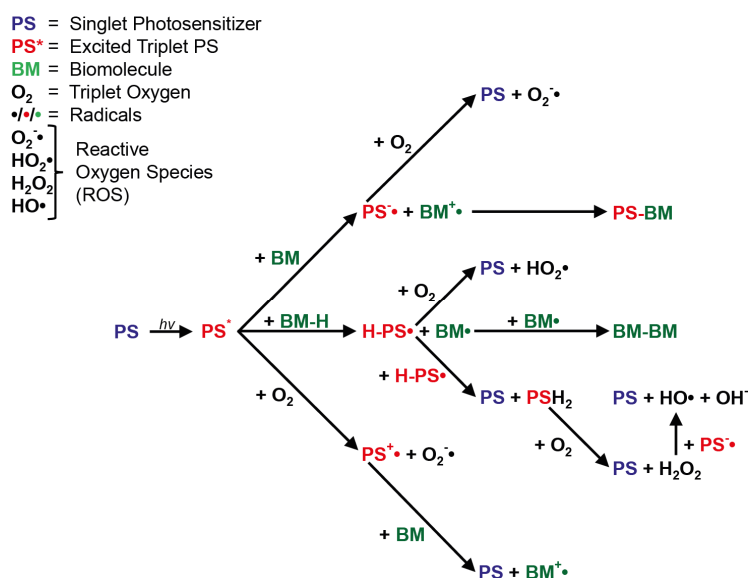


Fig. 1.9. Relevant type I reactions initiated by photon ($h\nu$) absorption of a PS elevating it to an excited triplet state PS^* . The activated PS can react with molecular triplet oxygen (O_2) and biomolecules. In some reactions PS is restored. Reactive oxygen species such as superoxide anion radicals ($O_2^{\cdot-}$), hydroxyl radicals (OH^{\cdot}), hydroperoxyl radicals (HO_2^{\cdot}), and hydrogen peroxide (H_2O_2) are also photogenerated and contribute to oxidatively-derived damage to cells.

Biomolecules such as proteins, lipids and nucleic acids are prone to oxidatively generated damage leading to cell death. Photo-induced modifications of proteins can cause unfolding, conformational changes, aggregation, fragmentation, and inactivation, which in turn lead to alteration of protein functions essential for cell signaling, redox homeostasis, and proteolytic pathways [177]. Lipid peroxidation mediated by photogenerated singlet oxygen and other ROS leads to lipid decomposition and gives rise to radicals, which initiate free-radical chain reactions resulting in lipid bilayer breakdown of biomembranes. Typical targets for lipid peroxidation are unsaturated fatty acids and glycolipids, phospholipids, and cholesterol [173, 176]. Oxidatively generated DNA damage in cells is characterized by single nucleobase lesions, single and double strand breaks, intrastrand base cross-links, DNA interstrand cross-links, DNA-protein cross-links, and nucleobase

adducts with lipid peroxidation breakdown products ^[178]. DNA insults caused by PDT can be genotoxic and mutagenic ^[168]. However, there is no data available yet, which show that PDT directly induces cancerogenesis *in vivo*. Hence, several authors consider the risk that PDT can give rise to secondary tumors as low ^[166, 168, 173].

Three distinct processes, elicited by PDT-derived oxidatively generated damage, have been recognized to contribute to tumor destruction: 1) direct cellular damage, 2) indirectly through shut-down of tumor-associated vasculature, and 3) by initiating an immune response against cancer cells (Fig. 1.10A) ^[155]. Direct cellular damage can be further divided into three different cell death pathways: 1) apoptosis, 2) necrosis, and 3) autophagy-associated cell death ^[165]. The lifetime of ¹O₂ in a single life rat neuron or HeLa cell was determined to be approximately 3 μs ^[179]. Based on this result and on values for the intracellular oxygen diffusion coefficient, it was estimated that the spatial domain of ¹O₂ reactivity within HeLa cells has a spherical radius of around 100 nm ^[180]. Therefore, the loci of subcellular damage due to PDT is determined mainly by the localization of the respective PS. *In vitro* data suggest that photosensitizers accumulating in mitochondria induce apoptosis while those targeting the plasma membrane are more likely to mediate necrosis. However, tumor destruction *in vivo* is expected to result from a mixture of apoptotic and necrotic cell death ^[181]. Autophagy promotes cell survival at low levels of photodamage. Yet, it can become a cell-death pathway, when cells attempt to recycle damaged biomolecules and organelles beyond their capacity for recovery. Furthermore, in cells with compromised apoptosis, autophagy is probably responsible for cell death. However, the exact role of autophagy in PDT-mediated cell death has still to be elucidated ^[182, 183]. Damage to tumor-associated vasculature can provoke thrombosis and hemorrhage in tumor blood vessels. As consequence of the ischemic condition, tumor cell death occurs because of lack of oxygen (hypoxia) and nutrients, which facilitates long-term tumor control ^[184, 185]. Like anthracycline-based chemotherapy, photodynamic therapy can act as an inducer of immunogenic cell death ^[186], which is accompanied by the release of immunostimulatory signals (see section 1.4.1.1). Accordingly, PDT can evoke an invasion of immune cells into the tumor tissue (Fig. 1.10B), which contributes to its destruction and enables the immune system to recognize malignant metastases ^[184, 187]. Several factors such as the nature of the applied photosensitizer, its localization within the neoplastic tissue during irradiation, the light exposure dose, the type of tumor, and the tumor microenvironment determine the relative contribution of each process to tumor eradication ^[155].

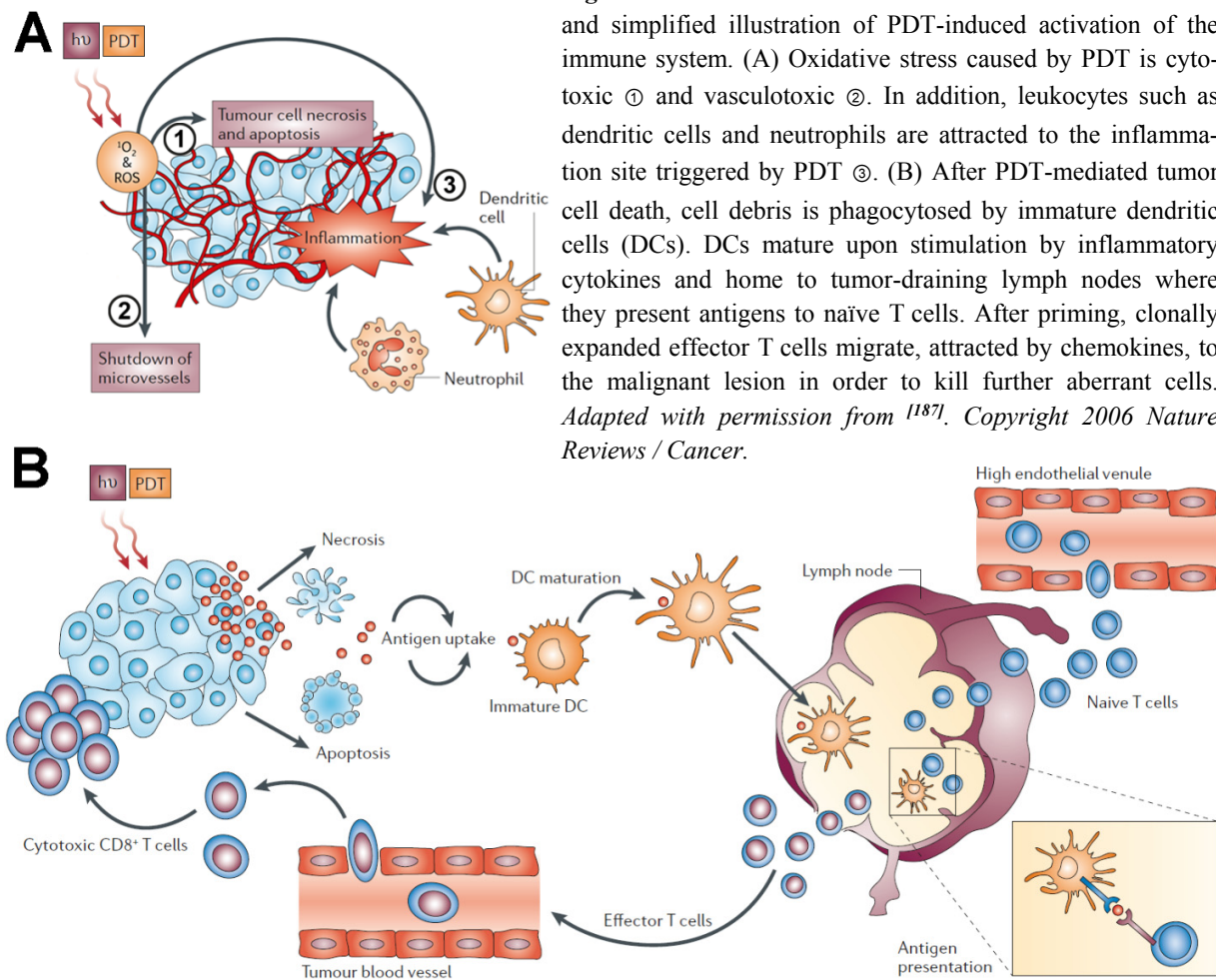


Fig. 1.10. Three modes of PDT-mediated tumor destruction and simplified illustration of PDT-induced activation of the immune system. (A) Oxidative stress caused by PDT is cytotoxic ① and vasculotoxic ②. In addition, leukocytes such as dendritic cells and neutrophils are attracted to the inflammation site triggered by PDT ③. (B) After PDT-mediated tumor cell death, cell debris is phagocytosed by immature dendritic cells (DCs). DCs mature upon stimulation by inflammatory cytokines and home to tumor-draining lymph nodes where they present antigens to naïve T cells. After priming, clonally expanded effector T cells migrate, attracted by chemokines, to the malignant lesion in order to kill further aberrant cells. Adapted with permission from ^[187]. Copyright 2006 Nature Reviews / Cancer.

1.4.2.3 Photosensitizers and PSS/mTHPP complex

Photosensitizing compounds can generally distinguished into porphyrins and non-porphyrins ^[188]. Well-known porphyrins are chlorophylls as well as the heme cofactors of hemoglobin, myoglobin, and cytochromes. Indeed, a mixture of photosensitizing molecules termed hematoporphyrin, later used in PDT, was isolated from hemoglobin by Scherer in 1841 ^[189]. Porphyrins are a class of heterocyclic macrocycle organic compounds, based on modified tetrapyrroles. In contrast, the class of non-porphyrin-based PS, encompassing amongst others hypericin, chalcogenopyrylium and phenothiazinium dyes, as well as cyanines, cannot be derived from a common parent chemical structure. Porphyrin-based PS are further subdivided into first, second, or third generation photosensitizers. Hematoporphyrin derivatives (HpD) such as the clinically approved Photofrin belong to first generation photosensitizers. However, drawbacks such as prolonged skin photosensitization and suboptimal tissue penetration led to the development of the next generation of

photosensitizers. Second generation PS such as clinically approved Foscan, Metvix or NPe6 absorb light of longer wavelengths (ensuring deeper tissue penetration ^[165]) and/or cause significantly less skin photosensitization compared with first generation PS. The ideal characteristics of a photosensitizer are shown in table 1.1. However, no clinically approved PS can be regarded as ideal so far. The search for agents fulfilling the chemical, physical and biological requirements of an optimal photosensitizer is the focus of current research. Candidates could be found among third generation photosensitizers, encompassing second generation PS, which are rendered more tumor tissue selective by conjugation to antibodies, liposomes, and nanoparticles ^[170, 188]. PS-loaded tumortropic cells, as investigated in this thesis, could meet some requirements, especially increased selectivity but reduced toxicity, for an ideal photosensitizer.

Table 1.1. Requirements for an ideal photosensitizer. *Adapted with permission from ^[188]. Copyright 2009 John Wiley & Sons, Inc.*

Activation	Significant absorption of wavelengths between 700 and 850 nm for maximum light penetration through tissue with minimum light scattering.
ADME	Optimal absorption, distribution, metabolism and excretion (ADME) properties for relevant indication.
Cost and availability	Inexpensive and commercially available in order to promote extensive utilization of treatment.
Mutagenicity/carcinogenicity	Neither mutagenic nor carcinogenic effects should result from the photosensitizer
Purity	Should be a single pure substance of known composition that is stable at room temperature.
Quantum yield	High single oxygen quantum yield for photochemical event, which is usually the production of singlet oxygen and other ROS.
Selectivity	Accumulation within tumor tissue is favorable.
Toxicity	Minimal toxicity in the absence of light and only cytotoxic in the presence of light of defined wavelengths. Photosensitizer should not yield toxic metabolites.

In this work, the porphyrin-based photosensitizer 5,10,15,20-tetrakis(3-hydroxyphenyl)porphyrin (mTHPP, Fig. 1.11) was used. mTHPP is the parent porphyrin of 5,10,15,20-tetrakis(3-hydroxyphenyl)chlorin (mTHPC, Fig. 1.11), which is a corresponding dihydroporphyrin ^[190]. mTHPC is the active pharmaceutical ingredient of Foscan, which is approved for the use in systemic cancer treatment. Foscan-PDT has been proven an effective measure in the treatment of cancer types related to chest, gastrointestinal tract, gynecological tissues, skin, and head and neck ^[153]. mTHPC appears to be one of the most potent photosensitizers. However, a major drawback of Foscan is still the prolonged skin photosensitivity that can last for several weeks post-treatment ^[188].

The reduction of one of the double bonds of tetrapyrrole (red oval in Fig. 1.11) causes a greater absorption of red light by mTHPC compared to mTHPP ^[191]. The molar extinction coefficients of mTHPP and mTHPC are $3400 \text{ M}^{-1} \times \text{cm}^{-1}$ at a wavelength of 644 nm and $29600 \text{ M}^{-1} \times \text{cm}^{-1}$ at a wavelength of 650 nm, respectively ^[190]. For PS with lower molar extinction coefficients a greater concentration of the PS or intensity of light are required to achieve adequate tumor eradication ^[188]. Therefore, red light-activated mTHPP is less cytotoxic than its derivative Foscan ^[192]. Nevertheless, the precursor has been frequently applied as model photosensitizer in basic research on photodynamic therapy (PDT) ^[153]. Likewise, a water-soluble formulation of mTHPP complexed with poly(styrene sulfonate) sodium salt (PSS) was used as a model in the present work, in order to evaluate whether polymeric photosensitizer preparations are suitable drug formulations for cell-mediated drug delivery (PSS/mTHPP, Fig. 1.11). mTHPP itself is practically insoluble in water. Originally, the negatively charged complex was designed as a layer material for a delivery system of water-insoluble drugs. PSS was chosen for its water solubility and its benzene rings that can interact with benzene rings of mTHPP. Reum and co-workers showed that within the complex one mTHPP molecule is noncovalently attached to around 11 monomer units of the polyelectrolyte PSS. Thus, the complexation efficiency is around 2 mTHPP molecules per polymer ^[193]. Noncovalent bonding is preferred in terms of drug efficiency and singlet oxygen quantum yield ^[194].

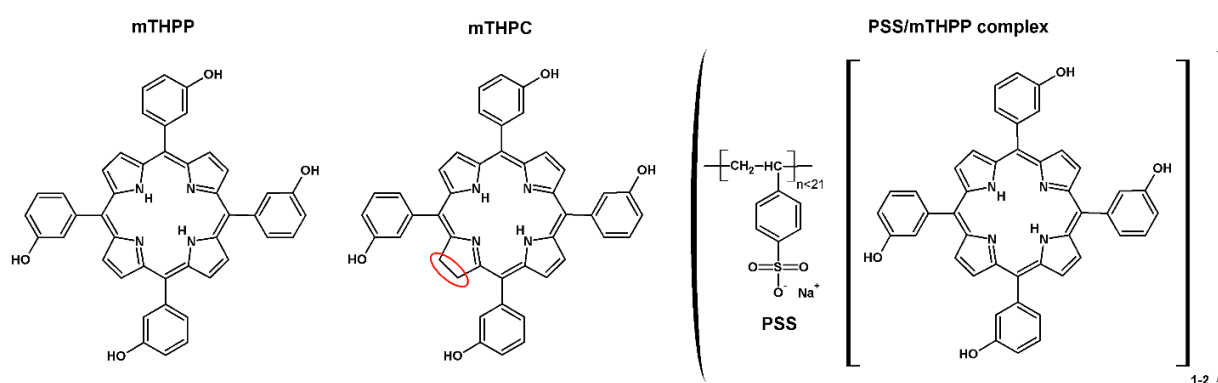


Fig. 1.11. Chemical structures of mTHPP, mTHPC (Foscan, Temopofrin), and PSS-complexed mTHPP. mTHPC is a derivative of mTHPP and lacks a double bond (red oval).

1.5 Aim of this thesis

One main objective of the thesis presented here was to identify anticancer drug formulations for human T lymphocyte-mediated drug delivery, which preserve loaded carrier cells from premature cell death. To this end, two different types of polymer-encapsulated therapeutics were investigated. The first approach pursued the idea of incorporation of an “active” drug into nanoparticulate systems in order to protect the living vehicles. In this regard, interactions between T cells and glycosylated polylysine polymers were studied in order to estimate which kind of polypeptide could be suitable as material for drug encapsulation (chapter 2). In addition, the protective effect on carrier cells of poly(lactic-*co*-glycolic-acid) nanoparticles (NPs), newly developed maleate-based polyester NPs and gold shell-coated polyester-based NPs, all enclosing the cytotoxic chemotherapeutic agent idarubicin, was examined (chapter 3). For the second approach, a “passive” drug represented by the photosensitizer 5,10,15,20-tetrakis (3-hydroxyphenyl)porphyrin (mTHPP) was used, the mode of action of which is only triggered by light irradiation (chapter 3 and 4). The tolerance of T lymphocytes for loading with a water-soluble formulation of this drug was tested. Classical pharmaceuticals applied in chemotherapy lack high specificity for tumor sites. The living cell-mediated drug deliver concept aims to improve the selectivity and efficacy of cancer treatment to reduce adverse effects by using tumor-specific T cells as transport vehicles. In the study presented here, tumor specificity was provided by bispecific antibodies, which cross-link T cells and cancer cells thereby triggering cytotoxic effector T cells to kill target cells. The T cell-based drug delivery approach aims to combine the cytotoxicity of cell-delivered pharmaceuticals with the cell-mediated cytotoxicity to improve the curative potential of adoptive cell therapy. Hence, the second main objective of this thesis was to prove the feasibility of this concept *in vitro*. Particularly, the question of whether this combination is synergistic or additive was addressed.

Within the scope of the presented thesis the following research questions were investigated:

1) What requirements do glycosylated polylysine polymers fulfill to be a potential material for drug encapsulation in T cell-mediated drug delivery?

The purpose of the encapsulation material is to protect the carrier cells against the toxicity of the drug. Therefore, it was tested whether the polylysine polymers are themselves toxic

for T lymphocytes. Furthermore, polymers were conjugated with sugar-based ligands. Therefore, it was tested whether these ligands facilitate the uptake of glycosylated polylysine polymers by T cells.

2) What formulations facilitates drug uptake by T cells?

The prerequisite for cell-based drug delivery is that the “Trojan horse” (the carrier) take up “greek soldiers” (drug molecules). Therefore, internalization of therapeutics by T lymphocytes was monitored.

3) To what extent do drug formulations harm the living vehicles?

Polyester-encapsulated idarubicin and complexed mTHPP must not harm loaded T cells to prevent impairment of physiological functions. Hence, the effect of the payload (associated materials and pharmaceuticals) on cell viability and cytolytic activity was studied.

4) Are pharmaceuticals released from carrier cells and transferred to target cells?

For the T cell-based drug delivery approach to function is it mandatory that the therapeutics are released or transferred to the target cells, where they can exhibit their cytotoxic potential. This question was tackled by tracking drug uptake by target cells over time.

5) Is the amount of released/transferred drug sufficient to kill tumor cells?

Drug delivery by loaded carrier cells is only feasible, when the anticancer drug is not trapped within the vehicles. To elucidate this question the viability of target cells was determined after the challenge with drug loaded T lymphocytes.

6) Is the combination of drug and cell cytotoxicity additive or synergistic *in vitro*?

This was the most important question addressed in this thesis. In case the use of loaded T cells would only achieve an additive killing effect, the loading process would not be needed. It would have the same effect as the administration of the free drug formulation in combination with empty bsAb-retargeted T cells. Consequently, the T cell-mediated drug delivery approach would presumably be unfeasible.

1.6 Statement of contributions

Chapter 2, 3, and 4 of this thesis contain parts, which were published in scientific journals. Section 1.5 explains, how each chapter is related to each other. The results described in each chapter are discussed and brought into context in chapter 5.

In the following, the author of the thesis state his contributions to these chapters.

Parts of chapter 2 were published in:

Stöhr T., **Blaudszun A.-R.**, Steinfeld U. and Wenz G.

Synthesis of glycosylated peptides by NCA polymerization for recognition of human T-cells.

Polymer Chemistry; 2011, 2: 2239-48

The second author contributed the following points to the chapter:

- Design, performance, and interpretation of all shown experiments.
- Writing of the chapter.

T. Stöhr provided the glycosylated peptides.

Parts of chapter 3 were published in:

Blaudszun A.-R., Lian Q., Schnabel M., Loretz B., Steinfeld U., Lee H.-H., Wenz G., Lehr C.-M., Schneider M., Philippi A.

Polyester-idarubicin nanoparticles and a polymer-photosensitizer complex as potential drug formulations for cell-mediated drug delivery.

International Journal of Pharmaceutics; 2014, 474: 70-79

The first author contributed the following points to the chapter:

- Design, performance, and interpretation of all shown experiments except generation and characterization of nanoparticles as well as synthesis and characterization of poly(diethylene glycol-maleate-*co*-sebacate)ester (MPE).
- Writing of the chapter.

Q. Lian provided and characterized the nanoparticles.

M. Schnabel characterized MPE. M. Schneider provided PSS/mTHPP.

Parts of chapter 4 were published in:

Blaudszun A.-R., Moldenhauer G., Schneider M., Philippi A.

A photosensitizer delivered by bispecific antibody retargeted human T lymphocytes enhances cytotoxicity against carcinoma cells upon light irradiation

Journal of Controlled Release; 2015, 197: 58-68

The first author contributed the following points to the chapter:

- Design, performance, and interpretation of all shown experiments.
- Writing of the chapter.

G. Moldenhauer provided the bispecific antibody.

M. Schneider provided PSS/mTHPP.

2. Interactions of statistical glycosylated copolypeptides with human T lymphocytes

Parts of this chapter were published in:

Stöhr T., **Blaudszun A.-R.**, Steinfeld U. and Wenz G. (2011)

Synthesis of glycosylated peptides by NCA polymerization for recognition of human T-cells.

Polymer Chemistry; 2: 2239-48

2.1 Abstract

There is evidence to suggest that targeted drug delivery increases the efficacy of chemotherapies. A wide variety of nanoparticulate systems composed of different materials such as inorganic compounds, lipids and polymers as artificial drug vehicles are used in approaches to accumulate therapeutics at the disease site. However, the concept has limitations such as recognition of drug carriers by the immune system and removal from the host by phagocytic cells of the reticuloendothelial system before they can reach their target site. Given the diverse restrictions of classical drug delivery systems, alternative more efficient drug targeting strategies are being investigated. Among them, cell-mediated transport of therapeutics has emerged as a new drug delivery concept. In order to protect cellular drug carriers against highly toxic pharmaceuticals, encapsulation of active drugs into protective nanoparticles has been proposed.

We plan to use human T lymphocytes as carriers for anticancer therapeutics. In the present study, we investigated interactions of potential compounds for polymeric nanoparticulate systems with *ex vivo* activated human T cells. Tested compounds comprised neutral *O*-glycosylated polylysine derivatives with attached diethylene glycol chains. To target cells, carbohydrate ligands such as β -D-galactopyranose, β -D-glucopyranose and α -D-mannopyranose were bound to the backbone of these statistical copolypeptides. Indeed, human T lymphocytes specifically took up galactosylated and mannosylated peptides at 37 °C but not at 4 °C. In addition, T cell viability was preserved for polymer concentrations of up to 0.33 mg/mL. Therefore, glycosylated polylysine derivatives are potentially useful for selective staining of cells or targeted drug delivery.

2.2 Introduction

Targeted drug delivery has emerged as a therapeutic concept to increase the effectiveness and specificity of chemotherapies. Most approaches use artificial drug carriers such as liposomes, polymeric, metallic, viral and many other varieties of nanoparticles (NPs) or nanoparticulate systems to concentrate therapeutics at the pathological site. Often, these classical drug vehicles are functionalized with monoclonal antibodies (mAb), cell-specific ligands (e.g. folate or transferrin), peptides or aptamers to further enhance the targeting effect [195, 196]. Numerous studies have demonstrated the benefits of targeted drug delivery, but they also revealed serious limitations of this concept. These restrictions include the recognition of particulate drug carriers as “foreign” by the immune system and removal from the bloodstream by phagocytic cells of the reticuloendothelial system before they reach the target site. Therefore, comparably high drug doses are still required to bring therapeutically effective drug amounts to pathological sites. Consequently, the adverse effects of many targeted drug delivery approaches are still severe. Toxic effects of carrier materials, chemical instability and inadequate tissue distribution are further problems of various drug delivery systems [39].

Given the diverse limitations of classical drug delivery systems, alternative more efficient drug targeting strategies are being investigated. Cell-mediated transport of therapeutics has emerged as a new drug delivery concept (reviewed in [12, 42]). Several mammalian cell types, such as immune and stem cells, have a number of natural properties, which make them ideal candidates for the development of novel drug targeting strategies. Unlike many artificial drug carriers, defense and stem cells can actively trace and infiltrate diseased sites (homing ability) and migrate across impermeable barriers, such as the blood-brain or the blood-tumor barrier [42, 197, 198]. These intrinsic abilities can be utilized to transport pharmaceuticals specifically to the target site. Furthermore, various types of immune cells like cytotoxic T lymphocytes and natural killer cells or monocytes/macrophages and neutrophils possess a natural killing function such as cytotoxic [199] or phagocytic activity [200], respectively, that can additionally be exploited to fight diseases. The biocompatibility of cellular drug carriers and diminished drug immunogenicity represents a further advantage of cell-based drug delivery strategies [12].

We aim to use human T lymphocytes as tumortropic vehicles for antineoplastic therapeutics to fight malignancies. In studies pursuing a similar approach, cell-delivered drugs included ricin [82, 84] and a doxorubicin derivative [81]. The efficacy of those delivered drugs was clearly shown.

However, the emerging strategy also revealed a major drawback. Carrier cells loaded with highly toxic pharmaceuticals showed a rapid loss of physiological functions and a decline in cell viability. To preserve cellular drug carriers from toxic effects of delivered therapeutics, incorporation of active drugs in protective nanoparticles has been proposed ^[12]. Ideal encapsulation materials are non-toxic and biodegradable and do not alter the physiological functions of loaded cells. Moreover, they show high drug encapsulation efficiencies and allow sustained release of enclosed pharmaceuticals inside the carrier cells. Given that many natural and synthetic polymers meet these requirements ^[201, 202], polymeric nanoparticles have recently attracted the attention of research groups working on cell-mediated drug delivery ^[203, 204].

Recognition between different cells, between viruses and cells, and between tissues and cells is controlled by the cooperativity of rather weak ligand-receptor interactions. Among others, carbohydrates like glucose, mannose, galactose, and lactose as well as complex oligosaccharides are well-known ligands for biological receptors expressed on cell membranes ^[205, 206]. Binding interactions between carbohydrate ligands and receptor proteins are indeed highly specific, but generally rather weak compared to other biological interactions ^[207]. Therefore, molecular recognition between biological entities requires the interplay of more than one receptor-ligand interaction.

Cooperativity of binding can also be used in artificial systems to improve binding affinities. In the so-called “multivalency approach,” many ligands are connected to an inert polymer backbone to reach manifold binding ^[208]. Therefore, many carbohydrate ligands have been attached to polymers ^[209, 210], carbon nanotubes ^[211], and cyclic scaffolds, e.g., cyclodextrins ^[212-214] or spherical molecules such as dendrimers ^[215]. The resulting so-called “glycoclusters” or “neoglycoconjugates” indeed showed improved binding to multivalent receptors, e.g., lectins ^[216-219], *in vitro* and to cells *in vivo* ^[220], and are potentially useful for targeted delivery ^[221]. Despite the successes of the multivalency approach, some drawbacks still obstruct broad application. Firstly, glycoclusters are often not biodegradable because mostly synthetic scaffolds are used in their synthesis. Secondly, polymers and high molecular weight glycoclusters tend to bind non-specifically to biological surfaces, i.e., by Coulomb interactions between oppositely charged species.

In the present study, we investigated interactions of potential compounds for polymeric nanoparticles with *ex vivo* activated human T cells. Tested compounds comprised neutral *O*-glycosylated polylysine derivatives with attached diethylene glycol chains. Nanoparticulate systems based on a variety of polypeptides derivatives were already produced for drug delivery (reviewed in ^[32]). Polypeptides have hydrolysable bonds and are therefore biodegradable by proteolytic enzymes

(proteases) [32]. Thus, glycosylated polylysine polymers meet at least one requirement (biodegradation) for an ideal encapsulation material. The use of oligo(ethylene glycol) side chains minimizes unspecific binding to cell surfaces [221] and to biomolecules such as serum proteins applied in cell culture like bovine serum albumin (BSA) [223]. The α -helical synthetic polypeptides [224] were used as a backbone for attachment of carbohydrate ligands such as β -D-galactopyranose (galactose), β -D-glucopyranose (glucose) and α -D-mannopyranose (mannose). To analyse and visualize interactions with biological systems like cells, fluorescein isothiocyanate (FITC) was coupled to free ϵ -NH₂ groups of lysine repeating units as well (compare Figure 2.1).

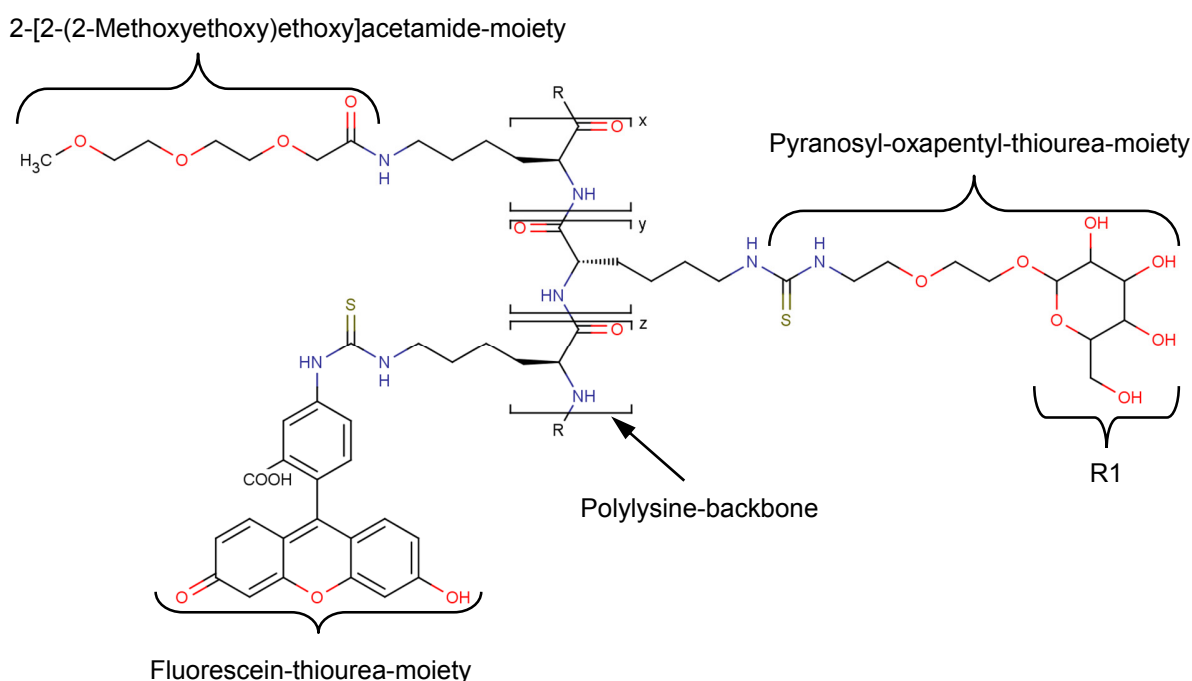


Figure 2.1. Chemical structure of the *O*-glycosylated (*y* units) polylysine derivative with attached fluorescein (*z* units) and diethylene glycol chain (*x* units). R = functionalized lysine repeating units, R1 = galactose, glucose or mannose.

T lymphocytes express a variety of glycoprotein-binding receptors on the cell surface such as L-selectin (CD62L) [225] which belongs to a subclass of the calcium-dependent (C-type) lectin family, galectins, a family of β -galactoside-binding lectins [226] and mannose-6-phosphate receptors (P-type lectins) [227, 228]. In addition, T cells express membrane transporters of the SLC2 (GLUT) family [229] which show affinity to saccharides such as galactose, glucose and mannose [230]. Thus, the introduced glycosylated polymers could be used to target T cells. To estimate which kind of glycosylated polylysine polymer could be suitable as material for drug encapsulating NPs, pre-

liminary studies to evaluate the cytotoxicity and binding/uptake capacity of polymers were performed. To this end, T cell viability after incubation with polymers, binding and internalization of glycopeptides were studied using an XTT based *in vitro* toxicology assay, flow cytometry and fluorescence microscopy, respectively. We demonstrate that T cell viability was preserved for polymer concentrations of up to 0.33 mg/mL. Furthermore, although all glycosylated polylysine derivatives were taken up by T lymphocytes, the preference for internalisation of particular polymers was clearly evident.

2.3 Materials and methods

Synthesis (section 2.3.1) of glycosylated peptides was not conducted by the author of this thesis.

2.3.1 Synthesis and handling of glycosylated peptides by *N*-carboxyanhydride polymerization

O-glycosylated polylysine (PL) polymers were synthesized as previously described [231]. In brief, peracetylated sugars (glucose, mannose and galactose) were attached via a thiourea linker to the 3-amino group of α -BOC-lysine and α -Z-lysine. After transformation to the *N*-carboxyanhydride (NCA), the product was copolymerized with both PEGylated lysine-NCA and ϵ -TFA-lysine-NCA by both tertiary amine and nickel complex catalysts. After deprotection fluorescein isothiocyanate (FITC) was coupled to the free ϵ -NH₂ groups of the lysine repeating units. The glucosylated polylysine (PL-Glu), the mannosylated polymer (PL-Man), and the galactosylated polymer (PL-Gal) as well as the unsubstituted polypeptide (PL) were dissolved in autoclaved purified water obtained from an Elix3 (UV) water purification system (Merck Millipore, Darmstadt, Germany) as stock solutions with a concentration of 2 mg/mL. Stock solutions were stored protected from light at -20 °C.

2.3.2 Fluorescence spectrometry of polymers

Thomas Stöhr (Organic Macromolecular Chemistry, Saarland University, Germany) kindly provided polypeptides PL-Gal, PL-Glu, PL-Man, and PL. These polymers were diluted in cell culture medium without phenol red (RPMI 1640 (PAN Biotech, Aidenbach, Germany) supplemented with 10% (v/v) heat-inactivated FBS (PAN Biotech), 100 U/mL penicillin and 0.1 mg/mL streptomycin (Sigma-Aldrich, Steinheim, Germany) (stock c(PL) = 20 μ g/mL, pH = 7.5). Fluoro-

rescence intensities of samples ($V = 100 \mu\text{L}$) at indicated concentrations were measured in a black 96-well microplate (Greiner Bio-One, Frickenhausen, Germany) with a Modulus Microplate Multimode Reader (Promega, Mannheim, Germany) at an excitation wavelength of 490 nm and emission wavelengths of 510-570 nm at 25 °C. Aliquots of 100 μL of pure cell culture medium served as blanks. Fluorescence intensities of blanks were subtracted from the intensities of polypeptides.

2.3.3 Isolation and activation of human T lymphocytes

Buffy coat blood of healthy donors was obtained from a local blood center (Blutspendezentrale Saar-Pfalz gGmbH, Saarbrücken, Germany) after informed consent according to the declaration of Helsinki. CD3⁺ T cells were enriched by using a RosetteSep Kit (StemCell Technologies, Grenoble, France) according to the manufacturer's instructions. Briefly, 0.5 mL RosetteSep antibody cocktail was added to 20 mL buffy coat blood and incubated at 25 °C for 20 min while gently shaking. Cells were isolated by centrifugation using a Pancoll human density gradient (PAN Biotech). Remaining erythrocytes were lysed with 2 mL of an ammonium chloride-based lysing buffer (BD Pharm Lyse, BD Biosciences, Heidelberg, Germany). Afterwards, enriched cells were resuspended in cell culture medium (supplemented RPMI 1640). Purity of isolated T lymphocytes was consistently higher than 90% when analyzed by flow cytometry (FACSCalibur, BD Biosciences) with antibodies against human CD3 (Bio-Rad AbD Serotec, Puchheim, Germany). Prior to experimental use, T lymphocytes were stimulated for at least 3 days using particles functionalized with antibodies against human CD2, CD3, and CD28 (MACS T Cell Activation/Expansion Kit, Miltenyi Biotec, Bergisch Gladbach, Germany). Expansion of T cells was achieved by adding 20 U/mL of recombinant human Interleukin-2 (IL-2, PAN Biotech), and fresh culture medium every 3 to 4 days.

2.3.4 *In vitro* toxicology assay

T lymphocytes were harvested from cultures and counted using an automated cell counter (CASY Model TT, OMNI Life Science, Bremen, Germany). Subsequently, cells were inoculated at a concentration of 2.5×10^5 cells/well in 100 μL fresh cell culture medium (supplemented RPMI 1640 without phenol red (PAN Biotech), containing 20 U/mL of IL-2) into 96-well microtiter plates. Triplicates of culture wells were subjected to 20 μL of stock solutions of polylysine PL-Man, PL-Glu, PL-Gal, and PL and incubated at 37 °C in a humidified atmosphere with 5% CO₂.

Likewise, negative control cells were treated with 20 μL of phosphate buffered saline (PBS, Life Technologies, Darmstadt, Germany). Additionally, triplicate blanks contained only culture medium with polypeptides or PBS. Prior to use, 5 mg of a mixture of 2,3-bis(2-methoxy-4-nitro-5-sulfophenyl)-5-[(phenylamino)carbonyl]-2H-tetrazolium hydroxide, XTT, and 1% phenazine methosulfate (PMS) (TOX-2, Sigma-Aldrich) were reconstituted with 5 mL of RPMI 1640 medium without phenol red. After 18, 42 and 66 h, 24 μL of XTT-PMS solution was applied to the cultures, which were further incubated for 6 h. Subsequently, samples were homogenized to completely disperse the XTT formazan. Finally, the absorbance was measured at 450 nm with a reference wavelength of 690 nm using an absorbance microplate reader (Spectra Rainbow Thermo, Tecan, Crailsheim, Germany). After subtracting blank values, all viability data obtained were normalized to the viability of the negative controls (PBS) which were set to 100%.

2.3.5 Flow cytometric analysis of polypeptide uptake by T lymphocytes

T cells were inoculated at a concentration of 5×10^5 cells per tube in 100 μL of fresh cell culture medium. Duplicates of T lymphocytes were subjected to 20 μg (10 μL of solution) of PL-Man, PL-Glu, PL-Gal and PL and incubated at 4 $^\circ\text{C}$ or 37 $^\circ\text{C}$ for 2, 4 or 8 h. Likewise, control cells were treated with 10 μL of PBS. Cells were washed twice with 1 mL of ice-cold PBS ($300 \times g$ and 4 $^\circ\text{C}$ for 10 min, centrifuge 5415 R, Eppendorf, Hamburg, Germany), resuspended in 500 μL of ice-cold PBS and kept on ice until analysis by flow cytometry. Fluorescence intensity of 10,000 events per sample was measured by using a FACSCalibur cytometer (BD Biosciences) and CellQuest Pro software (version 5.1.1, BD Biosciences). Fluorescence intensities of gated T cell populations are represented by histograms. Furthermore, geometric means (GMFI) calculated by CellQuest Pro for cells incubated with each polymer were normalized to the fluorescence intensities of the polymers determined at a concentration of 0.02 mg/mL using the following equation:

$$n\text{GMFI}_{\text{Pol}} = (\text{GMFI}_{\text{Pol}} - \text{GMFI}_{\text{Blank}}) \times \frac{\text{FI}_{\text{PL-Gal}}}{\text{FI}_{\text{Pol}}}$$

nGMFI_{Pol}: normalized GMFI of T cells incubated with the respective polymer

GMFI_{Pol}: GMFI of T cells incubated with the respective polymer

GMFI_{Blank}: GMFI of T lymphocytes

FI_{PL-Gal}: Fluorescence intensity of PL-Gal at 0.02 mg/mL

FI_{Pol}: Fluorescence intensity of the respective polymer at 0.02 mg/mL

2.3.5.1 Flow cytometric analysis of PL-Glu uptake by T cells in the absence of glucose

The culture medium used is supplemented with glucose as nutrient for cells (2 mg/mL according to data sheet provided by Pan Biotech). To verify whether medium related glucose is interfering with interactions between glucosylated polymers and T cells, the aforementioned experiment was performed using glucosylated polymers and a medium devoid of glucose (PBS containing 1% (v/v) BSA).

2.3.5.2 PL-Gal uptake by naïve/memory and activated T lymphocytes

Non-activated T cells consists of naïve and memory subsets (see section 1.1). However, in the following naïve and memory T cells are also referred to as non-activated T cells. We were interested in whether there is a difference between non-activated and activated T cells in binding/uptake of glycosylated polymers. Thus the previously described experiment was accordingly performed with freshly isolated non-activated T lymphocytes and galactosylated polylysine.

2.3.5.3 Inhibition of PL-Gal uptake with lactose

We also investigated whether PL-Gal uptake by T cells can be inhibited with β -D-galactopyranosyl-(1 \rightarrow 4)-D-glucose (lactose). To this end, lactose monohydrate (Carl Roth, Karlsruhe, Germany) was dissolved in PBS to produce a stock solution with a concentration of 120.11 mg/mL. T lymphocytes were inoculated at a concentration of 5×10^5 cells per tube in 90 μ L of cell culture medium. Duplicates of T cells were subjected to 90 μ L of lactose stock solution and incubated at 37 °C for 30 min. Likewise, control cells were treated with 90 μ L of PBS. Afterwards, 40 μ g (20 μ l of solution) was added and T cells were incubated at 37 °C for indicated periods (final concentration of lactose was then 0.15 mol/L). Finally, samples were processed as described in section 2.3.5.

2.3.6 Fluorescence microscopy of polypeptide treated T cells

For fluorescence microscopy, samples containing 2×10^6 T cells in 800 μ L of cell culture medium and 0.1 mg/mL of polypeptides were incubated protected from light at 4 °C or 37 °C for 6 h. Subsequently, T cells were washed twice with 1 mL of ice-cold PBS (300 \times g and 4 °C for 10 min, centrifuge 5415 R, Eppendorf, Germany). For fixation, sedimented cells were resuspended in 400 μ L of PBS containing 4% (w/v) formaldehyde (paraformaldehyde, Sigma-Aldrich) and

were incubated protected from light at 25 °C for 10 min. Afterwards, cells were washed twice with 1 mL of ice-cold PBS.

For experiments including cell membrane staining, samples containing 3×10^6 T cells resuspended in 1 mL of cell culture medium and 0.1 mg/mL of PL-Gal were incubated protected from light at 37 °C for 6 h. After washing, T lymphocytes were stained in serum-free culture medium containing 2.5 μ L/mL DiD (Vybrant cell-labeling solution (1 mM), Life Technologies) at 37 °C for 10 min. Afterwards, labeled cells were washed three times with warm cell culture medium ($300 \times g$ for 10 min, centrifuge 5415 D, Eppendorf, Germany) and were fixed as described above. Washing buffer was discarded and T cells were resuspended in 20 μ L of polyvinyl alcohol-based anti-fading mounting medium consisting of 25 mg/mL 1,4-diazabicyclo-[2,2,2]-octane (DABCO, Carl Roth), 9.1% (w/w) Mowiol 4-88 (Carl Roth), 22.7% (w/w) glycerol (Merck Millipore), 1 μ g/mL 4',6-diamidino-2-phenylindole dihydrochloride (DAPI, Sigma-Aldrich) and 0.1 M Tris-HCl pH 8.5 (Sigma-Aldrich). The mounting medium was allowed to harden overnight and kept protected from light at 4 °C. Fluorescence microscopy was performed using an IX71 inverted microscope (Olympus, Hamburg, Germany) equipped with U-MNU2, U-MWIBA2 and U-N41033 filters. DNA-intercalating DAPI was excited at wavelengths of 360-370 nm. Polypeptides were excited at wavelengths of 460-490 nm and DiD at wavelengths of 625-655 nm. Fluorescence, emitted by DAPI-DNA-complexes at wavelengths above 420 nm, by polypeptides at 515-550 nm or by DiD at 662.5-737.5 nm, was imaged through a 60 \times PlanApo N oil-immersion objective (Olympus) with a numerical aperture of 1.42 by a digital camera (F-View II, Olympus) attached to the microscope. Immersion oil Immersol 518N (Carl Zeiss Microscopy GmbH, Göttingen, Germany) was used. The camera was controlled by cell^P imaging software (version 2.8, Olympus). All images were digitalized using the same conditions (automatic gain disabled and fixed exposure times) to compare the fluorescence intensities of polypeptides, whereas the imaging of DAPI-stained cell nuclei and DiD-labeled cell membranes was automatically adjusted by cell^P (Olympus soft imaging solutions). Merged images were generated via cell^P imaging software.

2.4 Results

2.4.1 Fluorescence spectrometry of polypeptides

It was desirable to attach fluorescent labels, such as fluorescein, to the glycopolypeptides to allow the detection of any interaction with biological systems. As illustrated in Figure 2.2, all FITC-conjugated glycopolypeptides diluted in cell culture medium and the unsubstituted polypeptide exhibited a clear fluorescence signal at the greatest tested concentration.

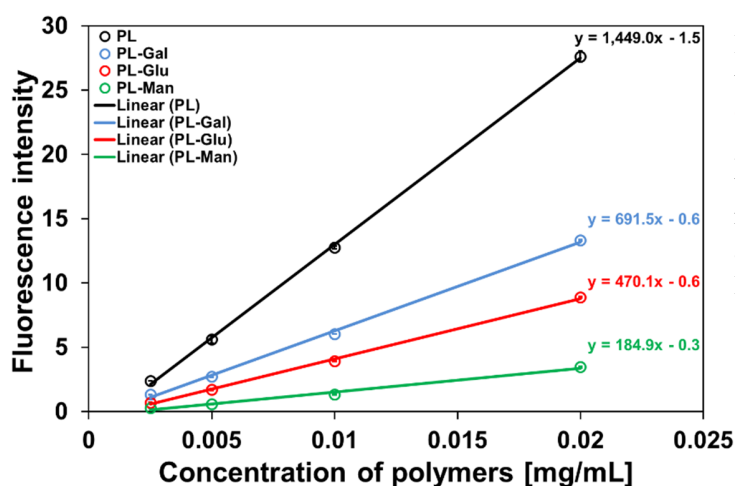


Figure 2.2. Fluorescence intensities in arbitrary units of glucosylated polylysine (**PL-Glu**), mannosylated polymer (**PL-Man**), galactosylated polymer (**PL-Gal**) as well as the unsubstituted polypeptide (**PL**). One representative experiment is shown. Results are expressed as means of duplicate samples. Error bars indicate standard deviations (SD).

Table 2.1. Fluorescence intensities (FI) of glycopolypeptides and the unsubstituted polymer at a concentration of 0.02 mg/mL

Polymer	PL	PL-Gal	PL-Glu	PL-Man
FI [arb. units]	27.6	13.3	8.9	3.5

The order of fluorescence intensity (PL > PL-Gal > PL-Glu > PL-Man) is consistent with the order of polypeptide absorbance at a wavelength of around 480 nm determined by Thomas Stöhr [224]. Accordingly, the unsubstituted polypeptide PL exhibiting the greatest absorbance also showed the greatest fluorescence intensity. Obviously, more fluorescein-molecules were attached to unsubstituted polypeptides than to mannosylated polymers. Possible reasons for different amounts of conjugated fluorochrome could be an initially different number of ϵ -TFA protected lysine units added to the terpolymerization (compare [224, 231]) and/or an uncompleted labeling process.

2.4.2 Analysis of T cell survival

In vitro toxicity of glucosylated polylysine (PL-Glu), mannosylated polymer (PL-Man), galactosylated polymer (PL-Gal) as well as the unsubstituted polypeptide (PL) was tested with *ex vivo* activated human T lymphocytes of two different donors using the XTT cell viability assay [232]. Fig. 2.3 clearly shows that cell viability remains preserved for polymer concentrations of up to 0.33 mg/mL. From these observations, we conclude that all tested polymers are sufficiently biocompatible.

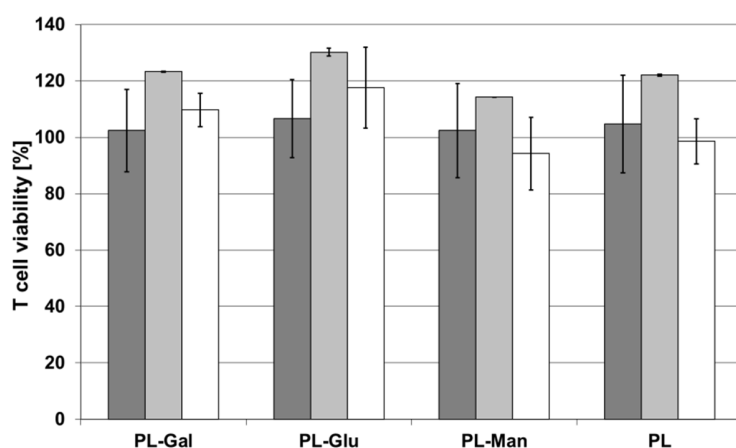


Figure 2.3. Viabilities of human T lymphocytes after ■ 24 h, ■ 48 h and □ 72 h of incubation with polylysine polymers ($c = 0.33$ mg/mL). Results are expressed as means of two independent experiments with 2 different donors ($n = 2$). Error bars indicate SD.

2.4.3 Flow cytometric analysis of polylysine polymer uptake by T cells

The interactions of polymers PL-Man, PL-Glu, PL-Gal as well as the unsubstituted polypeptide PL with *ex vivo* activated human T lymphocytes were investigated by flow cytometry (FCM). The fluorescence intensity distributions showed a pronounced shift to higher fluorescence intensities for the galactosylated polymer PL-Gal, especially for incubations at 37 °C as shown in Fig. 2.4D.

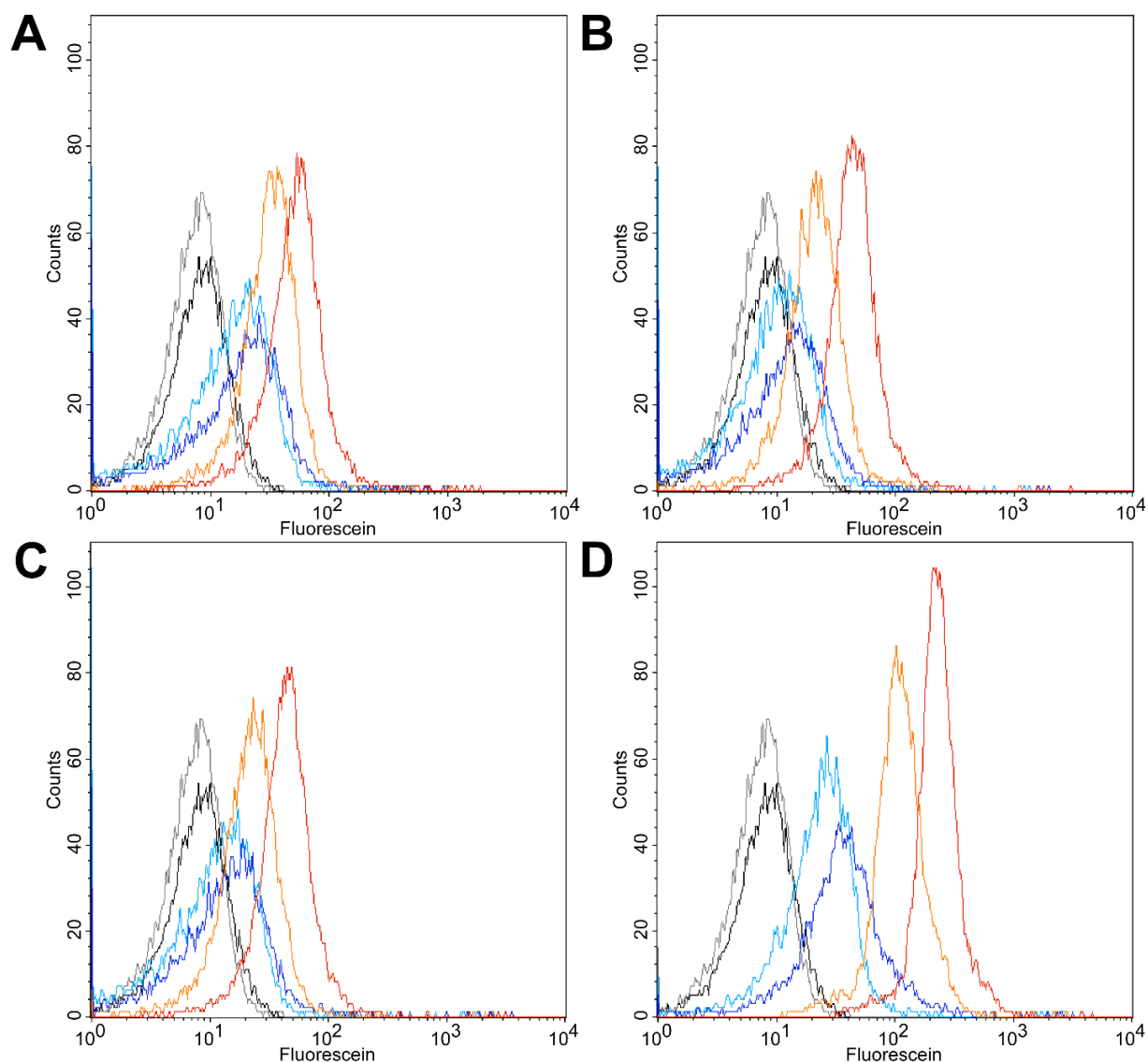


Figure 2.4. Fluorescence intensity distributions measured by FCM of T cell populations after incubation with polymers at 4 °C (—2 h, —8 h) and 37 °C (—2 h, —8 h) for (A) the unsubstituted polypeptide PL (B) the mannosylated polypeptide PL-Man (C) the glucosylated polymer PL-Glu, and (D) the galactosylated polylysine PL-Gal. As controls autofluorescence intensity distributions of T cells incubated at 4 °C (—8 h) and 37 °C (—8 h) are shown as well.

The uptake of each fluorescent polymers (Fig. 2.4) was quantified by calculating the geometric mean of fluorescence intensity (GMFI) over the cell populations. Moreover, these GMFI values were normalized to their respective fluorescence intensities taken from Table 2.1. While there was only little uptake of the fluorescent unsubstituted polymer PL and the glucose polymer PL-Glu, the mannose polymer PL-Man and the galactose polymer PL-Gal were readily taken up, especially at 37 °C (Fig. 2.5).

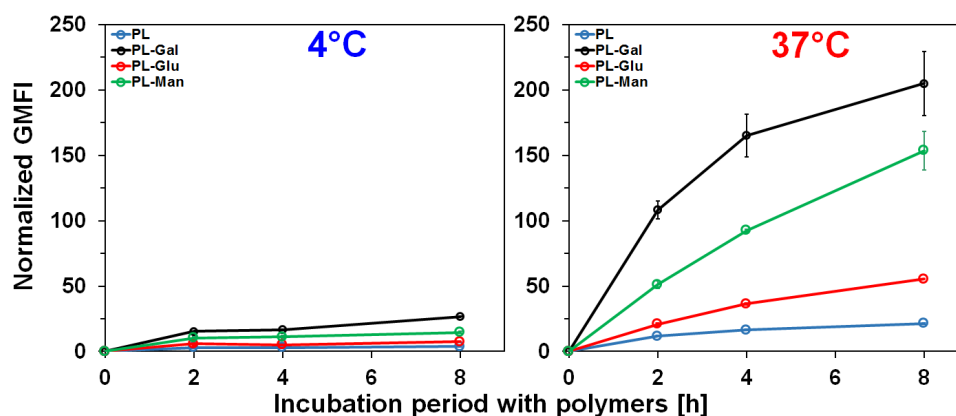


Figure 2.5. Uptake of the glycosylated polymers **PL-Gal**, **PL-Glu** and **PL-Man** and the unsubstituted polymer **PL** by T cells at 4 °C (left panel) and 37 °C (right panel), as determined from the geometric mean of FCM fluorescence intensities (GMFI), normalized to the fluorescence intensity of the respective polymer at a concentration of 0.02 mg/mL. One representative experiment is shown. Results are expressed as means of duplicate samples. Error bars indicate SD.

2.4.3.1 Flow cytometric analysis of PL-Glu uptake by T cells in the absence of glucose

Given that cell culture medium (supplemented RPMI 1640) in which interaction experiments were performed contained glucose as supplement (2 mg/mL according to data sheet provided by Pan Biotech), we verified whether medium related glucose interferes with the interaction between glycosylated polymers and T cells. To this end, T lymphocytes were incubated with PL-Glu in medium devoid of glucose (PBS + 1% BSA) at 4 °C and 37 °C for indicated periods of time. Interestingly, incubation in BSA supplemented phosphate buffered saline decreased uptake of PL-Glu by T cells as shown in Fig. 2.6. Obviously, the selected glucose free-medium was not suitable to answer the question whether medium related glucose impairs interactions between T cells and glycosylated polylysine.

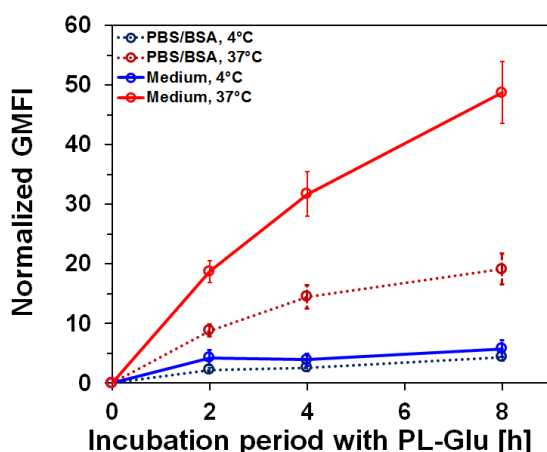


Figure 2.6. Uptake of the glycosylated polymer PL-Glu by T cells at 4 °C and 37 °C, as determined from the geometric mean of FCM fluorescence intensities (GMFI), normalized to the fluorescence of PL-Glu at 0.02 mg/mL. T lymphocytes were incubated with PL-Glu either in cell culture medium or in PBS containing 1% BSA. Results are expressed as means of two different experiments conducted with two different donors (n = 2). Error bars indicate SD.

2.4.3.2 PL-Gal uptake by non-activated and activated T lymphocytes

Upon activation of T cells, the expression of several cell-surface molecules, associated with activation, co-stimulation, and adhesion, changes [233]. In addition, T lymphocytes start to proliferate rapidly (clonal expansion) which requires an upregulating of metabolic pathways to provide the needed energy [234, 235]. This is accompanied by an increased expression of GLUT1 sugar transporters [236]. Accordingly, the transition from non-activated cell phenotype to activated cell phenotype could change the amount and specificity of binding-motifs for glycosylated polymers on the cell-surface. To gather preliminary information about the nature of those binding motifs, we investigated whether there is a difference between both states of T cells in binding/uptake of glycosylated polymers. To this end, non-activated and activated T lymphocytes were incubated with PL-Gal at 4 °C and 37 °C for the indicated periods of time. PL-Gal was chosen, because this glycosylated polylysine yielded the greatest GMFI values (Fig. 2.5).

As illustrated in Fig. 2.7, all GMFI values of activated T cell populations are greater than the values obtained from non-activated populations after incubation with PL-Gal. Interestingly, even activated T lymphocytes, which had been incubated at 4 °C, showed a greater fluorescence intensity than non-activated T cells. We conclude that *ex vivo* activation of T lymphocytes could possibly induce the expression of binding motifs for galactosylated polymers.

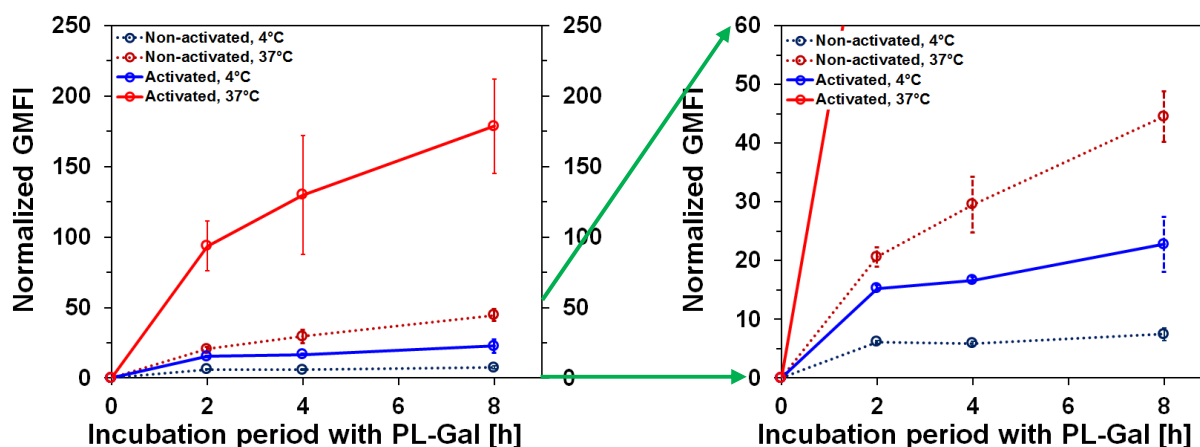


Figure 2.7. Uptake of the galactosylated polymer PL-Gal by non-activated or activated T cells at 4 °C and 37 °C, as determined from the geometric mean of FCM fluorescence intensities (GMFI), normalized by the fluorescence of PL-Gal. The diagram shown in the right panel represents a magnified version of the diagram shown in the left panel. Results are expressed as means of two different experiments conducted with two different donors (n = 2). Error bars indicate SD.

2.4.3.3 Inhibition of PL-Gal uptake with lactose

We also tried to impair the uptake of PL-Gal by T cells with β -D-galactopyranosyl-(1 \rightarrow 4)-D-glucose (lactose). Lactose (lac) was chosen because it contains a galactopyranose ring like PL-Gal (compare Fig. 2.1). As representatively shown in Fig. 2.8, the results are inconclusive. Control T cells, which had been incubated only with lactose, showed the usual autofluorescence. As expected, the longer the incubation period lasted the greater was the fluorescence intensity of cell populations treated with PL-Gal. However, there was no significant difference in GMFI values when lactose treated T cells were incubated with PL-Gal. In conclusion, under the chosen experimental conditions lactose did not inhibit uptake of the galactosylated polymer.

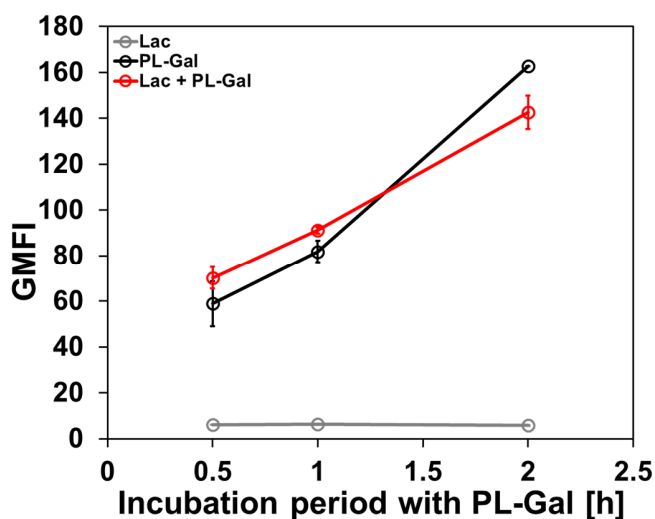


Figure 2.8. Uptake of the galactosylated polymer PL-Gal by activated T cells after treatment with 0.15 M lactose at 37 °C. Results are expressed as means of two samples derived from one donor (n = 1). Error bars indicate SD.

2.4.4 Fluorescence microscopy of polypeptide treated T lymphocytes

Fluorescence microscopy studies of T cells incubated with solutions ($c = 0.1$ mg/mL) of polymers PL as well as PL-Gal for 6 h, shown in Figure 2.9A, demonstrated that the galactosylated polymer exhibited significant interactions with *ex vivo* activated T lymphocytes. Almost all cells exhibited the green fluorescence of fluorescein. Furthermore, Figure 2.9B suggests that the PL-Gal is not only adsorbed at cell walls, but is also internalized by T cells. Merged fluorescence images clearly show that green fluorescent cell compartments are encircled by red stained cell membranes. Hence, the sites of green fluorescence emission were mainly located within T cells.

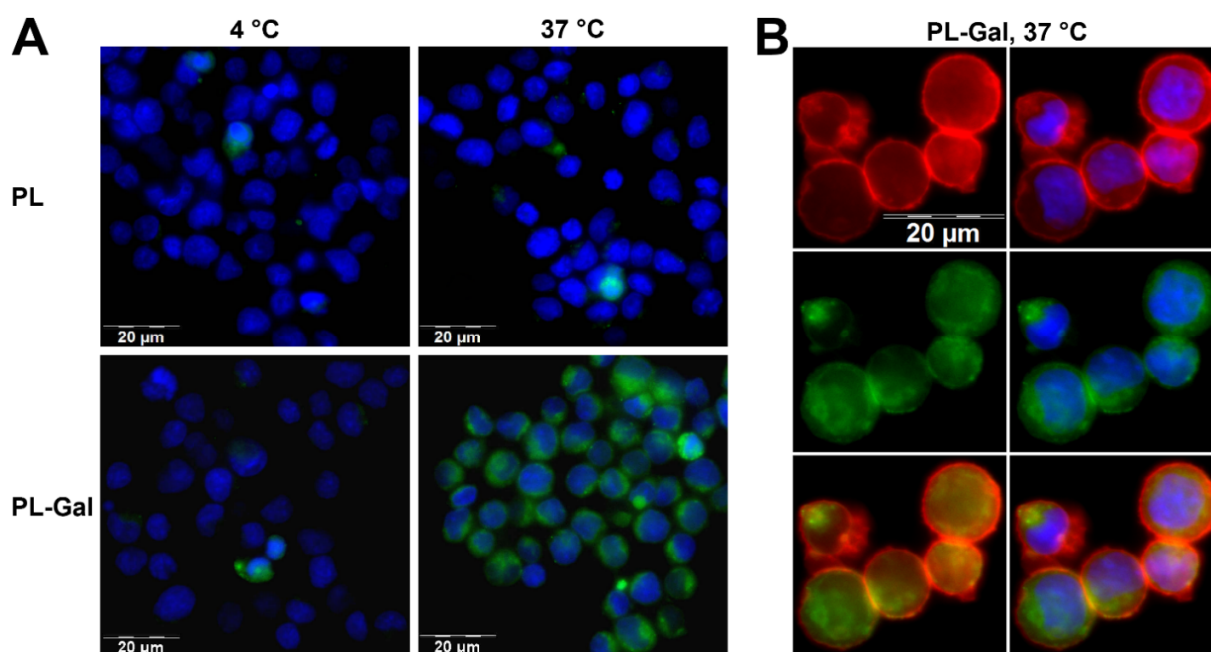


Fig. 2.9. Imaging of T lymphocytes by fluorescence microscopy. (A) After 6 h of incubation at 4 °C (left panels) and 37 °C (right panels) with unsubstituted polypeptide PL (upper panels) and galactosylated polymer PL-Gal (lower panels). Blue fluorescent cell nuclei were stained with DAPI before. The green color represents the emission of fluorescein, attached to the polymers. (B) Cell membranes were detected using DiD (red fluorescence). Galactosylated polypeptides are located within T cells as shown in the merged image (lower left panel) composed of the green (middle left panel) and the red fluorescence picture (upper left panel). Locations of blue stained cell nuclei are illustrated in right hand panels.

2.5 Discussion

We aim to use human T cells as carriers for antineoplastic drugs to fight cancer. To prevent premature death of cellular carriers due to toxic effects of delivered therapeutics, encapsulation of active drugs into protective nanoparticles has been suggested ^[12]. The purpose of the present work was to investigate the interactions between *ex vivo* activated T lymphocytes and neutral *O*-glycosylated polylysine derivatives that could serve as potential compounds for polymeric nanoparticulate systems. Non-toxicity and biodegradability are among the requirements for optimal encapsulation materials. Here, we demonstrated that polymer concentrations of up to 0.33 mg/mL did not impair T cell viability. In addition, glycosylated polylysine derivatives are biodegradable by hydrolytic processes occurring within cells (e.g. hydrolysis mediated by proteolytic enzymes) ^[32]. Hence, the tested polymers meet at least some requirements for an ideal encapsulation material.

Moreover, polylysine derivatives were functionalized with monosaccharides such as galactose, glucose and mannose to target binding-motifs on cell-surfaces. Indeed, we have shown that all glycosylated polymers were internalized to a greater extent than the non-glycosylated polylysine by T lymphocytes. However, the preference for uptake of particular polymers was evident. While there was only limited uptake of the fluorescent unsubstituted polymer PL and a slightly increased uptake of the glucose polymer PL-Glu, the mannose polymer PL-Man and the galactose polymer PL-Gal were readily internalized, especially at 37 °C.

Interestingly, we have demonstrated that populations of activated T cells are more intensely fluorescent than populations of naïve/memory T lymphocytes after incubation with PL-Gal at 4 °C or at 37 °C. At 4 °C galactosylated polymers have presumably only bound cell membranes, since endocytosis is an energy-dependent process and inhibited at low temperatures [237]. However, non-activated T cells are smaller than activated T lymphocytes (see Supplementary Information, Fig. S2.1). Consequently, the cell surface of activated cells is larger than the surface of non-activated cells. Therefore, activated T cells could bind more PL-Gal than naïve/memory T cells, which could explain the slightly increased fluorescent GMFI value of activated cell populations determined by flow cytometry at 4 °C. Upon activation, metabolism of T cells is upregulated to fuel bioenergetic demands for clonal expansion and differentiation into effector cells [235]. Upregulating is reflected in the increased reduction of tetrazolium salts, because energy metabolism is generally considered to correlate with the conversion of tetrazolium salts to formazans by cells [238]. Indeed, the bioreductive activity of non-activated T cells determined by a colorimetric XTT assay is much weaker than the activity of activated T lymphocytes (Supplementary Information, Fig. S2.2). In addition, proliferation and differentiation of cells requires increased uptake of nutrients for the biosynthesis of lipids, nucleic acids, and proteins as well [235]. Consequently, it is conceivable that activated T cells exhibit greater endocytic activity than naïve/memory T lymphocytes. For instance, increased macropinocytosis in activated T cells could cause greater unspecific uptake of polymers, which could explain the increased fluorescent GMFI value of activated cell populations compared to non-activated T cells at 37 °C.

However, cell size and increased unspecific binding upon activation cannot explain the preference for uptake of different glycosylated polylysine derivatives or the preference of T cells for the glycosylated polymers to the unsubstituted polymer. We conclude, that modification with sugars granted polymers a distinct specificity for activated T lymphocytes.

Activation could have led to a stronger expression of galactose binding-motifs than of mannose and glucose receptors incorporated into the cell membranes. These motifs could be related to L-selectin, which is known to bind the galactose-containing tetrasaccharide sialyl Lewis X and galactose clusters ^[239, 240]. The glycoprotein L-selectin (CD62L) is expressed on the surface of T lymphocytes and plays a crucial role during T cell recirculation ^[225, 241]. By binding to its ligands, CD62L initiates the extravasation of T lymphocytes into peripheral lymphoid tissues. However, during activation of T lymphocytes, CD62L is down-regulated ^[242], which is in contrast to our finding of activated T lymphocytes taking up polymer PL-Gal significantly. Consequently, L-selectin might not be the desired receptor. Another receptor candidate could be among the members of the galectin family. These mammal lectins exhibit affinity for β -galactosides ^[243]. Galectins can exist as dimers or even pentamers ^[226]. Therefore, extracellularly secreted galectins are able to form lattices with glycoprotein receptors on the cell surface. This process enables the cell to modulate various receptor functions ^[244]. Galactosylated polymers could bind multivalently to these extracellular galectin lattices. This hypothesis is supported by the experimental results of both galectin-1 and galectin-3 being upregulated upon T cell activation ^[245, 246]. Moreover, the multivalency of PL-Gal could be the reason, why lactose (concentrations up to 0.15 mol/mL) could not inhibit a presumably strong and irreversible interaction of the galactosylated polymer with the T lymphocytes.

One binding-motif for mannosylated polypeptides could be the cation-independent mannose-6-phosphate (M6P) receptor (CI-MPR), which is expressed on membrane surface of T cells as well ^[227]. CI-MPR facilitates endocytosis of CD26, a multifunctional cell surface glycoprotein, thereby contributing to T cell activation. The phosphomonoester group participates in the interactions between M6P and CI-MPR ^[228]. However, amino acid-residues essential for high-affinity binding of Mannose-6-phosphate form potential hydrogen bonds to hydroxyl-groups at the 2, 3 and 4 positions of mannose. Hence, mannosylated polylysine derivatives could have bound to CI-MPR, although glycosylated polymers did not contain phosphomonoester groups.

GLUTs (glucose transporters) show affinity for saccharides such as galactose, glucose and mannose ^[230]. Because of the size of those polylysine derivatives ($M_w = 38400 - 44500$ g/mol ^[231]), we do not assume that single transporters are able to mediate the uptake of glycosylated polymers. However, multivalent binding of polymers could induce clustering of transporters followed by endocytosis of those polymer-transporter complexes similar to antibody-antigen complexes ^[247] or artificial multivalent protein-receptor complexes ^[248]. Notably, the uptake of PL-Glu by

T cells was significantly decreased compared to that uptake of PL-Gal or PL-Man. This observation seems to be conflicting with the fact that activated T cells show an increased expression of GLUT1 transporter ^[236], which is specific for glucose, and also for galactose and mannose ^[230]. Either those transporters simply do not bind glycosylated polymers or cell-culture medium-related glucose competed with PL-Glu (and PL-Gal or PL-Man) for binding sites. To exclude this possibility, uptake experiments in medium (PBS + 1% BSA) devoid of glucose were performed. However, the use of this medium had an opposing effect on the uptake and even less PL-Glu was internalized. Several reasons for this observation could come into consideration. Cell culture medium, supplemented with 10% FBS, contains serum proteins, which can reduce unspecific adsorption to microtube walls. Alternatively, the amount of bovine serum albumin (1%) in PBS could have been insufficient to prevent unspecific binding. Thus, in interaction experiments less polymer molecules could have been available for uptake by T cell, because to some extent polymers could have been already adsorbed to laboratory plastic ware. However, in experiments 4.8 μM ($M(\text{PL-Glu}) = 37600 \text{ g/mol}$ ^[231]) of glycosylated polymers were used. This concentration is at least 100 times greater than the concentration at which adsorption effects are being considered to produce false or inconsistent results ^[249]. On the other hand, keeping cells for a longer period in PBS decreases cell viability due to lack of nutrients. Consequently, the ability to endocytose glycosylated polymers could have been impaired, which in turn would explain the decrease of GMFI values derived from T cell populations incubated in BSA supplemented PBS. It is important to note, that if glucose uptake is indeed impaired because of GLUTs inhibition, then the observed uptake of galactose and mannose is predominantly not mediated by GLUTs. Furthermore, glycosylated polymers are not natural ligands for transporters. Barnett and colleagues showed that glucose interacts with the GLUT1 transporter probably via hydrogen bonding at the 1, 3 and 4 positions of glucose ^[250, 251]. A potential hydrophobic interaction via the C-6 position was also suggested. Given that glucose is linked to polylysine derivatives via an oxapentylthiourea-spacer at the C-1 hydroxyl-group, binding to GLUT1 transporters is perhaps not impossible but seems to be unfavorable due to steric hindrance.

2.6 Conclusions

Ex vivo activated human T lymphocytes tolerated exposure to glycopolyptides concentrations of up to 0.33 mg/mL very well for at least three days. Furthermore, glycosylated polylysine derivatives can be used to target T cells, because those cells have readily taken up the galactosylated and mannosylated polymers. In contrast, uptake of glucosylated or unsubstituted polypeptides was rather poor or insignificant, respectively. Obviously, activated T cells show a greater density of galactose-binding motifs than non-activated T lymphocytes. However, inhibition with lactose could not be demonstrated. The small amounts of glycosylated polylysine derivatives available for the present work have precluded an exhaustive analysis of polymer-binding site interactions. Consequently, the true target sites for glycosylated polymers remain to be elucidated. Nevertheless, the work reported herein highlights the potential use of statistical glycosylated copolypeptides in biomedical applications such as selective staining of cells or protective encapsulation material for targeted cell-mediated drug delivery.

2.7 Supplementary Information

2.7.1 Size of non-activated and activated T lymphocytes

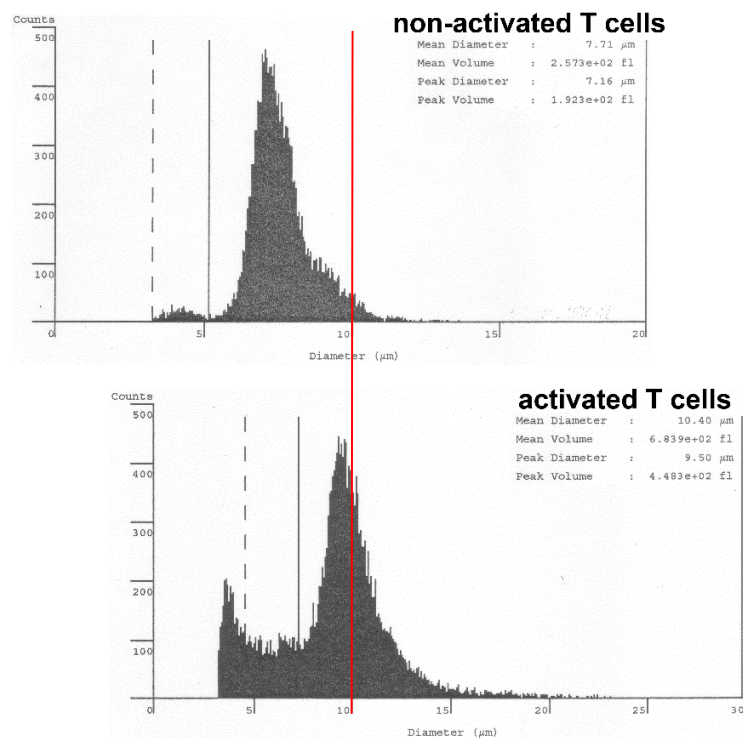


Fig. S2.1. Size distribution of T cell populations measured by an automated cell counter (CASY Model TT, OMNI Life Science). A red orientation line is laid over the 10 μm value of both histograms indicating that naïve/memory T cells (mean $\text{Ø} = 7.71 \mu\text{m}$) are smaller than activated T cells (mean $\text{Ø} = 10.40 \mu\text{m}$).

2.7.2 Reduction of XTT tetrazolium salt by T lymphocytes

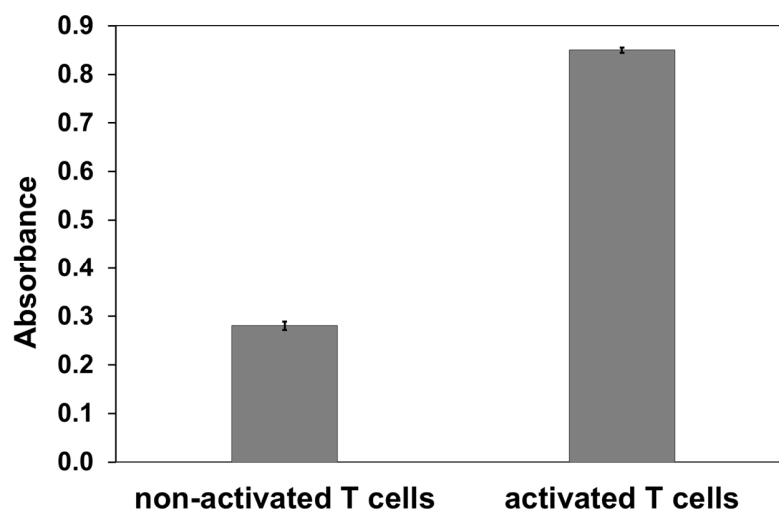


Fig. S2.2. Bioreductive activity of T cells obtained from two healthy donors represented as absorbance after incubation with XTT tetrazolium salt. Colorimetric XTT assay was performed as described in section 2.3.4. Freshly isolated naïve/memory T lymphocytes were used. Bioreductive activity of *ex vivo* activated T cells was determined four days after activation and is significantly increased compared to non-activated cells. Means of two different donors ($n = 2$) are shown. Error bars indicate standard deviations.

3. Interactions of polyester-idarubicin nanoparticles and polymer-photosensitizer complexes with human T lymphocytes

Parts of this chapter were published in:

Blaudszun A.-R., Lian Q., Schnabel M., Loretz B., Steinfeld U., Lee H.-H., Wenz G., Lehr C.-M., Schneider M., Philippi A. (2014)

Polyester-idarubicin nanoparticles and a polymer-photosensitizer complex as potential drug formulations for cell-mediated drug delivery.

International Journal of Pharmaceutics; 474: 70-79

3.1 Abstract

Cell-mediated transport of therapeutics has emerged as promising alternative to classical drug delivery approaches. To preserve viability and functions of carrier cells, encapsulation of active drugs in protective nanoparticles or the use of inducible therapeutics has been proposed. Here, we compared the effects of novel polymeric formulations of an active and a stimulus-sensitive anti-cancer drug on human T lymphocytes to identify suitable drug preparations for cell-mediated drug delivery. For the first approach, the chemotherapeutic agent idarubicin (IDA) was encapsulated in poly(lactic-co-glycolic-acid) (PLGA) and newly developed maleate-polyester (MPE) nanoparticles. PLGA- and MPE-encapsulated IDA was efficiently internalized by *ex vivo* activated human T lymphocytes; however, both encapsulations could not prevent premature T cell death resulting from IDA-uptake. In contrast, loading with a poly(styrene sulfonate) (PSS)-complex of the light-sensitive pharmaceutical 5,10,15,20-tetrakis(3-hydroxyphenyl)porphyrin (mTHPP) did not affect T cell viability if upon loading the cells were kept in the dark. The photosensitizer was transferred from loaded T lymphocytes to co-cultivated carcinoma cells, and induced cancer cell death if co-cultures were exposed to light. Inducible drugs, such as photosensitizers, thus, may help to overcome the limitations of encapsulated active drugs and open up new perspectives for the use of cells as drug transporters in cancer therapy.

3.2 Introduction

Cell-mediated transport of therapeutics has emerged as a new drug delivery concept in the past decade. Several mammalian cell types, including immune and stem cells, have a number of natural properties which make them ideal candidates for the development of novel drug delivery strategies. Unlike artificial drug carriers, defense and stem cells actively move towards sites of inflammation, injury, and cancer. This intrinsic homing ability and the capability of those cells to migrate across the blood–brain and the blood–tumor barrier can be utilized to transport pharmaceuticals specifically to diseased sites. Furthermore, some defense cells possess an intrinsic cytotoxic or phagocytic activity, that can additionally be exploited to fight diseases ^[12]. The drug targeting capabilities of living cells were demonstrated in various pre-clinical studies.

In a murine model of Parkinson’s disease, the homing ability of bone marrow-derived macrophages was exploited to transport catalase nanoparticles the blood-brain barrier to the target site ^[252]. For the treatment of experimentally induced tumors mainly lymphokine activated killer (LAK) cells, macrophages, mesenchymal stem cells, and erythrocytes were utilized as drug carriers ^[12]. Delivered therapeutics include ricin ^[82, 84], doxorubicin and derivatives ^[6, 46], liposomal 5-fluorouracil ^[72], nanoparticulate gold ^[104] as well as magnetic nanoparticles ^[73]. In addition, genetically modified cells expressing immunotoxins, apoptosis-inducing proteins, and immunomodulating cytokines were tested in cell culture and animal experiments ^[13].

Although in most of the studies above the efficacy of cell-delivered drugs was clearly demonstrated, some of them also revealed a major drawback of the emerging strategy: often, when carrier cells were loaded with highly toxic pharmaceuticals, a rapid loss of physiological functions and a decline in cell viability were observed ^[6, 82, 84]. To preserve cellular drug carriers from the toxic effects of delivered therapeutics, incorporation of active drugs in protective nanoparticles has been proposed ^[12]. Ideal encapsulation materials are non-toxic and biodegradable and do not alter the physiological functions of loaded cells. Moreover, they show high drug encapsulation efficiencies and allow sustained release of enclosed pharmaceuticals inside the carrier cells. Since many natural and synthetic polymers meet with these requirements ^[201], polymeric nanoparticles have recently attracted the attention of research groups working on cell-mediated drug delivery. As shown in two basic studies, uptake of fluorochrome-labeled polyelectrolyte-coated poly(lactic-co-glycolic acid) (PLGA) microparticles and amino functionalized polystyrene nanoparticles did not affect the physiological functions of monocytes-derived dendritic cells (DCs)

suggesting that these particles could serve as delivery systems for peptide antigens in DC-based vaccination strategies [203, 204]. In contrast, only few data exist on cellular drug vehicles loaded with polymeric anticancer drug formulations [101].

In the present study, we aimed to identify anticancer drug formulations for cell-mediated drug delivery which preserve loaded carrier cells from premature cell death. To this end, two different types of therapeutics, an active and an inducible drug, were encapsulated in polymers. For the first approach, the highly toxic chemotherapeutic agent idarubicin (IDA) was enclosed in PLGA and newly developed maleate-based polyester (MPE) nanoparticles (NPs). Both NP-preparations were subsequently introduced in activated polyclonal human T lymphocytes. Upon loading, T cell survival was characterized as a function of drug concentration and loading time. Furthermore, the protective effect of gold shell-coated MPE nanoparticles, referred to as AuSh NPs, was examined. For the second approach, T lymphocytes were loaded with a water-soluble poly(styrene sulfonate) (PSS)-complex of the light-sensitive anticancer drug 5,10,15,20-tetrakis (3-hydroxyphenyl)porphyrin (mTHPP) [193]. First, survival of polymer-photosensitizer-loaded T cells was analyzed. In a second step, mTHPP-transfer from T lymphocytes to co-cultivated carcinoma cells, and the phototoxic effect of T cell-delivered photosensitizer on tumor cells were studied.

3.3 Materials and methods

Methods described in section 3.3.1 to 3.3.3 and preparation of PSS/mTHPP were not conducted by the author of this thesis.

3.3.1 Synthesis of poly(diethylene glycol-maleate-co-sebacate)ester (MPE)

Poly(diethylene glycol-maleate-co-sebacate)ester (MPE) was prepared by melt condensation. In brief, 20 g (0.185 mol) of diethylene glycol, 5.405 g (0.0375 mol) of dimethyl maleate, 34.729 g (0.151 mol) of dimethyl sebacate and 1.5 g of p-toluene sulfonic acid (Sigma-Aldrich, Steinheim, Germany) were mixed in a plain glass flask with plain bottom and heated up to 170 °C for 1 day under stirring. After distilling off methanol produced during the reaction under reduced pressure (20 mbar), a viscous product was obtained by cooling to 25 °C. The product was dissolved in 200 mL of tetrahydrofuran and precipitated in 1000 mL of methanol. The oily precipitate was

collected by centrifugation and dried under reduced pressure (2×10^{-2} mbar). Polymer characterization was performed as described in the Supplementary information (S3.7.3).

3.3.2 Synthesis of PLGA-IDA, MPE-IDA, and AuSh-IDA nanoparticles

Idarubicin (IDA) ethyl acetate (EA) solution was prepared by extracting IDA as free base from aqueous idarubicin hydrochloride solution (IDA•HCl, 1 mg/mL, Sigma-Aldrich) after adding triethylamine (1%). To prepare PLGA-IDA and MPE-IDA NPs, polyesters poly(D,L-lactide-co-glycolide) 50:50 (Sigma Chemical Co., St. Louis, MO, USA) and MPE were first dissolved in ethyl acetate (Fluka Chemie, Buchs, Switzerland) mixed with IDA in a defined ratio (2:0.1, w/w, polymer:IDA). This organic phase was added gradually to an equal volume of polyvinyl alcohol in water (PVA, 2.5% aqueous solution, Sigma-Aldrich). The emulsion was then homogenized using an Ultra-Turrax T25 device (IKA-Werke, Staufen, Germany) at 13,500 rpm for 10 min. NPs were obtained by adding purified water dropwise under gentle stirring to obtain a final suspension. Stirring was continued overnight at room temperature to remove the organic solvent. To prepare AuSh-IDA NPs, an equal volume of chloroauric acid (1 mg/mL, Sigma-Aldrich) was added to the solution containing MPE-IDA NPs. Hydroxylamine (50%, Sigma-Aldrich) as reduction agent was further added dropwise under gentle stirring for 10 min. Gold nanoshells were self-assembling on the surfaces of MPE-IDA NPs.

3.3.3 Determination of colloidal characteristics, drug encapsulation efficiency, nanoparticle morphology and drug release kinetics

Average particle size, size distribution, and zeta potential were determined in purified water (MilliQ) using the Malvern Zetasizer Nano (Malvern Instruments, Malvern, UK). For each batch, three samples were measured (with 30 subruns for each sample) to determine the mean values.

Drug encapsulation efficiencies (EE) and drug loading values were determined indirectly by fluorescence spectrometry using an Infinite 200 PRO reader (Tecan, Crailsheim, Germany). The nanoparticle supernatant was used for fluorescence measurements. From the fluorescence of the supernatant, the IDA amount not encapsulated was determined using respective calibration of IDA fluorescence. Knowing the amount of drug used for NP-preparation (in the beginning) and the amount determined in the supernatant allowed to calculate the encapsulated drug amount.

The morphology of NPs was determined by scanning probe microscopy (SPM) with a Bioscope equipped with a Nanoscope IV controller from Digital Instruments (Veeco, Santa Barbara, CA,

USA). Samples were dried under a stream of compressed air after deposition on a freshly cleaved muscovite mica (Plano, Wetzlar, Germany) and investigated under ambient conditions in tapping mode using a scanning probe with a force constant of 40 N/m at a resonant frequency of around 300 kHz (Anfatec, Oelsnitz, Germany).

For determination of drug release kinetics, 1 mL aliquots of polyester-IDA NP suspensions were placed into a QuixSep Micro Dialyzer (Carl Roth, Karlsruhe, Germany). The capsules were then covered with dialysis membranes. The receptor compartments were filled with 100 mL of phosphate buffer solution (pH 7.4). Release studies were performed at 37 °C. At each selected time point, the buffered solution in the receptor compartment was taken for HPLC analysis and replaced with fresh buffer solution. The samples were analyzed using an HPLC apparatus consisting of a Dionex Pump P680 (Dionex, Idstein, Germany) with a Hitachi Fluorescence detector L-2480 (Hitachi, Darmstadt, Germany). The excitation and emission wavelengths used were 485 and 542 nm, respectively. The column used was LiChroCART 125-4 RP-18 (Merck Millipore, Darmstadt, Germany). The mobile phase consisted of water, acetonitrile, triethylamine, and phosphoric acid (624:370:4:2, v/v). The settings were as follows: flow rate = 1 mL/min; temperature = 25 °C; injection volume = 50 µL.

3.3.4 Preparation and handling of PSS/mTHPP

The photosensitizer (PS)-complex PSS/mTHPP was kindly provided by Hagar Ibrahim Labouta (Helmholtz Institute for Pharmaceutical Research Saarland (HIPS), Saarland University, Germany) and prepared as previously described ¹¹⁹³¹. Lyophilized PS-complex was dissolved in autoclaved purified water obtained from an Elix3 (UV) water purification system (Merck Millipore, Darmstadt, Germany) as a stock solution of 5 mg/mL (around 1 mg/mL drug) which was stored in the dark for up to 4 weeks at 4 °C. An LED lamp (SBAR I, TPL Vision, La Chevrolière, France) having a peak wavelength of 588 nm was used to handle the PS-complex and PSS/mTHPP-loaded T cells. Incubations were carried out in the dark to avoid premature activation of the photosensitizer.

3.3.5 Cell culture

Human T lymphocytes were isolated from day-fresh buffy coat preparations, activated and further expanded as previously described ¹²³¹¹. Buffy coat products were obtained from healthy donors of the Blutspendezentrale Saar-Pfalz (Saarbrücken, Germany) after informed consent ac-

according to the declaration of Helsinki. Prior to use, activation beads (T cell Activation/Expansion Kit human, Miltenyi Biotec, Bergisch Gladbach, Germany) were removed from T cell cultures by density gradient centrifugation using Pancoll (human, PAN Biotech, Aidenbach, Germany) as separating solution.

The human ovary carcinoma cell line SKOV-3 (HTB-77, American Type Culture Collection, Manassas, VA, USA) was maintained in RPMI 1640 medium (PAN Biotech) supplemented with 10% (v/v) heat-inactivated FBS (PAN Biotech), 100 U/mL penicillin, and 0.1 mg/mL Streptomycin (Sigma-Aldrich).

3.3.6 Loading of T lymphocytes with nanoparticles and PSS/mTHPP

Qiong Lian (Biopharmaceutics and Pharmaceutical Technology, Saarland University, Germany) kindly provided nanoparticles. For loading with NPs and the PS-complex PSS/mTHPP, T lymphocytes were adjusted 4-6 days post stimulation in cell culture medium (supplemented RPMI 1640) to a concentration of 2.5×10^6 cells/mL using an automated cell counter (CASY Model TT, OMNI Life Science, Bremen, Germany). After addition of the indicated amounts of PLGA-IDA, MPE-IDA, AuSh-IDA NPs and PSS/mTHPP (suspended/dissolved in purified water), T cells were incubated unless otherwise specified for 2 h in a humidified atmosphere at 37 °C and 5% CO₂. Moreover, by treating T lymphocytes under the same conditions with appropriate small quantities of sterile purified water unloaded (empty) control T cells were prepared. To remove non-internalized NPs and PS-complex, T cells were subsequently sedimented at 300×g and 4 °C for 10 min (centrifuge 5810 R, Eppendorf, Hamburg, Germany) and washed three times with ice-cold cell culture medium. Then, T lymphocytes were either immediately processed or adjusted in 20 U/mL interleukin-2 (IL-2, PAN Biotech) containing cell culture medium to a concentration of 2.5×10^6 cells/mL and further cultivated at 37°C/5% CO₂ for the indicated periods of time.

3.3.7 Analysis of particle and photosensitizer uptake by flow cytometry

For flow cytometry-based examination of NP and PSS/mTHPP uptake, 5×10^5 unloaded and loaded T lymphocytes were resuspended in 400 µL of ice-cold flow cytometer (FCM) buffer (MACS Buffer containing 2 mM EDTA and 0.5% BSA (Miltenyi Biotec) supplemented with 0.1% NaN₃ (Sigma-Aldrich)) and analyzed in a FACS Calibur flow cytometer (BD Biosciences, Heidelberg, Germany). Fluorescence intensities of 10,000 events were measured with the FL2 (idarubicin)

and FL3 (mTHPP) detector using the CellQuest Pro software (BD Biosciences). Cell debris was eliminated from the analysis by using a threshold of 80/120, before T cell populations were gated and the geometric mean (GeoMean) of fluorescence intensities was determined using the FlowJo software (Tree Star, Inc., Ashland, OR, USA). Results represent means of duplicate measurements with standard deviations (SD) indicated.

3.3.8 Fluorescence microscopy (FM) and confocal laser scanning microscopy (CLSM)

Intracellular uptake of IDA and PSS/mTHPP was confirmed by FM and CLSM. For FM analysis, 3×10^6 loaded T lymphocytes were first fixed for 10 min using 4% (w/v) formaldehyde (paraformaldehyde, Sigma-Aldrich) in phosphate buffered saline (PBS, Life Technologies, Darmstadt, Germany) and then embedded in 1 $\mu\text{g}/\text{mL}$ 4',6-diamidino-2-phenylindole dihydrochloride (DAPI, Sigma-Aldrich) containing FluorSave mounting medium (Merck Millipore). Images were captured with an F-View II CCD camera (Olympus, Hamburg, Germany) mounted on an inverted IX71 microscope (Olympus) equipped with a 60 \times oil-immersion objective (numerical aperture 1.42, Olympus) and the Cell^P software (version 2.8, Olympus). Immersion oil Immersol 518N (Carl Zeiss Microscopy GmbH, Göttingen, Germany) was used. To visualize idarubicin and mTHPP uptake, a MWG2 filter (excitation wavelength: 510-550 nm, emission wavelength: > 590 nm, Olympus) was used, whereas nuclei stained with DAPI were detected using a MNU2 filter (excitation wavelength: 360-370 nm, emission wavelength: > 420 nm, Olympus).

For CLSM analysis of PLGA-IDA NP-loaded T lymphocytes, cells were first fixed as previously described and then stained for 20 min at 37 °C with a membrane dye (5 $\mu\text{L}/\text{mL}$ of Vybrant DiO cell-labeling solution (1 mM), Life Technologies). Embedded cells were analyzed with a ZEISS LSM 510 META confocal laser scanning microscope (Carl Zeiss, Jena, Germany) equipped with a helium-neon laser with an excitation wavelength of 543 nm and a 560 nm long pass filter for detection of internalized idarubicin. Cell membranes stained with DiO were visualized using an argon-ion laser with an excitation wavelength of 488 nm and a 500-530 nm band pass filter, while a pulsed NIR laser (Chameleon-XR, Coherent, Dieburg, Germany) with an excitation wavelength of 720 nm (2×360 nm) and a 390-465 nm band pass filter served to detect DAPI stained nuclear DNA using two-photon excitation microscopy.

To visualize photosensitizer transfer from loaded T lymphocytes to co-cultivated cancer cells, 40,000 SKOV-3 ovary carcinoma cells were seeded in a μClear black 96-well plate (Greiner Bio-One, Frickenhausen, Germany), before PSS/mTHPP-loaded T cells were added to the tumor cells

in a ratio of 4:1. After a co-cultivation period of 27.5 h, cells were stained for 30 min with 5 µg/mL Hoechst 33342 (10 mg/mL solution in water, Life Technologies). Then, co-cultures were washed three times with cell culture medium to remove excess T cells. Subsequently, live cell fluorescence microscopy was performed using an inverted Olympus IX71 microscope equipped with an F-View II camera (Olympus) as described above.

3.3.9 Analysis of cell survival

Survival of NP- and PS-complex-loaded T lymphocytes was determined using colorimetric XTT and WST-1 cell viability assays. For both tests, 2.5×10^5 loaded T cells resuspended in RPMI 1640 medium w/o phenol red supplemented with 10% FBS, and antibiotics were transferred in triplicates to 96-well plates. Unloaded T cells were used as negative control, whereas T lymphocytes treated with Triton X-100 (Merck, Darmstadt, Germany) served as positive control. Blanks containing only medium and assay components were included, too. All samples were incubated unless otherwise specified at 37 °C until XTT (Sigma-Aldrich) and WST-1 (Roche Applied Science, Mannheim, Germany) assays were conducted according to the protocols provided by the manufacturers. XTT assays were started 6 h before the time points indicated by mixing 100 µL T cell culture with 20 µL reconstituted XTT reagent, while for the WST-1 assay 100 µL T cell culture were incubated for 1 h with 10 µL WST-1 solution. To analyze the viability of PSS/mTHPP-loaded T cells, part of the cultures was irradiated at the time points indicated for 2 min with a tungsten halogen light (Haloline Eco, 400 W, 9000 lm, OSRAM, Muenchen, Germany) which corresponds to a light dose (fluence) of 2.8 J/cm² (300-780 nm), whereas the remaining samples were kept in the dark. For absorbance measurements, a Spectra Rainbow Thermo microplate reader equipped with the Magellan software (Tecan, Crailsheim, Germany) was utilized. The measurement and reference wavelengths used were 450 and 690 nm, respectively. After subtracting the blanks all viability data obtained were normalized to the viability of the negative controls which were set to 100%.

To analyze cancer cell survival in irradiated co-cultures of PSS/mTHPP-loaded T lymphocytes and SKOV-3 ovary carcinoma cells, triplicates of 40,000 tumor cells were seeded in 96-well plates. Upon addition of different quantities of unloaded and PS-complex-loaded T cells, the samples were further incubated at 37°C/5% CO₂. In addition, positive (1% TX-100) and negative controls (untreated cancer cells) and blanks containing only loaded or unloaded T cells were prepared. To activate the photosensitizer, part of the co-cultures was illuminated after 16 and 20 h

for 2 min with a tungsten halogen light as specified above. After a total co-cultivation time of 23.5 h, all cultures were incubated for 30 min with WST-1 reagent (Roche Applied Science), before absorbance were measured at 450 nm as described in the previous section. For data analysis, first T cells blanks were subtracted. Then, all viability data obtained were normalized to the viability of untreated SKOV-3 cells which was set to 100%. In summary, cancer cell survival in the individual co-cultures was calculated using the following equation:

$$\% \text{ Cancer cell survival} = 100 \times \frac{(\text{A of co-cultures}) - (\text{A of T cells alone})}{(\text{A of cancer cells alone})}$$

(A = mean absorbance of samples – mean absorbance of background controls)

3.4 Results

Results described in section 3.4.1 and shown in Figure 3.1 as well as Fig. 3.4A, and Table 3.1 were not obtained by the author of this thesis.

3.4.1 Synthesis and characterization of MPE-IDA and PLGA-IDA nanoparticles

In order to evaluate whether encapsulation of highly toxic antineoplastic agents in polymeric nanoparticles prevents cellular drug carriers from premature cell death, a novel amphiphilic polyester composed of a hydrophilic monomer (diethylene glycol), a hydrophobic monomer (dimethyl sebacate), and dimethyl maleate units was synthesized by melt condensation. Poly(diethylene glycol-maleate-*co*-sebacate) ester (referred to as MPE, chemical structure depicted in Fig. 3.1A) has a melting point of 29°C and a molecular weight of 16,000 g/mol determined by DSC and GPC, respectively (M. Schnabel, personal communication). While the double bonds provided by the maleate units allow functionalization, the specific combination of the hydrophilic and hydrophobic component enables encapsulation of selected pharmaceuticals.

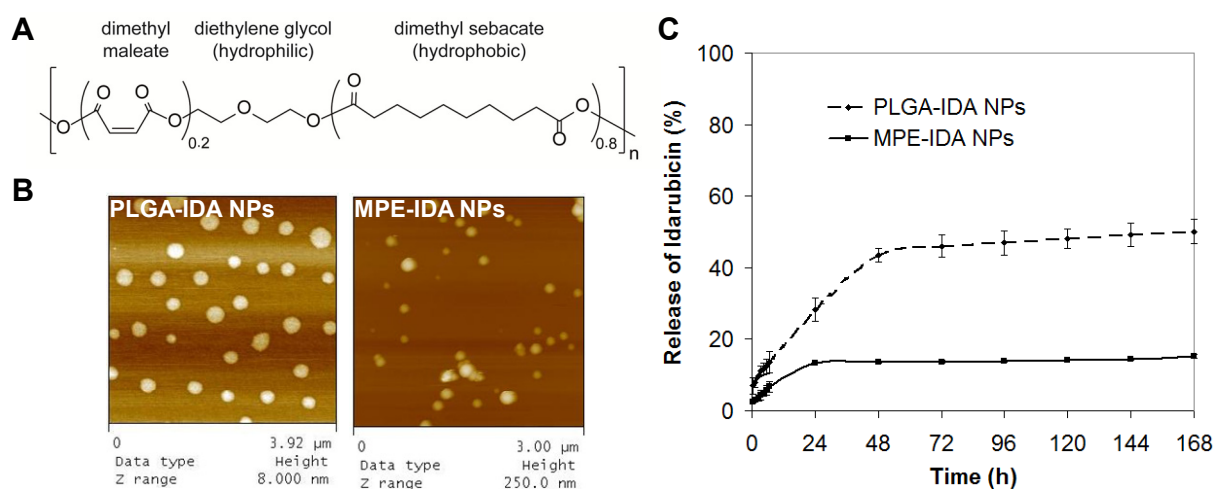


Figure 3.1. Nanoparticle characterization. (A) Chemical structure of poly(diethylene glycol-maleate-co-sebacate) ester used for preparation of MPE-IDA NPs by an emulsification-solvent evaporation-based technique. (B) Scanning probe microscopy (SPM) images of PLGA-IDA and MPE-IDA nanoparticles. (C) Drug release profiles of PLGA-IDA and MPE-IDA NPs in PBS buffer (pH 7.4), $n = 3$.

In the present study, MPE was used to encapsulate the hydrophobic anthracycline idarubicin (IDA) serving simultaneously as active drug and fluorescent probe. In addition, reference nanoparticles (NPs) composed of IDA and the well-known biocompatible polyester poly(lactic-co-glycolic-acid) (PLGA) were synthesized. Using the emulsification-solvent evaporation technique almost spherical PLGA-IDA and MPE-IDA nanoparticles were obtained as shown by scanning probe microscopy (SPM) (Fig. 1B). The average particle diameter ranged between 216 nm (PLGA-IDA NPs) and 227 nm (MPE-IDA NPs), with the PLGA-IDA preparation exhibiting a better size distribution (PDI, Table 3.1). In terms of encapsulation efficiency (EE) and drug loading PLGA-IDA NPs (EE = 92.6%, drug loading = 2.26%) were also slightly superior to MPE-IDA particles (EE = 81.4%, drug loading = 1.97%).

Table 3.1.

Physicochemical characteristics of PLGA-IDA and MPE-IDA nanoparticles ($n = 2$)

	PLGA-IDA	MPE-IDA
Size [nm]	215.8 ± 9.6	226.8 ± 7.1
PDI	0.067 ± 0.001	0.116 ± 0.001
Zeta potential [mV]	-20.57 ± 0.76	-1.88 ± 0.28
EE [%]	92.6 ± 0.2	81.4 ± 1.34
Drug loading [%]	2.26	1.97

Abbreviations: PDI, polydispersity index; EE, encapsulation efficiency

However, MPE-IDA NPs displayed better drug release kinetics at physiological pH. While in PBS buffer (pH 7.4) PLGA-IDA NPs lost almost 50% of the encapsulated drug within the first 48 h, MPE-IDA NPs showed only a minimal burst release of about 15% within 24 hours (Fig. 1C). Consequently, MPE-IDA nanoparticles should be better suited than the reference NPs to protect loaded cells against the toxic effect of encapsulated idarubicin.

3.4.2 Uptake of PLGA- and MPE-encapsulated idarubicin by *ex vivo* activated human T lymphocytes

To evaluate whether the newly prepared idarubicin loaded polyester NPs can serve as drug payload in cell-mediated drug delivery, particle uptake by *ex vivo* activated, polyclonal human T lymphocytes was studied. In contrast to other carrier cells polyclonal T cells, possess a natural cytotoxic activity which can be exploited in combination with the delivered drug [12]. However, to take advantage of the natural cytotoxicity of polyclonal T lymphocytes, it is required to activate and expand those cells *ex vivo*. In this study, naïve/memory T cells isolated from the blood of healthy donors were incubated with anti-CD3, -CD28 and -CD2 antibodies coupled to magnetic beads in order to obtain the required amounts of activated cells. After an activation-expansion period of 4-6 days, drug-loaded T lymphocytes were prepared. To this end, 2.5×10^6 cells/mL were incubated at 37 °C for a total period of 4 h with different amounts of MPE-IDA and PLGA-IDA reference NPs. At the time points indicated, incorporation of the red fluorescent drug was examined using both flow cytometry and fluorescence microscopy.

When nanoparticle treated T cells were analyzed by flow cytometry, a significant dose- and time-dependent increase of fluorescence intensities was observed strongly suggesting that drug uptake occurred. Interestingly, T lymphocytes incubated with MPE-IDA NPs (Fig. 3.2B) produced weaker fluorescence signals than reference NP-loaded cells (Fig. 3.2A) indicating that MPE-encapsulated IDA was less efficiently internalized than the PLGA-enclosed drug. Furthermore, signals began to plateau after 2 h irrespective of the particle type and amount used.

When PLGA- and MPE-IDA NP-loaded T lymphocytes were analyzed by fluorescence microscopy, drug uptake could be confirmed (Fig. 3.2C and 3.2D). To study IDA incorporation in more detail, T cells loaded with PLGA-IDA NPs were stained with the membrane dye DiO and additionally characterized by confocal laser scanning microscopy. The CLSM image displayed in Fig. 3.2E clearly shows that PLGA-encapsulated idarubicin was internalized by the cells. Furthermore, a strong accumulation of the red fluorescent drug in the cytoplasm could be recog-

nized, whereas only little idarubicin was detected in the nuclei. Taken together, intracellular uptake of polyester-enclosed idarubicin by *ex vivo* stimulated T lymphocytes could be demonstrated.

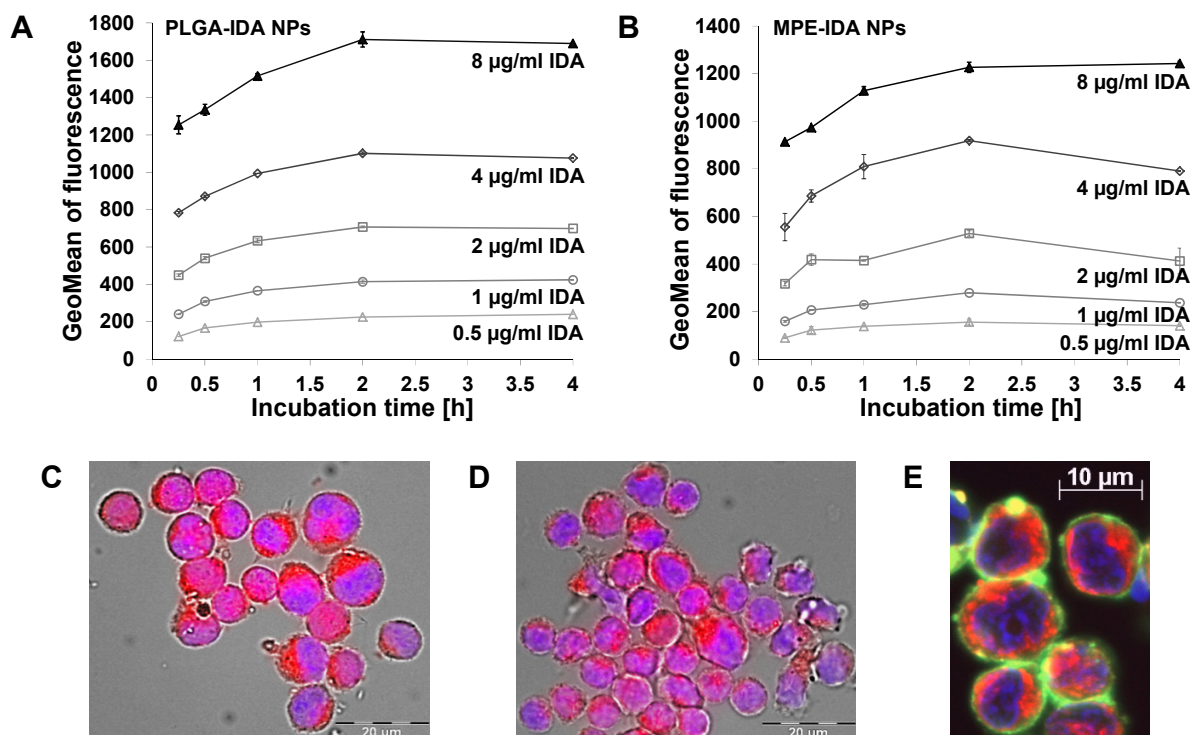


Fig. 3.2. Uptake of PLGA- and MPE-encapsulated idarubicin (IDA) by activated, polyclonal human T lymphocytes. Drug incorporation was examined by flow cytometry (A, B). In each panel, one of two independently performed experiments is exemplarily shown. T lymphocytes loaded for 2 h with 4 µg/mL PLGA- and MPE-encapsulated IDA (red fluorescence) were additionally analyzed by fluorescence microscopy (C, D). The nuclear DNA of fixed and embedded cells was stained with DAPI (blue fluorescence). Overlay images of fluorescence and bright field images are shown. (E) Confocal laser scanning microscopy of T lymphocytes loaded for 2 h with PLGA-IDA NPs (4 µg/mL IDA). Cell membranes were detected using DiO (green fluorescence), whereas nuclei were stained with DAPI.

3.4.3 Survival of PLGA-IDA and MPE-IDA NP-loaded T lymphocytes

To examine whether polymeric drug encapsulations prevent loaded T lymphocytes from premature cell death, the viability of unloaded and loaded T cells was compared over a total period of 3 days. To prepare loaded cells, *ex vivo* stimulated T lymphocytes were incubated for 2 h with 0.04, 0.4 and 4 µg/mL PLGA- and MPE-encapsulated idarubicin. Upon three washing steps, the lymphocytes were put back into culture, before a colorimetric XTT cell viability assay was performed at the time points indicated. To exclude toxic effects of the polymeric drug encapsulations, T cells incubated with empty PLGA and MPE particles were analyzed too, whereas T lymphocytes exposed to 4 µg/mL free idarubicin served as positive control.

Figure 3.3A reveals that irrespective of the particle concentration used PLGA-IDA NPs were as toxic for activated T cells as 4 $\mu\text{g/mL}$ free idarubicin. Already after 8 h NP-loaded T cells showed a clearly reduced viability which further declined to an average value of 12.5% after 24 h. In contrast, the viability of T lymphocytes exposed to empty PLGA nanoparticles was not impaired. When T cells were incubated with 0.4 and 4 $\mu\text{g/mL}$ MPE-encapsulated IDA, a dramatic loss of cell viability within 24 h was detected as well (Fig. 3.3B). However, in the presence of 0.04 $\mu\text{g/mL}$ nanoparticle-enclosed drug a delayed decrease of T cell viability was observed. At the lowest IDA concentration, it took 52 h until the minimum viability rate was reached, and only 12.5% viable T lymphocytes were left. Though, a significant protective effect of the maleate polyester-based drug encapsulation cannot be deduced from this result, since MPE-encapsulated IDA was less efficiently internalized by activated T cells than PLGA-enclosed IDA as shown in Figure 3.2. Rather it appears that both particle preparations released the drug too early to prevent premature death of NP-loaded T lymphocytes.

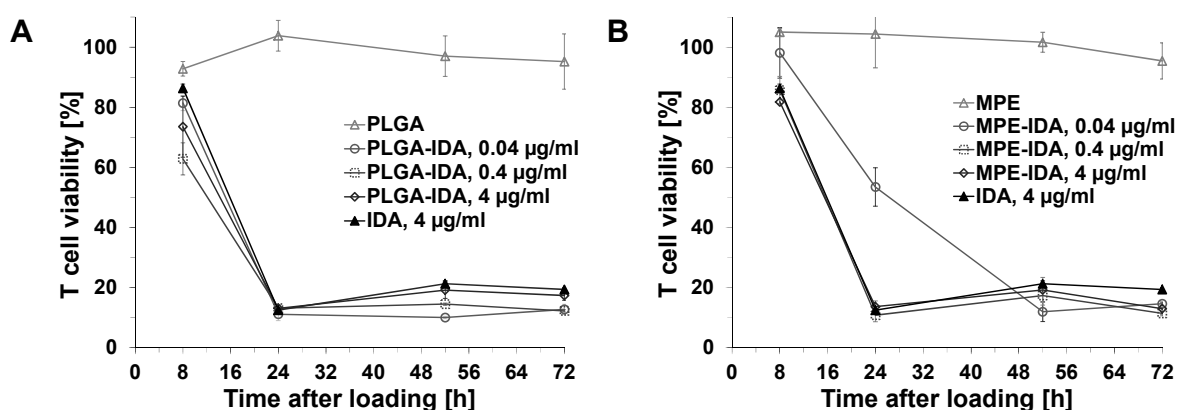


Fig. 3.3. Survival of PLGA-IDA (A) and MPE-IDA (B) NP-loaded T lymphocytes. After incubation with different amounts of PLGA- and MPE-encapsulated idarubicin, T cell viability was analyzed using a XTT colorimetric assay. T lymphocytes loaded with empty particles and free idarubicin served as negative and positive control, respectively. All viability data obtained were normalized to the viability of unloaded T cells. Results are expressed as means of two independent experiments with standard deviations (SD) indicated.

3.4.4 Uptake and cytotoxicity of gold-coated MPE-IDA nanoparticles

Coating of doxorubicin-loaded PLGA NPs with a gold layer enables NIR irradiation-dependent controlled drug release as demonstrated in several comprehensive studies [253, 254]. To verify in this work whether an additional gold layer would reduce premature drug release from idarubicin-loaded polymeric nanoparticles, and thus, extend the life span of particle-loaded T cells, MPE-IDA NPs were coated with a gold shell (AuSh) using a novel one-step deposition method. In par-

allel, AuSh nanoparticles without drug payload were prepared. Both, AuSh-IDA and control NPs had comparable hydrodynamic diameters and zeta potentials as determined by Zetasizer Nano measurements (Fig. 3.4A).

To characterize nanoparticle uptake by activated human T lymphocytes, 2.5×10^6 cells/mL were incubated at 37 °C for a total period of 3.5 h with 4 and 8 µg/mL AuSh NP-encapsulated idarubicin. In addition, loading with the highest NP concentration (8 µg/mL IDA) was carried out at 4 °C. In this way, endocytosis-mediated uptake, which only occurs at elevated temperatures could be distinguished from non-specific particle binding and drug diffusion processes that also may happen at 4 °C. When analyzed by flow-cytometry, again a dose- and time-dependent increase of fluorescence intensities could be observed (Fig. 3.4B). Moreover, the fluorescence intensities of the 37 °C samples were significantly higher than the 4 °C values; thus, particle uptake most probably occurred. The low GeoMean values, however, suggest that only small quantities of AuSh-IDA NPs were incorporated by the lymphocytes. As for non-AuSh NPs, the highest uptake was reached after 2 h. Thereafter, fluorescence intensities of analyzed cells decreased.

For analysis of cell viability, T lymphocytes were incubated for 48 h with different amounts of AuSh-IDA and control AuSh NPs. Since the gold coated particles did not remain in the supernatant during centrifugation, washing was omitted here. At the time points indicated, a colorimetric WST-1 cell viability assay was performed. Although only small amounts of IDA containing NPs (0.4 and 0.8 µg/mL IDA) were used for loading, strong toxic effects on T cells were detected (Fig. 3.4C). Within 24 h, viability rates declined to 20-30% and reached 13% after 48 h. At longer incubation times, the survival of control particle-loaded T lymphocytes was impaired as well. Since toxic effects of the new maleate-based polyester could be excluded (compare Fig. 3.3B), the observed loss of T cell viability was most probably due to the additional gold coating. But regardless of any possible negative impact of gold shells on T lymphocytes, no significant protective effect of the additional drug encapsulation could be determined.

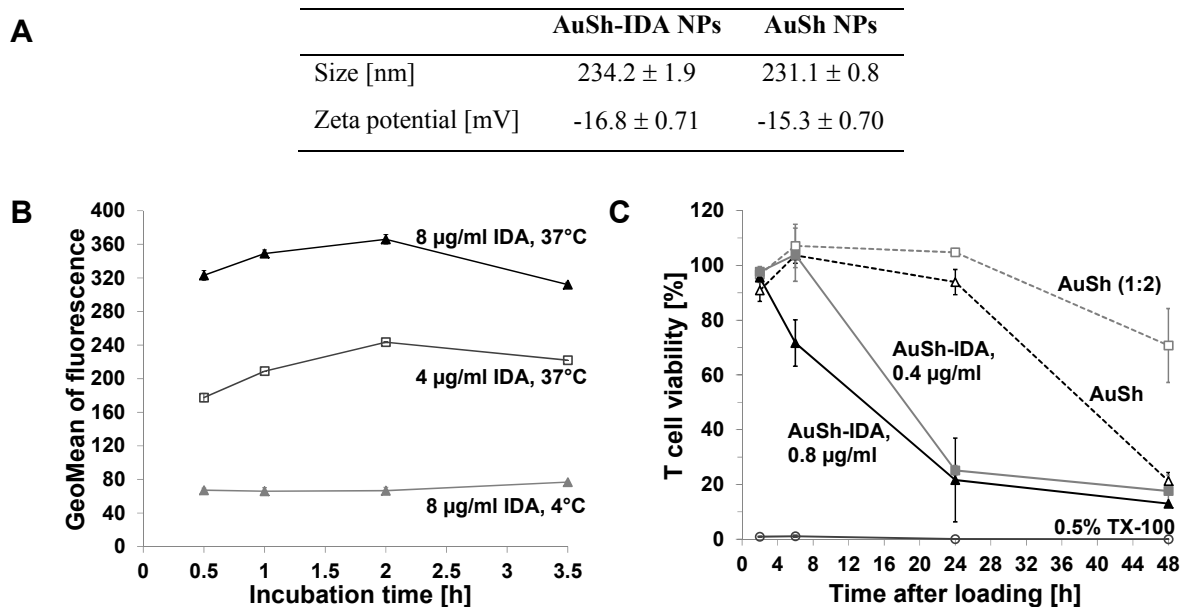


Fig. 3.4. Intracellular uptake and protective effect of AuSh-IDA nanoparticles. (A) Average hydrodynamic diameter and zeta potential of newly prepared gold shell-coated MPE-IDA nanoparticles (AuSh-IDA NPs) and AuSh-coated MPE NPs without drug content (AuSh NPs), $n = 2$. (B) Particle uptake by *ex vivo* activated human T lymphocytes was studied at 37 and 4 °C by flow cytometry. (C) Survival of particle-loaded T cells was determined using a WST-1 colorimetric assay. Results represent the means of two independent experiments \pm SD. TX-100: Triton X-100 (positive control).

3.4.5 Intracellular uptake of the polymer-photosensitizer complex PSS/mTHPP

Given the strong toxic effect of polyester-IDA and AuSh-IDA nanoparticles on activated human T lymphocytes, a change in strategy was necessary to protect the cells more effectively against delivered anticancer drugs. In the treatment of many tumors light-inducible drugs such as Photofrin or Foscan have become an attractive alternative to conventional chemotherapeutic agents. While in the dark light-sensitive therapeutics do not affect cell viability, strong cytotoxic effects can be observed if treated cells are exposed to light [165]. Recently, preparation of a water-soluble poly(styrene sulfonate) (PSS)-complex of the hydrophobic photosensitizer 5,10,15,20-tetrakis(3-hydroxyphenyl)porphyrin (mTHPP) was described [193]. Although red light-activated mTHPP is less cytotoxic than its approved derivative Foscan [192], the precursor has been frequently applied as model photosensitizer (PS) in basic research on photodynamic therapy (PDT) [153]. In the present study, PSS/mTHPP was used exemplarily in order to evaluate whether polymeric photosensitizer preparations are suitable drug formulations for cell-mediated drug delivery.

For analysis of intracellular uptake, *ex vivo* activated human T lymphocytes were incubated in the dark for a total period of 8 h with 1 and 10 $\mu\text{g/mL}$ PSS-complexed mTHPP. To distinguish spe-

cific energy-dependent drug uptake from unspecific drug binding and diffusion processes, only half of the samples were kept at 37 °C, while the other part was incubated at 4 °C. The flow-cytometer analysis shown in Figure 3.5A reveals a clear time- and concentration-dependent increase of fluorescence intensities at both incubation temperatures. Moreover, the values measured at 4 °C were well below the values of the 37 °C samples strongly suggesting that activated T cells internalized the red fluorescent drug at elevated temperatures with energy-dependent processes being the basis of the uptake mechanism. To confirm drug incorporation, T cells incubated for 2 h with 10 µg/mL complexed mTHPP were additionally studied by fluorescence microscopy (Fig. 3.5B). The strong photosensitizer signal detected in the cytoplasm of formaldehyde-fixed cells supports the findings of the flow cytometer analysis. Thus, intracellular photosensitizer uptake by PSS/mTHPP-incubated T lymphocytes could be demonstrated.

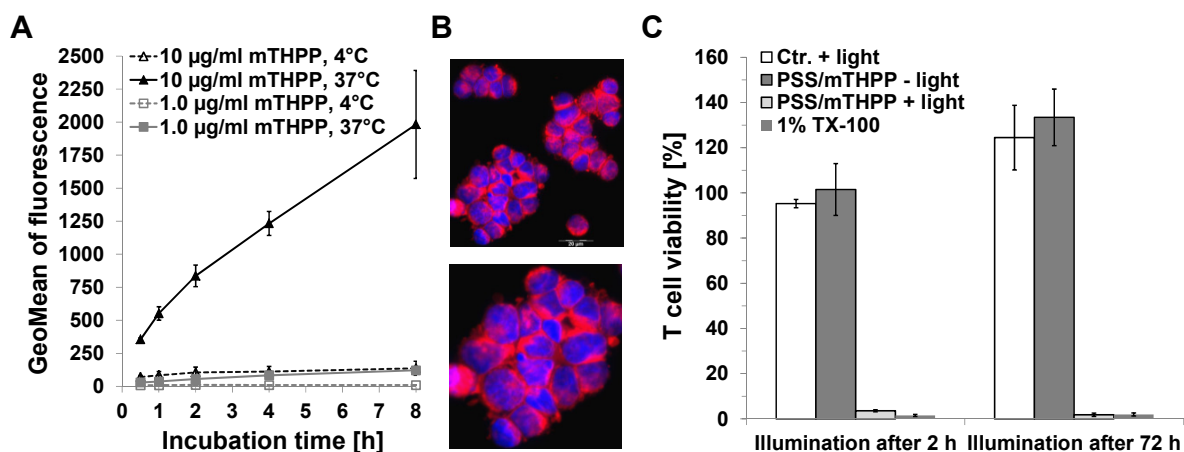


Fig. 3.5. Uptake studies with the water-soluble polymer-photosensitizer complex PSS/mTHPP. Internalization of mTHPP (red fluorescence) by *ex vivo* activated human T cells was detected using flow cytometry (A) and fluorescence microscopy (B). Nuclei were stained with DAPI (blue fluorescence). In the lower image a magnified area of the upper image is shown. (C) Survival of PSS/mTHPP-loaded T lymphocytes was analyzed using a WST-1 cell viability assay. Both, non-illuminated (- light) and illuminated cells (+ light) were examined. All viability data obtained were normalized to the viability of non-illuminated, unloaded T cells. Data represent the means of at least two independent experiments \pm SD. TX-100: Triton X-100 (positive control).

3.4.6 Viability of PSS/mTHPP-loaded T cells before and after illumination

In the next experiment, both dark toxicity and phototoxic effect of the incorporated photosensitizer were evaluated. To prepare PS-loaded cells, T lymphocytes were again incubated for 2 h in the dark with 10 µg/mL complexed mTHPP or treated with the appropriate amount of sterile purified water (control). Thereafter, T cells were transferred to fresh culture medium and further cultivated at 37 °C. At two different time points, either 2 or 72 h upon loading, the photosensitiz-

er was stimulated in a portion of the cultures using a tungsten halogen light which was set to deliver a 2-minute light pulse of 2.8 J/cm² (300-780 nm). 18-24 h upon illumination, the viability of irradiated and non-irradiated T cells was analyzed using a WST-1 assay.

Although in the 72 h approach T lymphocytes were exposed to the photosensitizing agent for up to 96 h, no toxic effects could be detected if the loaded cells were kept in the dark (Fig. 3.5C). Thus, at a loading concentration of 10 µg/mL PSS-complexed mTHPP, no dark toxicity occurred during 4 days. However, upon irradiation, PS-loaded T lymphocytes were efficiently killed, irrespective of the time of light exposure. The irradiation itself had no negative effect on the lymphocytes, since illuminated, empty cells were not affected. Taken together, by loading T lymphocytes with a polymer formulation of a light-inducible anticancer agent, T cell survival and drug effect could be precisely controlled.

3.4.7 Transfer and phototoxic effect of T cell-delivered mTHPP

To characterize PSS/mTHPP-loaded T cells in more detail, first drug transfer from T lymphocytes to co-cultivated SKOV-3 ovary carcinoma cells was analyzed. In order to obtain strong fluorescence signals, the loading concentration was increased to 45 µg/mL. Furthermore, an incubation period of 3 h was chosen. Upon loading, T cells were washed three times with culture medium to remove non-internalized polymer-PS complex. Then, T lymphocytes were added to confluent SKOV-3 cells in a ratio of 4:1. After a co-cultivation period of 27.5 h, first the nuclear DNA was stained, before live cell microscopy was performed to visualize the distribution of the red fluorescent drug. Within the specified period of time, considerable amounts of mTHPP were transferred from loaded T lymphocytes to co-cultivated SKOV-3 cells as displayed in Figure 3.6A. Interestingly, the transferred photosensitizer was not equally distributed within tumor cells. As the images show, accumulation of the drug in the perinuclear region of SKOV-3 cells could be recognized. PS-uptake by tumor cells upon co-cultivation with PSS/mTHPP-loaded T lymphocytes was confirmed by flow cytometric analysis. In the 25-hour experiment shown in Figure S3.1 only SKOV-3 cells co-cultured with loaded T cells produced detectable fluorescence signals, whereas incubation with empty T lymphocytes did not result in an increase in fluorescence.

Finally, co-cultures of complex-loaded T lymphocytes and SKOV-3 cells were utilized to evaluate the phototoxic effect of T cell-delivered mTHPP on tumor cells. To prepare co-cultures, T lymphocytes were again loaded for 3 h with 45 µg/mL PSS-complexed mTHPP and, after ex-

tensive washing, added in three different ratios (1:1, 2:1 and 4:1) to SKOV-3 ovary carcinoma cells. As a control, tumor cells were also incubated with unloaded T cells. Moreover, blanks containing only loaded or unloaded T lymphocytes were prepared. To trigger the drug effect, a portion of the cultures was exposed twice to a 2-minute light pulse (after 16 and 20 h), while the remaining samples were constantly kept in the dark. After a total co-cultivation period of 24 h, a WST-1 assay was performed.

In the samples containing only T lymphocytes (= blanks), very low viability values were measured (compare Fig. S3.2). Thus, in the determination of cancer cell survival the T cell contribution to total viabilities could be neglected. However, in order to determine specifically SKOV-3 survival, first T cell blanks were subtracted from the measured overall viabilities, before in a second step all viability data obtained were related to the viability of untreated SKOV-3 cells which was set to 100%. Fig. 3.6B reveals that in co-cultures of SKOV-3 cells and PSS/mTHPP-loaded T lymphocytes cancer cell viability decreased significantly if samples were exposed to light. Furthermore, the strength of the phototoxic effect was dependent on the amount of loaded T cells used. In contrast, the viability of non-illuminated, drug-containing cancer cells was not affected indicating that in the dark the transferred photosensitizer was not cytotoxic. Similarly, tumor cells co-cultivated with empty T cells (control) were not impaired by light. Thus, a specific phototoxic effect of T cell-delivered mTHPP on co-cultivated tumor cells could be demonstrated.

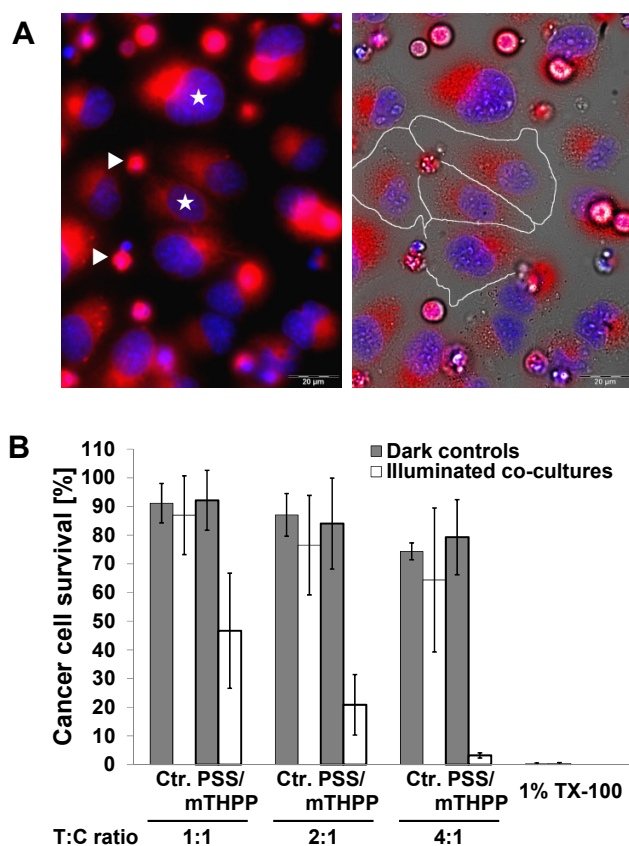


Fig. 3.6. Photosensitizer transfer from loaded T lymphocytes to co-cultivated cancer cells and phototoxic effect of T cell-delivered mTHPP. (A) mTHPP-transfer (red fluorescence) from loaded T lymphocytes (▶) to co-cultivated SKOV-3 ovary carcinoma cells (★) was visualized after 28 hours by live cell fluorescence microscopy. Nuclei were stained with Hoechst 33342 (in blue). Left panel: Fluorescence image. Right panel: Overlay of fluorescence and bright field images. White lines were drawn to highlight cell membranes of representative SKOV-3 cells. (B) To detect the phototoxic effect of T cell-delivered mTHPP, co-cultures containing unloaded (control) or PSS/mTHPP-loaded T lymphocytes were either illuminated twice (after 16 and 20 h) or not illuminated at all (dark controls). A WST-1 assay was performed to determine cancer cell survival in the individual cultures. To detect only the viability of SKOV-3 cells, T cell blanks were included in the calculation of viabilities. All viability data obtained were normalized to the viability of untreated SKOV-3 cells ($n = 3 \pm \text{SD}$). T:C ratio = T cell-to-cancer cell ratio, TX-100 = Triton X-100.

3.5 Discussion

Living cells can be utilized to transport therapeutics to diseased sites as demonstrated in various pre-clinical studies [12, 13]. However, severe adverse effects of anticancer agents on carrier cells have prevented the use of cellular drug vehicles in cancer therapy until now. To preserve viability and physiological functions of carrier cells, several strategies including encapsulation of active drugs in protective nanoparticles or the use of inducible therapeutics have been proposed [12]. The present study aimed to identify anticancer drug formulations which do not impair the viability of human T lymphocytes thus allowing the use of drug-loaded T cells for treating cancer. To ensure T cell survival, novel polymeric nanoparticles (NPs) loaded with an active chemotherapeutic agent and a polymer-complex of a stimulus-sensitive drug were tested.

For the first approach, a specific biocompatible polyester composed of diethylene glycol, dimethyl maleate and dimethyl sebacate monomers (maleate-based polyester, MPE) was synthesized to encapsulate the hydrophobic anthracycline idarubicin (IDA). In a physiological buffer MPE-

IDA nanoparticles displayed a minimal burst release of 15%, whereas reference NPs consisting of poly(lactic-*co*-glycolic-acid) (PLGA) and IDA lost half of the encapsulated drug, suggesting that MPE-IDA NPs were less leaky than PLGA-IDA NPs, and therefore, better suited to protect loaded T lymphocytes from the toxic effect of delivered IDA.

For the examination of particle uptake *ex vivo* activated, polyclonal human donor T lymphocytes were incubated with different concentrations of PLGA- and MPE-encapsulated IDA and subsequently analyzed by flow cytometry and fluorescence microscopy. Both techniques revealed efficient incorporation of the red fluorescent drug. However, irrespective of the particle type used the viability of loaded T cells substantially declined as determined by a standard cell viability assay. Thus, the polymeric drug encapsulations specifically prepared in this study did not exert a significant protective effect on loaded T lymphocytes. The observed decrease in T cell viability rather suggests that upon contact with T lymphocytes idarubicin was rapidly released from both nanoparticle preparations. Whether premature drug release from polyester-IDA NPs occurred early during the uptake process or after particle internalization cannot be decided on the basis of the experiments performed.

In order to protect loaded T lymphocytes more effectively from the toxic effect of encapsulated idarubicin, MPE-IDA nanoparticles were subsequently coated with a gold shell (AuSh) using a simple one-step deposition method. As shown in a parallel study, AuSh-IDA NPs containing an additional magnetite core were internalized well by human CaCo-2 colon carcinoma cells. 48 hours upon loading, only a slight cytotoxic effect (10%) was detected which was attributed to minor drug amounts released from a small fraction of non- or partially gold-coated nanoparticles (Schneider, personal communication). When in this study, activated human T lymphocytes were loaded with AuSh-IDA NPs without magnetite core, strong toxic effects were observed. Furthermore, the gold layer itself seemed to impair T cell viability. Thus, in contrast to CaCo-2 cells, which were only slightly affected by comparable particles, T cells did not tolerate the gold-coated MPE-IDA NPs specifically prepared for this work. Primary human T lymphocytes are, therefore, either more sensitive to idarubicin than CaCo-2 cells, or the proportion of non- and incompletely coated AuSh NPs was higher in this work than in the study conducted in parallel.

In accordance with our results, the viability of Jurkat T cells loaded with magnetite-starch-doxorubicin NPs was severely impaired [101]. Similarly, uptake of liposome-encapsulated doxorubicin had a negative impact on the survival of murine peritoneal macrophages [74]. Others, who studied immune cell-mediated transport of liposomal drug formulations did not analyze cell via-

bility ^[72] or showed only short-term survival data ^[74]. Even though therapeutic effects of defense cells loaded with free or encapsulated anticancer drugs were detected in tumor-bearing mice ^[6, 72, 74, 82], long-term survival of loaded carrier cells could not be demonstrated until now. Probably for this reason, clinical data are still missing. To test anticancer drug-loaded immune cells on human patients, cell viability and physiological functions need to be preserved. Research in this area, therefore, should focus on developing improved encapsulation strategies. Coating of polymeric NPs with a gold layer might help to reduce or even prevent premature drug release. Moreover, due to surface plasmon resonance in the near infrared AuSh NPs allow triggered release of enclosed pharmaceuticals ^[254]. Therefore, the AuSh-IDA nanoparticles presented in this work should be specifically optimized for use on primary human T lymphocytes.

In addition to improved encapsulation strategies for active drugs, stimulus-sensitive pharmaceuticals could help to ensure survival of cellular drug vehicles. Therefore, a recently developed hydrophilic polymer-formulation of the model photosensitizer (PS) 5,10,15,20-tetrakis(3-hydroxyphenyl)porphyrin (mTHPP) was included in the present study ^[193]. Like its clinically approved derivative 5,10,15,20-tetrakis(3-hydroxyphenyl) chlorin (mTHPC, the active pharmaceutical ingredient of Foscan), mTHPP shows virtually no dark toxicity. However, upon photo-activation, the precursor generates reactive oxygen species (ROS) which can destroy cells and tissues ^[192]. While mTHPP has been used in many basic studies ^[153], mTHPC is clinically applied in photodynamic therapies (PDT) to treat malignancies such as head and neck, lung, and skin cancer ^[165].

In the present work, uptake of a water-soluble poly(styrene sulfonate) (PSS)-complex of mTHPP by activated polyclonal human T lymphocytes was demonstrated using flow cytometry and fluorescence microscopy. In contrast to polyester-IDA NP-loaded T cells, lymphocytes incubated with PSS/mTHPP survived for at least 4 days if the cells were cultivated in the dark. However, immediate or time-delayed irradiation with a tungsten halogen light induced massive cell death. Thus, PSS/mTHPP-loaded T lymphocytes were protected against their toxic payload, until the drug effect was specifically activated.

Using live cell fluorescence microscopy, PS-transfer from loaded T lymphocytes to co-cultivated SKOV-3 ovary carcinoma cells could be demonstrated. Upon transfer, the red fluorescent drug accumulated in the perinuclear region which is consistent with findings of Teiten and colleagues who localized Foscan specifically in the endoplasmic reticulum and Golgi apparatus of MCF-7 breast cancer cells ^[255]. Furthermore, by illuminating co-cultures of complex-loaded T cells and

SKOV-3 cells, a specific phototoxic effect of T cell-delivered mTHPP on co-cultivated tumor cells could be detected. In view of these promising initial results, more detailed studies on PSS/mTHPP-loaded T lymphocytes need to follow.

In 1994, a work about photosensitizer- and methotrexate-loaded rabbit erythrocytes was published. Light-activated release of the chemotherapeutic agent as well as a combined chemophototherapy effect on co-cultivated HeLa cells was observed [47]. Despite these promising *in vitro* results, the erythrocyte-based drug delivery system was not further developed, possibly because red blood cells do not possess any targeting capabilities. In contrast, polyclonal T lymphocytes can be redirected to various tumors either using a bispecific antibody (bsAb) as retargeting device or by genetic engineering yielding chimeric antigen receptor (CAR)-expressing T cells [7, 256]. CAR- or bsAb-mediated binding of activated, polyclonal T cells to target cells stimulates the cytolytic activity of cytotoxic T lymphocytes. Consequently, in a cancer immunotherapy involving redirected, photosensitizer-loaded T cells the carrier cells would first exert their natural killing function, before the tumor is irradiated to activate the delivered drug. Thus, tumors would be eliminated through the consecutive action of redirected, cytotoxic T lymphocytes and a cell-delivered, light-activated photosensitizing agent. The cytotoxic T cell effect that can be exploited using a retargeting strategy makes polyclonal T lymphocytes superior to erythrocytes and other cells serving merely as drug carriers. Most importantly, by loading T cells with a light-inducible agent, we have found a way to preserve T cell viability.

Hence, polymeric photosensitizer formulations such as PSS/mTHPP might help to overcome the drawbacks of existing cellular delivery systems for anticancer drugs. At the same time redirected, PS-loaded T lymphocytes open up new perspectives in the area of T cell therapy. Furthermore, the selectivity of photodynamic therapy (PDT) could be improved by using living cells as transport vehicles for photosensitizing agents.

3.6 Conclusions

Neither polyester-based polymeric drug encapsulations nor gold shell-coated polyester nanoparticles were able to protect activated human T lymphocytes from the toxic effect of the active chemotherapeutic agent idarubicin. In contrast, uptake of the polymer-photosensitizer complex PSS/mTHPP did not impair T cell viability as long as the cells were kept in the dark. However,

upon exposure to light PSS/mTHPP-loaded T lymphocytes as well as co-cultivated cancer cells was efficiently killed. Thus, by loading living cells with a polymeric formulation of a light-inducible anticancer drug, we provide a promising new way to prevent premature death of carrier cells, which has been a main drawback of cell-mediated drug delivery until now.

3.7 Supplementary Information

3.7.1 Analysis of PS-transfer from T cells to cancer cells by flow cytometry

SKOV-3 ovary carcinoma cells resuspended in RPMI 1640 medium w/o phenol red supplemented with 10% FBS and antibiotics were seeded in 24-well cell culture plates and allowed to adhere for at least 3 h. Then, SKOV-3 cells were treated in triplicate with PSS/mTHPP-loaded T cells (45 $\mu\text{g/mL}$, 3 h) at an T cell-to-cancer cell (T:C) ratio of 2:1 and 4:1. As control, cancer cells were also treated with medium and unloaded (empty) T cells (T:C = 4:1). Co-cultures were incubated for 25 h at 37°C/5% CO₂, before cells were rinsed three times with PBS. Subsequently, cells were detached using 0.05% trypsin/0.02% EDTA (PAN Biotech) and resuspended in ice-cold FCM buffer (Miltenyi Biotec). To label the T cell population, a fluorescein-isothiocyanate (FITC)-conjugated anti-CD3 antibody (0.1 mg/ml, Bio-Rad AbD Serotec, Puchheim, Germany) was added to all samples. After 30 min at room temperature, cells were analyzed in a FACS Calibur flow-cytometer (BD Biosciences). 10,000 events were acquired using the CellQuest Pro software (BD Biosciences). First, the bulk of T cells were excluded by gating SKOV-3 cells in a FSC-SSC dot plot. Then, remaining green fluorescent T lymphocytes were removed from analysis by a second gating of only cancer cells in a FSC-FL1 dot plot, before fluorescence intensities of gated SKOV-3 cells were determined in the FL3 channel.

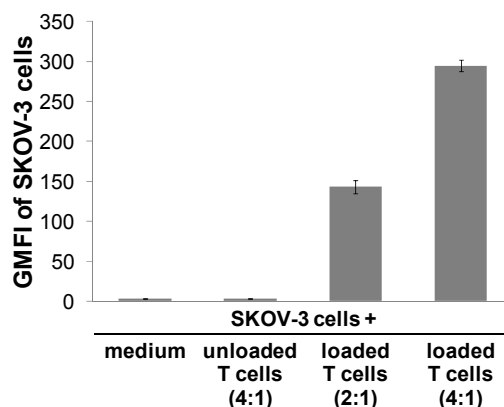


Fig. S3.1. Flow-cytometry analysis of photosensitizer uptake by SKOV-3 ovary carcinoma cells upon co-cultivation with PSS/mTHPP-loaded T lymphocytes. T cell-to-cancer cell ratios in the 25-hour co-culture experiment were 2:1 and 4:1. Fluorescence intensities of gated cancer cell populations are expressed as GeoMean of fluorescence intensity (GMFI) values \pm SD. One representative experiment is shown.

3.7.2 Phototoxic effect of T cell-delivered mTHPP on cancer cells

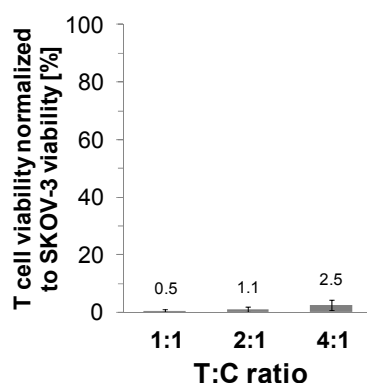


Fig. S3.2. The viabilities of PSS/mTHPP-loaded T cells prepared as blanks for dark controls (= non-illuminated SKOV-3 cells) were normalized to the calculated cancer cell viabilities (compare Fig. 3.6B). Data represent the means of three independently performed experiments \pm SD. T:C ratio = T cell-to-cancer cell ratio.

3.7.3 Characterization of poly(diethylene glycol-maleate-co-sebacate)ester (MPE)

The polymer was characterized by DSC, GPC and C/H-NMR. NMR results were: $^1\text{H-NMR}$ (DMSO- d_6 , 400 MHz): δ = 1.23 (bs, $\text{CH}_2\text{-Seb}$), 1.49 (bs, $\text{CH}_2\text{-Seb}$), 2.24 (t, $\text{CH}_2\text{-Seb}$), 3.58-3.67 (m, $\text{CH}_2\text{O-DEG}$, OMe), 4.10 (t, $\text{CH}_2\text{OCO-DEG}$), 4.20 ($\text{CH}_2\text{OH-DEG}$), 6.47 (bs, C=C , Mal); $^{13}\text{C-NMR}$ (DMSO- d_6 , 100 MHz): δ = 24.4, 28.4, 28.5, 33.2 ($\text{CH}_2\text{-Seb}$), 51.0 (OMe), 60.2, 62.9, 63.8 ($\text{CH}_2\text{OCO-TEG}$), 67.9, 68.2, 69.7, 72.2 ($\text{CH}_2\text{O-TEG}$), 130.1 (C=C , Mal), 164.9, 172.7 (C=O). GPC for molecular weight and PDI measurement: M_n = 8000, M_w = 16000 Dalton. The polydispersity index (PDI) of MPE was 2.1.

4. Detailed analysis of interactions of PSS/mTHPP with human T lymphocytes and bispecific antibody mediated redirection of PSS/mTHPP-loaded T cells to carcinoma cells

Parts of this chapter were published in:

Blaudszun A.-R., Moldenhauer G., Schneider M., Philippi A. (2015)

A photosensitizer delivered by bispecific antibody retargeted human T lymphocytes enhances cytotoxicity against carcinoma cells upon light irradiation

Journal of Controlled Release; 197: 58-68

4.1 Abstract

Recently conducted clinical trials have provided impressive evidence that chemotherapy resistant metastatic melanoma and several hematological malignancies can be cured using adoptive T cell therapy or T cell-recruiting bispecific antibodies. However, a significant fraction of patients did not benefit from these treatments. Here we have evaluated the feasibility of a novel combination therapy which aims to further enhance the killing potential of bispecific antibody-redirectioned T lymphocytes by using these cells as targeted delivery system for photosensitizing agents. For a first *in vitro* proof-of-concept study, *ex vivo* activated human donor T cells were loaded with a poly(styrene sulfonate) (PSS)-complex of the model photosensitizer 5,10,15,20-tetrakis(3-hydroxyphenyl)porphyrin (mTHPP).

In the absence of light and when loading with the water-soluble PSS/mTHPP-complex occurred at a tolerable concentration, viability and cytotoxic function of loaded T lymphocytes were not impaired. When “drug-enhanced” T cells were co-cultivated with EpCAM-expressing human carcinoma cells, mTHPP was transferred to target cells. Notably, in the presence of a bispecific antibody, which cross-links effector and target cells thereby inducing the cytolytic activity of cytotoxic T lymphocytes, significantly more photosensitizer was transferred. Consequently, upon irradiation of co-cultures, redirectioned drug-loaded T cells were more effective in killing A549 lung and SKOV-3 ovarian carcinoma cells than retargeted unloaded T lymphocytes. Particularly, the additive approach using redirectioned unloaded T cells in combination with appropriate amounts of

separately applied PSS/mTHPP was less efficient, as well. Thus, by loading T lymphocytes with a stimulus-sensitive anticancer drug, we were able to enhance the cytotoxic capacity of carrier cells. Photosensitizer boosted T cells could open new perspectives for adoptive T cell therapy as well as targeted photodynamic therapy.

4.2 Introduction

Although chemotherapy, radiation therapy and surgery are the primary modalities to treat cancer, limitations such as systemic toxicity and drug resistance, limited repeatability of treatments and inoperable tumors, respectively, have motivated investigators to seek alternative therapies. Photodynamic therapy (PDT) is such an emerging treatment, in which a light-sensitive photosensitizer (PS) is either topically or systemically administered. After a latency period, the malignant lesions are selectively irradiated with light of a specific wavelength, thereby exciting the photosensitizing agent. In the presence of oxygen, activated PS-molecules generate singlet oxygen ($^1\text{O}_2$) and reactive oxygen species (ROS), which provoke lethal oxidative damage in aberrant cells. In addition, PDT also causes damage to the tumor vasculature and evokes immune responses, which contribute to tumor destruction as well [165, 257, 258]. However, tumor selectivity after systemic application of classical photosensitizers is limited and healthy tissues also accumulate PS [169]. The general distribution of PS leads to adverse effects, like prolonged eye and skin photosensitivity. To circumvent these obstacles, several tumor-targeting PDT strategies are under investigation [170].

Adoptive transfer of tumor-specific T lymphocytes (ACT) is another alternative for treatment of cancer and has shown curative potential [1]. It has been proven to be effective in clinical trials with hematological malignancies (complete remissions in two of three patients [21], remissions in six of eight patients [22]), metastatic melanoma (durable complete responses in 20 of 93 patients [2]) and other types of neoplastic diseases [23]. In these trials, tumor-reactive autologous tumor-infiltrating lymphocytes (TILs) or patient-derived genetically engineered T cells were used for ACT. Transduced T lymphocytes have been redirected towards tumor-associated antigens (TAAs) through genetic modification with T cell receptor (TCR) or chimeric antigen receptor (CAR) genes [24]. A different option to guide T lymphocytes to sites of malignancies is the utilization of bispecific antibodies (bsAb). These engineered molecules possess dual specificity for two

different antigens. One antigen-binding site of bsAb recognizes a surface marker, such as a TAA, on the target cell. In T lymphocyte-based therapies, the other moiety binds specifically to a component of CD3, a signaling complex located on the plasma membrane of T cells. At the target site, bsAb-molecules cross-link effector to target cells thereby inducing the cytolytic activity of cytotoxic T lymphocytes (CTLs) in a non-major histocompatibility complex-restricted manner [7]. Adoptive cell therapy with TILs has been proven successful in treatment of metastatic melanoma. However, long-term follow-up data revealed that not all patients could benefit from ACT (5-year survival rate was 29% [2]). Moreover, not all tumors generate TILs which are appropriate for ACT [25]. Notably, even though transduced T cells have been shown very effective against hematological malignancies, solid tumors represent a major obstacle for successful treatments [24]. Thus, further improvements are necessary to increase the curative potential of ACT.

Since immune cells possess an intrinsic homing capability and are able to migrate to sites of inflammation initiated by injury, infection or neoplasms, cell-mediated drug delivery has emerged as an alternative to classical drug delivery strategies based on artificial drug carriers [12]. Considering the tumor-specificity of redirected T lymphocytes, we propose that a targeted PTD approach involving bsAb-guided T cells as a living drug delivery system to transport photosensitizing agents to tumor sites will be promising. The concept aims at enhancing the selectivity and efficacy of PDT for cancer, while simultaneously reducing adverse effects. Notably, the approach intends to combine the phototoxicity of PS-molecules delivered by redirected CD3+CD4+ helper T cells and CD3+CD8+ cytotoxic T lymphocytes (drug effect) with the cytotoxicity of retargeted CTLs (T cell effect) in a synergistic manner (compare Fig. 4.1).

The photosensitizer 5,10,15,20-tetrakis(3-hydroxyphenyl)-porphyrin (mTHPP) is the parent porphyrin of the second-generation photosensitizer mTHPC (the active pharmaceutical ingredient of Foscan, approved for PDT in Europe) and is often used as model PS in basic research [153]. Recently, preparation of a water-soluble complex (PSS/mTHPP) composed of hydrophobic mTHPP and poly(styrene sulfonate) sodium salt (PSS) was reported [193]. In a previous work, we have shown that PSS/mTHPP is internalized and tolerated by human T lymphocytes. In addition, un-specific mTHPP transfer from loaded T cells to SKOV-3 ovarian carcinoma cells was observed, which impaired cancer cell proliferation after illumination *in vitro* [260]. In the present study, we demonstrate that a PSS/mTHPP payload did not impair the cytolytic function of T cells. Moreover, the bispecific antibody HEA125×OKT3 (EpCAM×CD3 [8, 10]) was used to redirect PS-loaded T lymphocytes to epithelial cell adhesion molecule (EpCAM, CD326) expressing carcinoma cells

in vitro. We show that these retargeted photosensitizer enhanced T cells were more efficient in killing tumor cells than non-redirected loaded and bsAb-guided unloaded T lymphocytes. Notably, the additive approach using redirected unloaded T cells in combination with separately applied PS-complex equal to the amount of mTHPP carried by T lymphocytes was less effective, as well. Thus, the combined cytotoxicity of transferred drug and T cells exhibited synergistic anti-tumor effects. Our findings support the feasibility of the envisioned T cell-based targeted PDT approach.

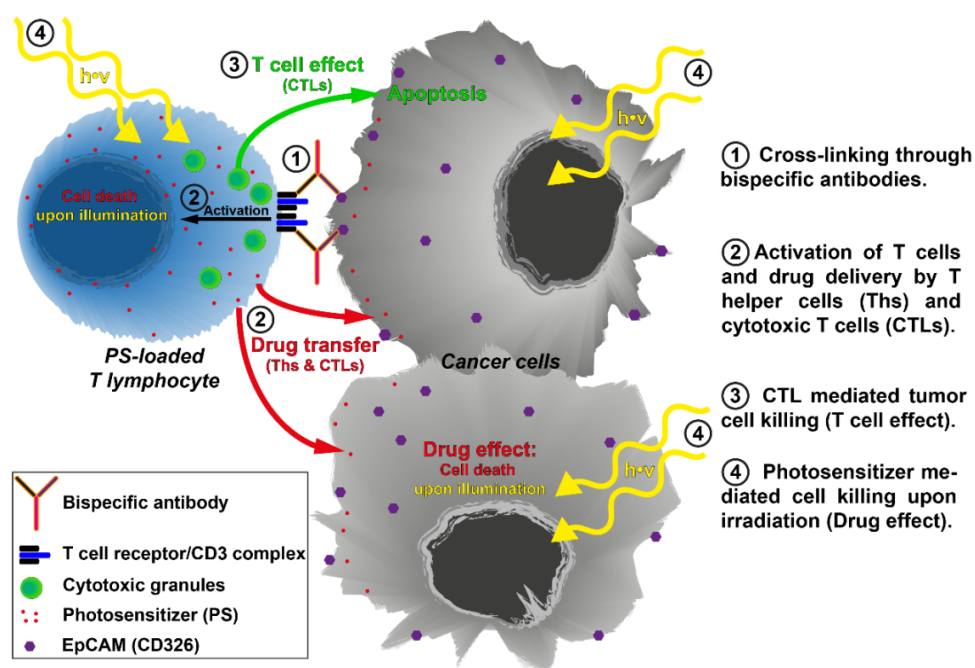


Fig. 4.1. Schematic illustration of the proposed mode of action of the T cell-based targeted PDT approach.

4.3 Materials and methods

4.3.1 T cell isolation, activation and expansion

Human T lymphocytes were prepared as previously described [231]. In brief, CD3⁺, CD4⁺ and CD8⁺ T cells were isolated from buffy coat preparations by using the respective RosetteSep Kits (StemCell Technologies, Grenoble, France) according to the manufacturer's instructions. Informed consent for the use of buffy coats was obtained from healthy donors. After isolation, remaining red blood cells were lysed with 3 mL of an ammonium chloride-based lysing buffer (BD Pharm Lyse, BD Biosciences, Heidelberg, Germany). Enriched T lymphocytes were resuspended

in cell culture medium (i.e., RPMI 1640 medium (PAN Biotech, Aidenbach, Germany) containing 10% (v/v) heat-inactivated FBS (PAN Biotech), 100 U/mL penicillin and 0.1 mg/mL streptomycin (Sigma-Aldrich, Steinheim, Germany)). T cells were activated using MACSiBeads functionalized with antibodies against human CD2, CD3, and CD28 (MACS T Cell Activation/Expansion Kit, Miltenyi Biotec, Bergisch Gladbach, Germany) at a density of 2.5×10^6 cells/mL according to the manufacturer's instructions. Expansion of T lymphocytes was achieved by suspending cells in fresh cell culture medium containing 20 U/mL of recombinant human Interleukin-2 (IL-2, PAN Biotech) at a density of 2.5×10^6 cells/mL 3 days after activation. Five to six days after stimulation, beads were removed from cultures by density gradient centrifugation using Pancoll (human, PAN Biotech) as separating solution. T lymphocytes were resuspended in fresh cell culture medium with 20 U/mL of IL-2 at a density of 2.5×10^6 cells/mL. Purity of expanded CD4⁺ and CD8⁺ T lymphocytes was determined by flow cytometry (FACSCalibur, BD Biosciences) using 5 μ g/mL FITC-conjugated antibodies against human CD4 or CD8 (Bio-Rad AbD Serotec, Puchheim, Germany) (see Supplementary Information, Fig. S4.1).

4.3.2 Tumor cell lines

Cells of the human lung carcinoma cell line A549 (CCL-185, American Type Culture Collection (ATCC), Manassas, VA, USA) and of the human ovary adenocarcinoma cell line SKOV-3 (HTB-77, ATCC) were maintained in cell culture medium (i.e., RPMI 1640 medium (PAN Biotech) containing 10% (v/v) heat-inactivated FBS (PAN Biotech), 100 U/mL penicillin and 0.1 mg/mL streptomycin (Sigma-Aldrich) at 37 °C in a humidified atmosphere with 5% CO₂.

4.3.3 Fluorimetric calibration of complexed mTHPP

Biolitec AG (Jena, Germany) kindly supplied 5,10,15,20-tetrakis(3-hydroxyphenyl)-porphyrin (mTHPP, MW = 678.75 g/mol). To determine mTHPP content of different PS-complex preparations a mean calibration curve derived from solutions of pure mTHPP was used (Fig. S4.2A, see Supplementary Information, section 4.6). To this end, triplicate split samples of mTHPP were dissolved in ice-cold ethyl acetate (UV/IR-grade, Carl Roth, Karlsruhe, Germany) to produce stock solutions with a concentration of 1 mg/mL. Serial dilutions of each split sample were prepared in duplicate in a cooled black 96-well polypropylene (PP) microplate with flat bottoms (Greiner Bio-One, Frickenhausen, Germany). Fluorescence of 100 μ L aliquots of serial mTHPP-solutions were measured in duplicate using a Modulus Microplate Multimode Reader (Promega,

Mannheim, Germany). Aliquots of pure ethyl acetate served as blanks. Fluorescence intensities of samples were measured (red optical kit: excitation wavelength $\lambda_{ex} = 625$ nm; emission wavelengths $\lambda_{em} = 660-720$ nm) using a Modulus Microplate Multimode Reader (Promega).

Complexed mTHPP was kindly provided by Hagar Ibrahim Labouta (Helmholtz Institute for Pharmaceutical Research Saarland (HIPS), Saarland University, Germany). Split samples of PSS/mTHPP lyophilizate preparations with defined masses of approximately 1 mg were dissolved in 500 μ L of purified water obtained from an Elix3 (UV) water purification system (Merck Millipore, Darmstadt, Germany) in silanized glass vials (Medchrom, Flörsheim-Dalsheim, Germany). The drug was extracted by adding 400 μ L of ethyl acetate to the aqueous phase followed by vigorous mixing. The vials were placed in tubes (50 mL, Greiner Bio-One) and the biphasic organic-aqueous solvent system was briefly centrifuged ($1000 \times g$ for 0.5 min, 5810, Eppendorf, Hamburg, Germany). Afterwards the organic solvent was aspirated and extraction procedure was repeated four times. All drug containing supernatants were pooled. Extracted mTHPP was dried in a desiccator attached to a diaphragm pump (MZ 2C, Vacuubrand, Wertheim, Germany) by solvent evaporation at 20 mbar for around 3 h. Each dried PS sample was dissolved in a defined volume of ice-cold ethyl acetate. For each extract 1:10-dilutions were prepared in triplicate and the fluorescence emissions of 100 μ L aliquots of dilutions were measured in triplicate (= 9 measured values per extraction-sample). Pure ethyl acetate (also in triplicate) served as blanks. To calculate the total mTHPP mass of PSS/mTHPP-complex samples the concentration of extracted and dissolved mTHPP was determined using the calibration curve. The ratio of PSS/mTHPP mass per mTHPP mass obtained from two PS-complex preparations is shown in Fig. S4.2B & S4.2C. All PS-complex stock solutions could now be adjusted to 1 mg mTHPP per mL. For all experiments the concentration of mTHPP and not of PSS/mTHPP is indicated.

4.3.4 Preparation and handling of PSS/mTHPP-complex

Poly(styrene sulfonate) sodium salt (PSS, MW = 4.23 kDa) was purchased from Sigma-Aldrich. PSS/mTHPP-complex was kindly provided by Hagar Ibrahim Labouta (Helmholtz Institute for Pharmaceutical Research Saarland (HIPS), Saarland University, Germany) and prepared as described before ^[193]. After calibration of complex preparations, lyophilized PSS/mTHPP-complex was dissolved in purified water as stock solution containing 1 mg mTHPP per mL. Specified concentrations refer to pure mTHPP. Experiments involving PS-complex were prepared using an

LED light source (SBAR I, TPL Vision, La Chevrolière, France) with a peak wavelength of 588 nm. (UV/Vis spectra of PSS/mTHPP are provided in the Supplementary Information, Fig. S4.3). Direct exposure to LED light was avoided. Incubations were performed protected from light to prevent premature activation of mTHPP at 37 °C in a humidified atmosphere containing 5% CO₂.

4.3.5 Loading of peripheral blood CD3+, CD4+ and CD8+ T lymphocytes

T cells were loaded with PSS/mTHPP in cell culture medium (compare section 4.3.2) at a density of 2.5×10^6 cells/mL. If not otherwise indicated, T lymphocytes were treated with 25 µg/mL of complexed mTHPP for 2 h at 37 °C/5% CO₂. Cells were sedimented ($300 \times g$ and 4 °C for 10 min, centrifuge 5810 R, Eppendorf, Germany) and washed three times with ice-cold supplemented RPMI 1640 to remove non-internalized drug. T lymphocytes not immediately processed were stored on ice protected from light.

4.3.6 Fluorimetric quantitative determination of mTHPP mass in CD3+ T lymphocytes

2×10^7 CD3+ T cells were loaded in duplicate with PSS/mTHPP. As control 2×10^7 T lymphocytes were also incubated in cell culture medium. Afterwards, T lymphocytes were washed three times as described before. Cell sediments were resuspended in 400 µl of PBS and cell concentration was determined using an automated cell counter (CASY Model TT, OMNI Life Science, Bremen, Germany). Moreover, to calculate the precise number of loaded T lymphocytes, the suspension volume was determined by weighing a reference sample with a defined volume of cell suspension. After adding 100 µL of cell culture lysis reagent (Promega) T cells were lysed for 30 min. Then, 400 µL of ethyl acetate was added to extract mTHPP and samples were vigorously mixed. The biphasic organic-aqueous solvent system was centrifuged at $16100 \times g$ for 5 min (5415 R, Eppendorf). The ethyl acetate phase was aspirated and collected. Extraction procedure was repeated three times and pooled samples were vacuum dried. Extracts were resuspended in 1 mL of ice-cold ethyl acetate. Fluorescence intensities of samples were measured (red optical kit: excitation wavelength $\lambda_{ex} = 625$ nm; emission wavelengths $\lambda_{em} = 660-720$ nm) in triplicate using a Modulus Microplate Multimode Reader (Promega). Extracts obtained from unloaded T lymphocytes served as blanks. A calibration curve of pure mTHPP (Fig. S1A, see Supplementary Information, section 4.6) was used to determine the total mass of PS. This value was also used to calculate the uptake efficiency. It should be noted that mTHPP of

T cells which had been used to determine the cell concentration after the loading process, were lost prior to the ethyl acetate extraction. Hence, all respective values were corrected accordingly. The average mass of mTHPP, taken up by a single T cell, was calculated by dividing the total mTHPP mass by the number of extracted cells.

4.3.7 Flow cytometric analysis of mTHPP uptake by CD3+ T lymphocytes

CD3+ T cells were loaded in duplicate for different periods with indicated concentrations of PSS/mTHPP at 4 °C or at 37 °C. As control, T lymphocytes were treated with an appropriate but small aliquot of purified water. Prior to treatment, cells were either pre-chilled or pre-warmed at 4 °C or at 37 °C, respectively. After washing, T cells were resuspended in ice-cold flow cytometer (FCM) buffer (MACS Buffer containing 2 mM EDTA and 0.5% BSA (Miltenyi Biotec) supplemented with 0.1% NaN₃ (Sigma-Aldrich)). Fluorescence intensities ($\lambda_{\text{ex}} = 488 \text{ nm}$, $\lambda_{\text{em}} > 670 \text{ nm}$) of 10,000 events were measured using a FACSCalibur cytometer (BD Biosciences, Heidelberg, Germany) controlled by CellQuest Pro software (BD Biosciences). Geometric means (GeoMean) of fluorescence intensities (GMFI) derived from gated populations were calculated with FlowJo software (Tree Star, Ashland, OR, USA) and normalized to the maximum GMFI.

4.3.8 Fluorescence microscopy of loaded CD3+ T cells

Nuclei of CD3+ T lymphocytes were stained in supplemented RPMI 1640 (w/o phenol red (PR), PAN Biotech) containing 10 $\mu\text{g/mL}$ of Hoechst dye (Hoechst 33342, trihydrochloride, trihydrate, Life Technologies, Darmstadt, Germany) at 37 °C in the dark for 30 min. After washing, cell membranes were stained with fluorescein-isothiocyanate (FITC)-labeled anti-CD3-mAb (0.1 mg/mL, Bio-Rad AbD Serotec, Puchheim, Germany) in FCM buffer at room temperature for 30 min. Washed T lymphocytes were resuspended in ice-cold FCM buffer. Around 3×10^5 cells per well were seeded onto black μClear 96-well microplates (Greiner Bio-One) and sedimented ($300 \times g$, 4 °C for 5 min) again. T cells were imaged using a digital camera (F-View II, Olympus, Hamburg, Germany) controlled by cell^P imaging software (Olympus) and attached to an IX71 inverted microscope (Olympus) equipped with a 60 \times PlanApo N oil-immersion objective (Olympus; NA of 1.42). Immersion oil Immersol 518N (Carl Zeiss Microscopy GmbH, Göttingen, Germany) was used. Image overlays illustrating blue (Hoechst dye; $\lambda_{\text{ex}} = 360\text{-}370 \text{ nm}$; $\lambda_{\text{em}} > 420 \text{ nm}$), green (anti-CD3-mAb; $\lambda_{\text{ex}} = 460\text{-}490 \text{ nm}$; $\lambda_{\text{em}} = 510\text{-}550 \text{ nm}$), and red fluorescence (mTHPP; $\lambda_{\text{ex}} = 510\text{-}550 \text{ nm}$; $\lambda_{\text{em}} > 590 \text{ nm}$) were generated via cell^P imaging software.

4.3.9 Bispecific antibody EpCAM×CD3

BsAb was kindly provided by Gerhard Moldenhauer (Department of Translational Immunology, German Cancer Research Center and National Center for Tumor Diseases, Heidelberg, Germany) and was produced as previously described¹¹⁰. A concentration of 0.1 µg bsAb/mL was used in all experiments.

4.3.10 Flow cytometric analysis of drug transfer

2×10^5 A549 cells resuspended in 400 µl of supplemented RPMI 1640 (w/o PR) were seeded onto wells of 24-well cell culture plates (Greiner Bio-One) and were allowed to adhere for at least 3 h. CD3⁺ T cells were labeled with 0.2 µM CFSE (5-(and-6)-carboxyfluorescein diacetate, succinimidyl ester, mixed isoforms (Life Technologies); 10 mM in DMSO (Hybri-Max grade, Sigma-Aldrich)). To this end, sedimented T lymphocytes were resuspended in pre-warmed phosphate buffered saline (PBS, Life Technologies) containing 0.2 µM CFSE and were incubated in the dark at 37 °C for 15 min. Afterwards, cells were centrifuged again and supernatant was discarded. Then, cells were resuspended in pre-warmed supplemented RPMI 1640, incubated protected from light at 37 °C for another 30 min and washed. A549 cells were treated in duplicate with CFSE-labeled and loaded T cells at an effector to target cell ratio (E:T ratio) of 2:1 either with or without bsAb. Co-cultures were incubated for increasing periods as indicated. After each time point, cells were rinsed with PBS. Subsequently, cells were trypsinized (0.05% trypsin/0.02% EDTA (PAN Biotech)) and after washing resuspended in ice-cold FCM buffer. Ten thousand events were accumulated via live gating in a predefined cancer cell gate. The bulk of T cells were excluded by gating A549 cells in an FSC-SSC dot plot. Remaining green fluorescent T lymphocytes were removed from analysis by a second gating of only cancer cells in an FSC-FL1 dot plot. GeoMean of red fluorescence intensities ($\lambda_{ex} = 488$ nm, $\lambda_{em} > 670$ nm) derived from successively gated A549 cell populations were determined and normalized to the maximum GMFI.

4.3.11 Fluorescence microscopic analysis of drug transfer

Co-cultures were prepared as described in the previous section but incubated in black µClear 96-well microplates for either 2 h or 22 h. A549 cells were also rinsed but not trypsinized. Imaging of cells was conducted as already described in section 4.3.8, but with one different dye (CFSE:

$\lambda_{\text{ex}} = 460\text{-}490\text{ nm}$; $\lambda_{\text{em}} = 510\text{-}550\text{ nm}$). To compare mTHPP fluorescence intensities, cells were imaged using the same conditions (automatic gain disabled, exposure time = 50 ms).

4.3.12 Viability assay

CD3⁺ T lymphocytes were loaded with different concentrations of PSS/mTHPP up to 45 $\mu\text{g}/\text{mL}$ for 2 h. Cells were also incubated with 0.2 mg/mL of PSS (MW = 4.23 kDa, Sigma-Aldrich). Upon loading and washing, cell concentration was determined and T lymphocytes were adjusted to a density of 2.5×10^6 cells/mL. Subsequently, 100 μL of cell suspensions was transferred in triplicate into wells of 96-well microplates (for suspension cells, Greiner Bio-One). As negative control or as positive control cell culture medium or a detergent (Triton X-100, 1% (v/v), Merck Millipore, Darmstadt, Germany) was used, respectively. To determine the bioreductive activity [238] of cells, WST-1 colorimetric assays (Roche, Mannheim, Germany) were performed according to the manufacturer's instructions. In brief, 10 μL of WST-1 reagent was added to samples 2 h before the end of the incubation period. Background controls contained the corresponding medium and WST-1 reagent. Absorbance of samples was measured against background controls at a wavelength of 450 nm (reference: 690 nm) using an absorbance reader (Spectra Rainbow Thermo, Tecan, Crailsheim, Germany). Values of mean absorbance derived from negative control samples represented 100% bioreductive activity denoted as viability.

4.3.13 Cytotoxicity assay

SKOV-3 cells suspended in 50 μl of supplemented RPMI 1640 (w/o phenol red) were seeded onto 96-well cell culture plates (Greiner Bio-One) at a density of 40,000 cells per well. After 3 h, 80,000 unloaded or PSS/mTHPP loaded CD3⁺ T lymphocytes also suspended in 50 μl of cell culture medium containing bsAb but devoid of PR were added in triplicate. To remove the contribution of effector cells to the absorbance measured in co-cultures, wells containing only loaded or unloaded T cells and bsAb served as blanks (similar as shown in [261]). As positive control or as negative control, tumor cells were treated in triplicate with Triton X-100 (2% (v/v)) or with supplemented RPMI 1640 (w/o PR), respectively. WST-1 assays were started 30 min before the end of indicated incubation periods. The percentage of cancer cell viability for each time point was calculated via the following equation:

$$\% \text{ viability} = 100 \times \frac{(A \text{ of co-cultures}) - (A \text{ of effectors alone})}{(A \text{ of targets alone})}$$

Where A represents the mean absorbance of samples minus the mean absorbance of background controls.

4.3.14 Cytotoxicity assay after light irradiation

Tumor cells were prepared as aforementioned and were treated in triplicate with bsAb and either unloaded CD3⁺ T cells, PSS/mTHPP loaded CD3⁺ T cells or unloaded CD3⁺ T cells plus separately applied PSS/mTHPP (final concentration = 0.23 µg/mL) at an E:T ratio of 2 to 1. The concentration of added PS was deduced from the greatest determined value for the internalized mass of mTHPP per T cell (0.29 pg, Fig. 4.2D, donor 2). As control, tumor cells were co-incubated with unloaded or loaded CD3⁺ T lymphocytes. Appropriate background controls were prepared as well. WST-1 assays were performed 20 min (for A549 cells) or 30 min (for SKOV-3 cells) before the end of indicated incubation periods. To activate the photosensitizer, co-cultures were exposed to a fluence of 8.3 J/cm² applied over a period of 15 min using a tungsten halogen light source (Haloline Eco, 400 W, 9000 lm, Osram, München, Germany) 2 hours before absorbance measurements. Co-cultures which were measured after one hour had not been irradiated. Percentages of cancer cell viability were determined using the aforementioned equation (section 4.3.13). Absorbance of mTHPP internalized by CD3⁺ T cells and of separately applied mTHPP and was negligible (see Supplementary Information, Fig. S4.4A & B). Cytotoxicity assay was repeated with A549 cells co-cultured either with loaded CD4⁺ or loaded CD8⁺ T lymphocytes.

4.3.15 Viability assay after incubation with supernatants obtained from loaded CD3⁺ T cells

After loading and washing of CD3⁺ T cells, cell density was adjusted to 1.6×10⁶ cells/mL using ice-cold medium (w/o PR). Cell suspensions were divided into several aliquots, which were transferred into wells of 24-well microplates for suspension cells (Nunc, Thermo Fisher Scientific, Roskilde, Denmark). Samples were collected after culturing for 0 h, 2 h, 6 h, 14 h, 22 h and 46 h at 37 °C / 5% CO₂ protected from light. Cells were sedimented and aspirated supernatants were stored at 4 °C. Unloaded T cells were used as control. Solutions composed of supplemented RPMI 1640 (w/o PR) containing either 0.46 µg/mL or 2 µg/mL of complexed mTHPP were also prepared. Aliquots of these solutions were collected and stored at 4 °C after the same incubation

periods. 40,000 A549 cells were prepared as described before and treated in triplicate with 50 μ l of supernatants and of PSS/mTHPP-solutions. Background controls were prepared accordingly. The experiment was exactly carried out like the cytotoxicity assay described in the previous section including a corresponding illumination schedule. For instance, samples which had been treated with supernatants collected after 6 h were also irradiated after an incubation period of 6 h.

4.3.16 Fluorimetric detection of mTHPP

Supernatants were transferred in duplicate into wells of a black 96-well microplate with flat bottoms (Greiner Bio-One). In an additional experiment, solutions composed of supplemented RPMI 1640 (w/o PR) containing either 0.2 μ g/mL or 0.46 μ g/mL of complexed mTHPP were prepared and aliquots of these solutions were collected and stored at 4 °C after the same incubation periods indicated in the previous section. Aliquots of cell culture medium were processed in the same way. Fluorescence emissions of samples were detected using the red optical kit of the Modulus Microplate Multimode Reader.

4.3.17 Statistical analysis

Significant differences between tested groups were calculated with a two-tailed unpaired Student *t* test using GraphPad Prism for Windows (GraphPad Software, La Jolla, CA, USA). P values of < 0.05 were considered as significant and are indicated with star or plus symbols as follows: */+ P < 0.05, **/++ P < 0.01 and ***/+++ P < 0.001.

4.4 Results

4.4.1 Qualitative and quantitative analysis of mTHPP uptake

Recently, uptake of PSS/mTHPP by peripheral blood CD3⁺ T cells has been demonstrated for low loading concentrations (1 and 10 μ g/ mL [260]). In the present study, uptake experiments with the maximum tolerable loading concentration (see next section) of PSS/mTHPP were carried out. To this end, CD3⁺ T lymphocytes were incubated with 12.5 and 25 μ g/mL of PSS/mTHPP at 37 °C and 4 °C. Reducing the incubation temperature is a simple method to gather preliminary information about a possible internalization mechanism. After the indicated incubation periods, cells were washed to remove excess drug and then analyzed by flow cytometry (Fig. 4.2A).

Complexed mTHPP was internalized by T lymphocytes at 37 °C in a concentration and time-dependent manner, whereas drug uptake was strongly impaired at 4 °C. Obviously, the process was energy dependent indicating drug uptake via endocytosis [237]. Furthermore, the capacity for PS-uptake was not reached within 8 h of incubation suggesting the potential to improve the loading process.

Live cell fluorescence microscopy was performed to illustrate a more realistic intracellular distribution of mTHPP in T cells compared to formaldehyde fixed and mounting medium embedded T lymphocytes (compare [260]). In contrast to unloaded T lymphocytes, loaded T cells emitted an intense red fluorescence (Fig. 4.2B). Merged fluorescence images clearly show that red fluorescent cell compartments are encircled by green stained cell membranes, which do not contain mTHPP in observable amounts. Hence, the sites of red fluorescence emission were mainly located within T cells. This is supported by the red stained structures of yet to be determined cell compartments in the perinuclear area of the cytoplasm, which resemble intracellular located endoplasmic reticulum and Golgi apparatus (Fig. 4.2C, middle panels) and could not be distinguished in fixed cells.

Subsequently, the amount of mTHPP incorporated by T cells was quantitatively determined. From the mass of mTHPP determined after ethyl acetate extraction by fluorescence spectrometry, the drug payload transported by a single carrier cell was calculated. As shown in Fig. 4.2D on average 0.24 ± 0.03 pg of mTHPP were internalized by a single T cell. However, the overall uptake efficiency was low (Fig. 4.2E). On average only 2.3% of the mTHPP used was taken up.

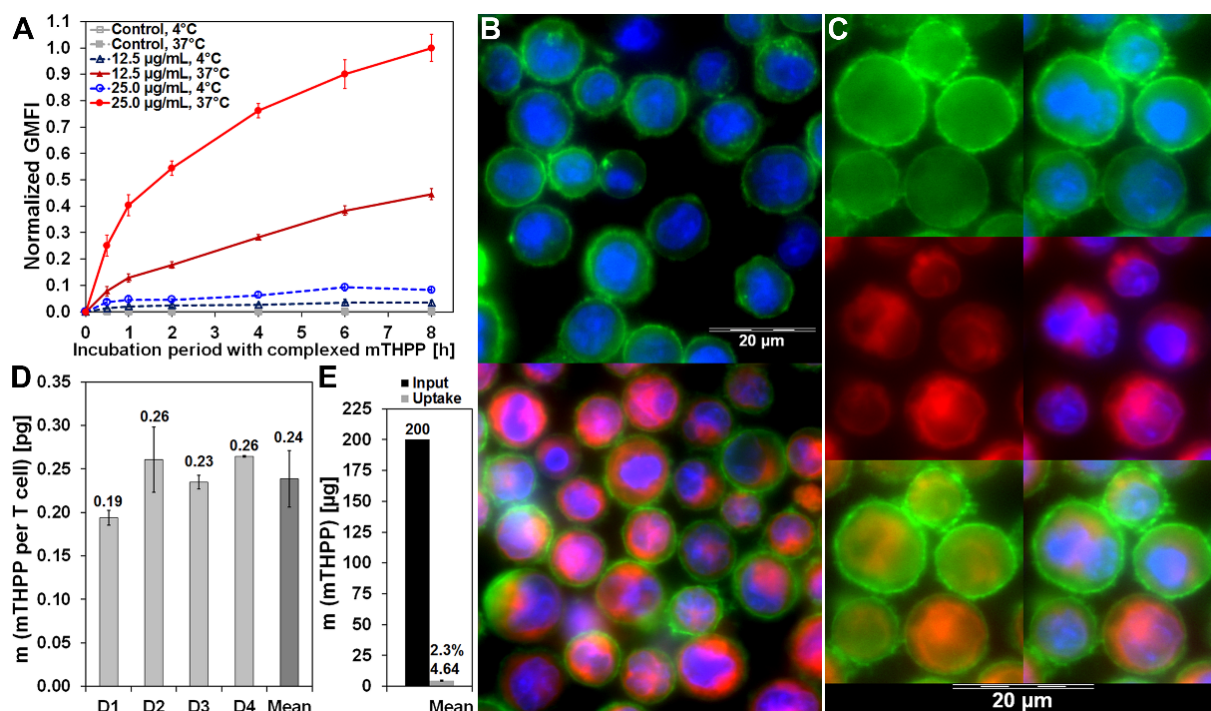


Fig. 4.2. Qualitative and quantitative determination of PSS/mTHPP internalization by *ex vivo* activated human CD3+ T lymphocytes. (A) Flow cytometric analysis of T cells upon incubation in medium as control or in medium containing indicated concentrations of PSS/mTHPP at 4°C versus 37°C. Fluorescence intensities of gated populations are expressed as normalized GMFI values \pm SD of 2 independent experiments using 2 different donors ($n = 2$). (B) Representative fluorescence images of unloaded (upper panel) and loaded (lower panel & C) T lymphocytes. Nuclei and membranes of live cells are blue and green fluorescent, respectively. T lymphocytes showing red fluorescence contain mTHPP (C) The photosensitizer is located within the lymphocytes and is not observable in cell membranes as shown in the merged image (lower left panel) composed of the green (upper left panel) and the red fluorescence picture (middle left panel). Locations of blue stained cell nuclei are shown in right hand panels. (D) Mass means \pm SD derived from T cell-loadings each conducted in duplicate after ethyl acetate extraction are shown for 4 donors (D1-D4). The overall mean \pm SD for the internalized mTHPP mass per cell is also shown ($n = 4$). (E) Illustration of uptake efficiency of loading procedures conducted with 4 different donors (mean \pm SD, $n = 4$). The black bar represents the total mass of complexed mTHPP (200 μg) used for T cell loading. The gray bar shows the mass of PS extracted from cells ($4.6 \pm 0.4 \mu\text{g}$).

4.4.2 Viability and cytotoxic function of loaded peripheral blood CD3+ T lymphocytes

To determine a safe maximum loading concentration of complexed mTHPP, CD3+ T cells were incubated with indicated amounts of PS-complex for 2 h. Bioreductive activity (i.e. viability) of loaded T cells was analyzed at indicated time points (Fig. 4.3A). Incubation with poly(styrene sulfonate) sodium salt, used in the same concentration equal to 45 $\mu\text{g}/\text{mL}$ of complexed mTHPP, did not affect T cell viability. Thus, at this concentration the complexing agent itself can be considered as non-toxic. T lymphocytes which had been incubated only with 20 or 25 $\mu\text{g}/\text{mL}$ of PSS/mTHPP tolerated the payload well. Even after 48 h, cell viability was still not impaired compared to the viability of untreated control group. However, dark toxicity was observed at loading concentrations greater than 25 $\mu\text{g}/\text{mL}$ and bioreductive activity was decreasing in a con-

centration-dependent manner. Therefore, a loading concentration of 25 $\mu\text{g/mL}$ of complexed mTHPP was fixed for later experiments.

To analyze whether loaded T cells have the same capacity to kill tumor cells as unloaded T lymphocytes, EpCAM-positive SKOV-3 ovarian adenocarcinoma cells were treated with T cells in combination with bispecific antibody (bsAb) EpCAM \times CD3, which induces cytolytic activity of cytotoxic T lymphocytes against EpCAM-expressing target cells. After addition of immune cells the viability of tumor cells was analyzed at indicated time points (Fig. 4.3B). No significant difference in redirected lysis of SKOV-3 cells was observed. Over the course of time, the progression of both viability curves is nearly identical. In conclusion, mTHPP-loaded T cells were as lethal as unloaded T lymphocytes. Obviously, the drug payload did not impair the natural cytotoxicity of T cells towards target cells.

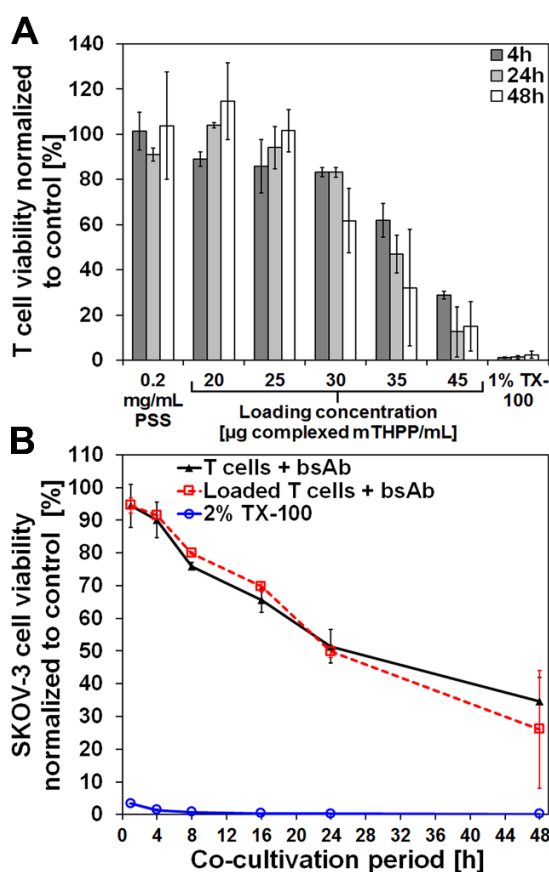


Fig. 4.3. Maximal tolerable mTHPP payload and cytolytic capacity of loaded CD3⁺ T cells were assessed using WST-1 colorimetric assays. (A) T cells were incubated for 2 h with indicated concentrations of complexed mTHPP and the greatest respective concentration of the complexing agent PSS. The bioreductive activity expressed as percentage of viable cells normalized to untreated control cells was determined 4 h, 24 h and 48 h after transfer of washed T cells into PS-complex and PSS free cell culture medium. (B) Cytolytic function of unloaded and loaded T lymphocytes (loading concentration = 25 $\mu\text{g/mL}$ of complexed mTHPP), in the presence of bsAb was compared for up to 48 h in co-cultures with SKOV-3 cells as target cells. The effector to target cell ratio was 2:1. (A, B) All cells were kept protected from light during the experimental period. Mean values \pm SD of 2 representative experiments with 2 different donors are shown ($n = 2$).

4.4.3 Photosensitizer transfer from loaded peripheral blood CD3⁺ T lymphocytes to co-cultivated carcinoma cells

It was shown that unspecific transfer of mTHPP from CD3⁺ T cells to target cells is possible [260]. In the present study, drug transfer was characterized in more detail. To this end, EpCAM-expressing A549 lung carcinoma cells were co-incubated with unloaded or PS-complex-loaded T cells in the presence or absence of bsAb over a total period of 22 h. The transfer of mTHPP was visualized by live cell fluorescence microscopy (Fig. 4.4A, C). After 2 h and 22 h of co-cultivation, A549 cells treated with CFSE-labeled, loaded T lymphocytes plus bsAb showed a more intense red fluorescence than lung carcinoma cells, which had been co-incubated with CFSE-labeled, non-redirected loaded T cells (Fig. 4.4A). In either case, the emission of fluorescence observed after 22 h (Fig. 4.4A, lower panels) was more intense than after 2 h (Fig. 4.4A, upper panels) of co-cultivation. The photosensitizer was accumulated in specific compartments of A549 cells, which are likely to be the endoplasmic reticulum and the Golgi apparatus (Fig. 4.4C). Although we have used PSS-complexed mTHPP, those findings are consistent with the observations of Teiten and colleagues, which had used mTHPC [255].

Fluorescence microscopy images suggest that the presence of bsAb increases drug transfer in co-cultures. To confirm this effect, mTHPP transfer was further evaluated via flow cytometry (Fig. 4.4B). As expected, the GMFI derived from A549 cells, which had been co-incubated with loaded T lymphocytes, increased constantly. The longer the co-cultivation lasted, the more mTHPP was transferred and the greater were the determined GMFI of analyzed tumor cells. However, when incubated with bsAb-retargeted loaded T cells, A549 cells showed much stronger fluorescence signals than upon co-cultivation with non-redirected loaded T lymphocytes. Thus, drug transfer was more efficient when T cells and tumor cells were cross-linked through bsAb. Fig. 4.4D shows some of the data used to calculate GMFI values for cancer cells which had been co-cultivated with loaded carrier cells plus bsAb. Notably, the PS transfer is also illustrated by a population shift of A549 cells and drug loaded T lymphocytes along the logarithmic x-axis representing mTHPP fluorescence intensity over the course of time. While the drug is transferred, the red fluorescence intensity of the loaded T cells population is shifting to smaller values. In contrast, the fluorescence intensity of the A549 cell population is increasing, indicating an internalization of transferred mTHPP by cancer cells.

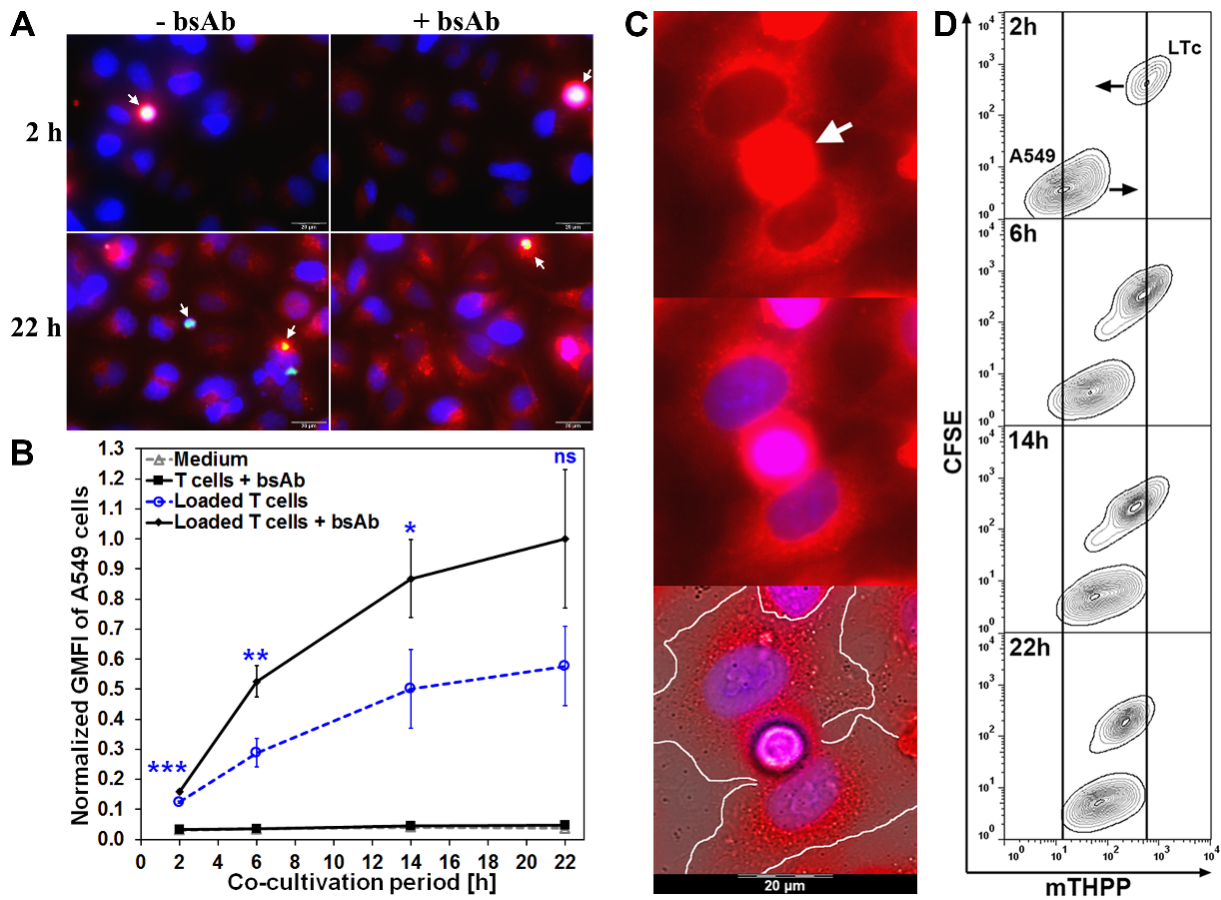


Fig. 4.4. Assessing mTHPP transfer from carrier CD3+ T cells to target carcinoma cells. For all experiments the E:T ratio was 2:1. (A) Representative merged fluorescence images of rinsed and live A549 cells 2 h and 22 h after co-cubation with loaded T lymphocytes either in the presence or absence of bsAb. Cell nuclei were stained with Hoechst dye and are blue fluorescent. Areas mostly devoid of CFSE-T cells (white arrows) are shown. Cell compartments containing mTHPP are red fluorescent. (B) A549 lung carcinoma cells were co-cultivated with unloaded and loaded T cells in combination with bsAb as well as with loaded T lymphocytes without bsAb for up to 22 h at 37°C. Fluorescence intensities of gated cancer cells populations are expressed as normalized GMFI values \pm SD (n = 3). Statistically significant differences in drug transfer are indicated by P-values represented by star symbols (* P < 0.05, ** P < 0.01 and *** P < 0.001, ns = not significant). (C) A very bright red fluorescent mTHPP loaded T lymphocyte (white arrow) attached to two A549 cells after 22 h of co-cultivation in combination with bsAb is shown. The sample had been rinsed before imaging. Cancer cells have internalized a considerable amount of mTHPP (upper panel). Sites with accumulated photosensitizer are mainly located around the cell nuclei (upper panel and middle panel). In the lower panel, the combined fluorescence images were merged with the corresponding bright field image. White lines highlight the estimated location of tumor cell membranes. (D) Contour plots, obtained from one of the experiments shown in B, of A549 cells and CFSE-labeled loaded T cells (LTc) for indicated co-incubation periods are illustrated. Black orientation lines are laid over the center of populations measured after 2 h of co-cultivation in the presence of bsAb.

4.4.4 Enhanced cytotoxicity of bsAb-redirectioned, photosensitizer-loaded CD3+ T lymphocytes

We addressed the crucial question of whether redirectioned mTHPP-loaded CD3+ T lymphocytes are more efficient in killing EpCAM-expressing carcinoma cells than unloaded T cells after irradiation. As shown in Fig. 4.5A and B, co-incubation with unloaded T lymphocytes had no significant effect on the viability of ovarian and lung carcinoma cells. In contrast, cancer cell viability considerably decreased to less than 60% following treatment with loaded T lymphocytes and exposure to light after 24 h. This result is owed to the fact that loaded T cells are able to transfer mTHPP to cancer cells as shown in the previous section. Since loaded T lymphocytes were killed upon exposure to light ^{1260l} and viability measurements were carried out 2 h after irradiation of co-incubation, redirectioned unloaded T cells had more time to kill target cells than retargeted carrier cells. However, in irradiated co-cultures, redirectioned loaded T lymphocytes inhibited tumor cell growth more efficiently than bsAb-guided T cells. For instance, after 8 h and 24 h of co-cultivation, retargeted loaded T lymphocytes had killed 39% and 21%, respectively, more SKOV-3 cells than redirectioned unloaded T cells. The treatment with redirectioned loaded T cells was even more effective in experiments with A549 cells (Fig. 4.5B). In comparison to retargeted unloaded T cells, the viability of A549 cells was significantly reduced by 52% and by 31% after 8 h and 24 h, respectively. Importantly, we could also demonstrate, that drug effect and T cell effect synergistically act together. The combination of retargeted T lymphocytes, separately applied PSS/mTHPP (0.23 µg/mL) and light was less effective in killing cancer cells than PS-complex-loaded, redirectioned T cells after illumination. Only when the tumor cells had enough time to accumulate the dissolved PS-complex were comparable killing percentages observed after 24 h.

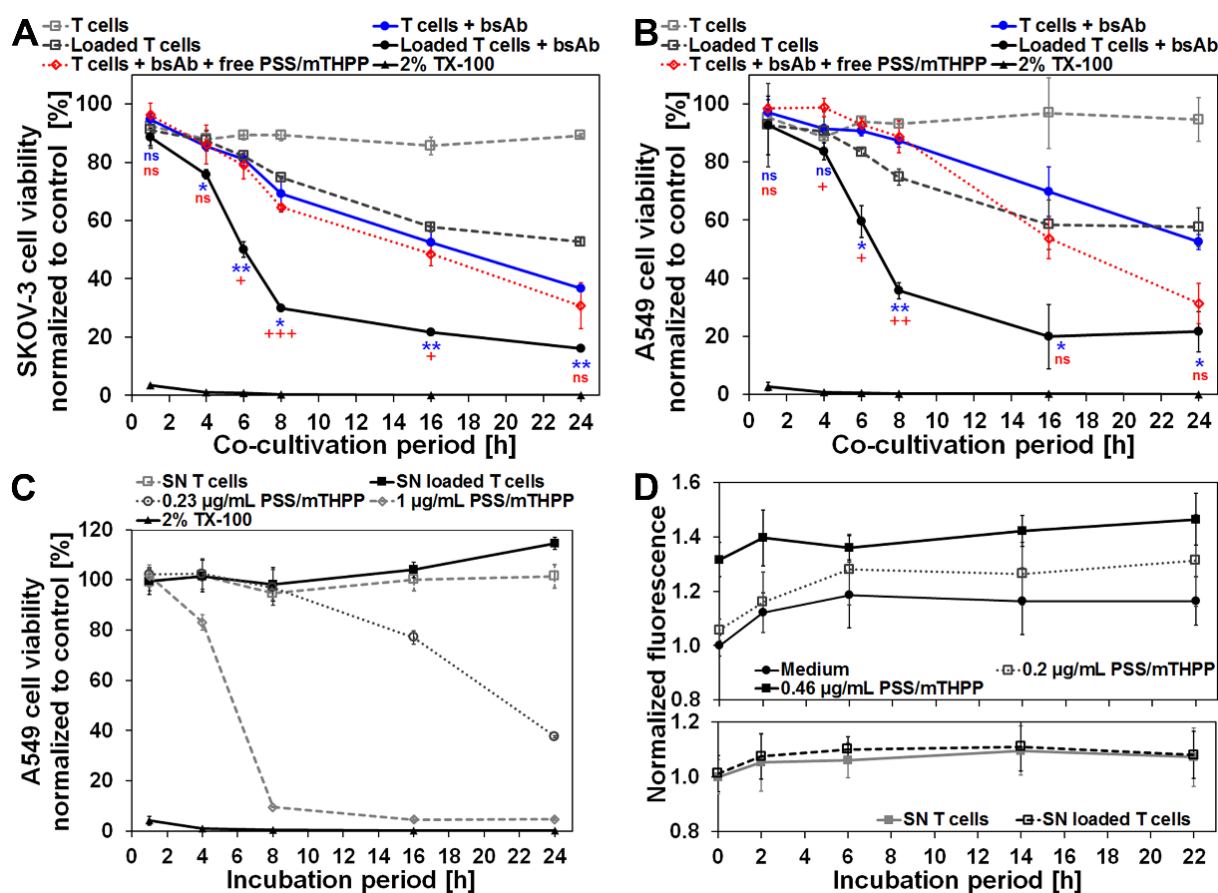


Fig. 4.5. Evaluation of killing potential of bispecific antibody-redirection, photosensitizer-loaded T cells by WST-1 assays and fluorimetric detection of mTHPP in supernatants (SN) harvested from loaded carrier cells. Time-dependent redirected killing of SKOV-3 ovarian carcinoma cells (A) and of A549 lung carcinoma cells (B) by unloaded and loaded T cells is shown. The mass of separately applied complexed mTHPP was equal to the greatest mass, which had been internalized by 80,000 T cells. Thus, the final concentration of free PSS/mTHPP in WST-1 assays was 0.23 µg/mL. The effector to target cell ratio in all experiments was 2:1. Statistically significant differences (P-values) between the viability of cancer cells co-cultivated with loaded T cells + bsAb and cancer cell viability after treatment with T cells + bsAb or with T cells + bsAb + free PSS/mTHPP for each incubation period are indicated with star or plus symbols, respectively (*/+ P < 0.05, **/++ P < 0.01 and ***/+++ P < 0.001; ns = not significant). Mean values ± SD of 2 representative experiments with 2 different donors (n = 2) for each carcinoma cell line are shown. (C) WST-1 assay conducted with supernatants obtained from unloaded and loaded T cell cultures analogous to the experiment presented in (B). Mean values ± SD of 4 different donors (n = 4) are shown. For free complexed drug controls (0.23 & 1 µg/mL) and detergent control, n was equal to 2. (A, B, C) Samples were exposed to light 2 h before determination of cell viability. Co-cultures measured after 1 h of incubation were not irradiated. (D, lower panel) Detection of mTHPP in aliquots of the same supernatants obtained from loaded T cells tested in the experiment shown in (C). Mean values ± SD of 4 different donors (n = 4) are shown. For drug controls n was equal to 2 (upper panel).

4.4.5 Cytotoxicity of supernatants obtained from loaded CD3+ T lymphocyte cultures

Subsequently, we examined whether PSS/mTHPP, which could have been released by loaded CD3+ T cells into cell culture medium, has an impairing effect on cancer cell viability. However, A549 cells, which had been incubated with supernatants, either collected from cultures of loaded T lymphocytes or as control from unloaded T cells, showed no reduced viability upon exposure

to light (Fig. 4.5C). Cancer cells were also treated with 0.23 $\mu\text{g}/\text{mL}$ of PSS/mTHPP, which is equal to the concentration that would have been achieved had 80,000 carrier cells released their entire drug payload into the co-culture medium. After 22 h of incubation and subsequent irradiation, A549 cells were clearly affected by PSS/mTHPP mediated phototoxicity. Fluorescence spectrometry measurements support that supernatants obtained from loaded T cells did not contain the pharmaceutical in cytotoxic doses. As shown in Fig. 4.5D, there is no difference in fluorescence emissions detectable when supernatants harvested from unloaded T cell cultures are compared to those of loaded carrier cells (lower panel). In contrast, mTHPP at concentrations of 0.2 $\mu\text{g}/\text{mL}$ and 0.46 $\mu\text{g}/\text{mL}$ is actually measurable (Fig. 4.5D, upper panel). The former value corresponds to one-tenth of the undiluted concentration of PSS/mTHPP used as positive control in the experiment shown in Fig. 4.5C, whereas latter value matches the concentration which could have been theoretically achieved by a complete release of drug by loaded T cells.

4.4.6 Boosted cytotoxicity of bsAb-redirectioned, photosensitizer-loaded CD4⁺ and CD8⁺ T lymphocytes

In the presence of the bispecific antibody HEA125 \times OKT3, CD4⁺ T cells can exhibit a cytotoxic effect against EpCAM-expressing target cells [10]. Therefore, we analyzed whether PSS/mTHPP-loaded CD4⁺ T cells would be suitable as carrier cells as well. In addition, we were interested whether we could increase the synergistic effect demonstrated for drug-loaded CD3⁺ T cells (Fig. 4.5A & B) by using only loaded CD8⁺ T lymphocytes. The results shown in Fig. 4.6A and 4.6B confirm both assumptions. The purity of both T cell subsets was consistently greater than 96% (Supplementary Information, Fig. S4.1.).

Co-incubation with unloaded CD4⁺ T lymphocytes had no significant effect on the viability of A549 cells. Likewise, background lysis of unloaded CD8⁺ T lymphocytes was insignificant. As expected, cancer cell viability was considerably decreased following treatment with both subsets of loaded T lymphocytes and exposure to light. After 24 h bsAb-retargeted CD4⁺ T cells had killed 47% of lung carcinoma cells. At that time point, cytotoxic CD8⁺ T cells had already eliminated 66% of target cells. In irradiated co-cultures, redirectioned loaded CD4⁺ T lymphocytes inhibited tumor cell growth more efficiently than bsAb-guided CD4⁺ T cells and non-redirectioned loaded cells. Therefore, CD4⁺ T lymphocytes could be of use as carrier cells. Within the first 8 h of co-incubation, bsAb-mediated cytolytic activity of CD3⁺ (Fig. 4.5B), CD4⁺ (Fig. 4.6A) or CD8⁺ T cells (Fig. 4.6B) was comparable. In contrast, retargeted loaded CD8⁺ T lymphocytes had erad-

icated 85% of target cells, while CD3⁺ and CD4⁺ loaded T cells had only killed 64% and 59%, respectively, of cancer cells after illumination. Thus, loaded CD8⁺ T lymphocytes were the most effective subset in killing A549 cells, which was still the case after 24 h of co-cultivation.

We have not investigated whether there is a difference in drug uptake by different subsets of T cells. However, had the CD4⁺ and CD8⁺ T cells internalized significant different amounts of PSS/mTHPP, two distinguishable populations should have appeared in flow cytometry drug loading experiments with CD3⁺ T lymphocytes (Fig. 4.2A). However, that was not the case. Hence, we tested the additional approach using free PSS/mTHPP as well. Again, we could demonstrate, that drug effect and T cell effect act synergistically. The combination of bsAb-redirected CD4⁺ or CD8⁺ T lymphocytes, separately applied PSS/mTHPP and light was less effective in killing A549 cells than drug-loaded, redirected T cells of both subsets after illumination. Interestingly, the synergistic effect demonstrated for loaded CD3⁺ (Fig. 4.5B) and CD4⁺ T lymphocytes was less pronounced, especially within the first 8 h, than the synergy shown for drug-loaded CD8⁺ T cells.

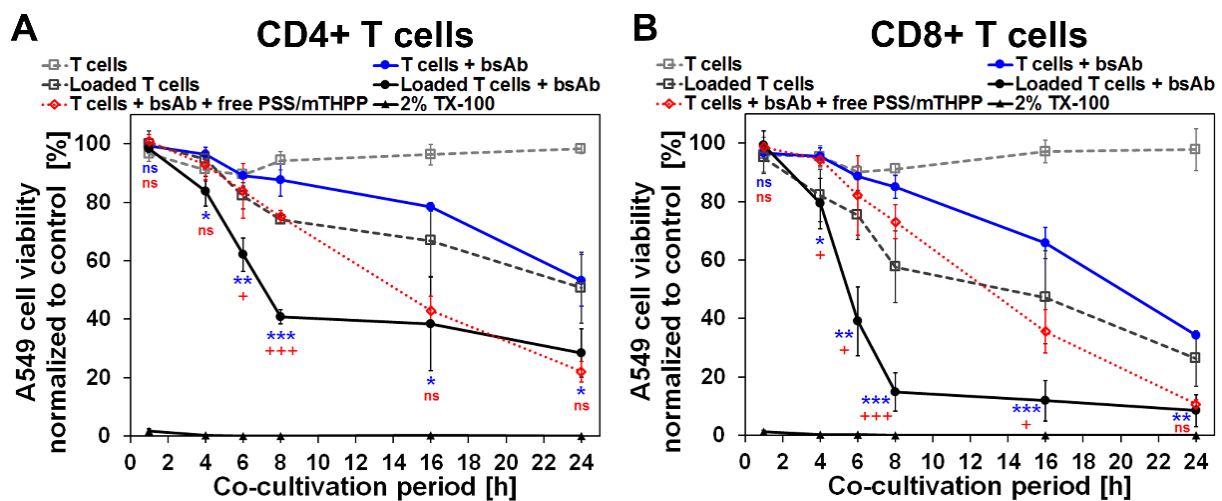


Fig. 4.6. Determination of the killing potential of bsAb-redirected, PS-loaded subsets of T lymphocytes by WST-1 assays. Time-dependent redirected killing of A549 lung carcinoma cells by unloaded and loaded CD4⁺ (A) and CD8⁺ (B) T cells is shown. The concentration of separately applied complexed mTHPP was 0.23 $\mu\text{g}/\text{mL}$. The effector to target cell ratio was 2:1 in all experiments. Statistically significant differences (P values) between the viability of cancer cells co-cultivated with loaded T cells + bsAb and cancer cell viability after treatment with T cells + bsAb or with T cells + bsAb + free PSS/mTHPP for each incubation period are indicated with star or plus symbols, respectively (*/+ P < 0.05, **/+ P < 0.01 and ***/+++ P < 0.001; ns = not significant). Mean values \pm SD of 3 experiments with 3 different donors (n = 3) are shown.

4.5 Discussion

In the present work, we have demonstrated the feasibility of a novel T cell-based targeted PDT approach *in vitro*. To this end, we have used a water-soluble formulation of the model photosensitizer mTHPP complexed with poly(styrene sulfonate) sodium salt (PSS). The photosensitizer itself is practically insoluble in water. In preliminary experiments, we could confirm that free mTHPP is also taken up by T lymphocytes (Supplementary Information, Fig. S4.5). Additional data imply that concentrations up to 10 $\mu\text{g}/\text{mL}$ of mTHPP are non-toxic for T cells (Supplementary Information, Fig. S4.6). However, while loading T cells with PSS/mTHPP was very reproducible, loading with free mTHPP was obviously not. This is indicated by huge standard deviations shown in Fig. S4.7 (Supplementary Information). Adding an organic mTHPP solution to an aqueous cell-suspension seems to generate inhomogeneous loading conditions. This was not the case when PSS/mTHPP was used. Therefore, we decided to use the water-soluble drug formulation throughout the present study.

An important part of our approach is to exploit the natural cytotoxic potential of drug-loaded T lymphocytes against malignant neoplasms in the context of adoptive T cell therapy. Therefore, it is essential that loaded T cells survive the drug payload until their arrival at tumor sites. Additionally, the internalized pharmaceutical must not impair the intrinsic cytotoxicity of T lymphocytes. It has been demonstrated that CTLs can be detected at neoplastic sites within 48 h to 72 h after reinfusion into patients [262, 263]. Here, we have shown that CD3+ T cells tolerated loading concentrations of up to 25 $\mu\text{g}/\text{mL}$ of complexed mTHPP for at least 48 h after the end of the loading procedure. In particular, loaded CD3+ T lymphocytes exhibited the same killing capacity as unloaded CD3+ T cells when kept protected from light. Therefore, the obtained data supports the hypothesis that loaded T cells could be functional for ACT and following PDT in patients.

Although we have demonstrated that, of the tested T cells, bsAb-guided drug-loaded CD8+ T lymphocytes were most effective in killing cancer cells *in vitro*, we aim to use all peripheral blood T cells *in vivo*. The rationale behind this is the specificity of the bispecific antibody, which cross-links all CD3+ T cells to target cells. Thus, all these cells could be exploited as drug carrier cells. This includes CD4+ T cells, which exert a cytotoxic phenotype in combination with bsAb (Fig. 4.6A) [10]. Furthermore, cells of the CD4+ subset could augment the response to adoptive T cell transfer when co-administered with CD8+ T cells *in vivo* [122, 123].

After intravenous injection, T lymphocytes reside for several hours in the lungs of humans and mice. Thereafter, the bulk of T cells redistributes to liver, spleen and secondary lymphoid organs [262, 264-266]. Furthermore, on the way to tumor sites drug-loaded T cells will interact with other cells. For instance, when circulating T lymphocytes extravasate through endothelial barriers [267], a part of the pharmaceutical payload will probably be transferred to these endothelial cells. However, off-target toxicity to the mentioned tissues is not to be expected, as long as no light activation occurs in that area. Presumably, not all carrier cells will be able to deliver the drug to targeted sites. Nevertheless, Cerundolo and co-workers demonstrated that adoptively transferred tumor-specific cytotoxic T lymphocytes, loaded with the plant toxin ricin, had a greater therapeutic effect on peripherally localized tumors than unloaded CTL [84]. It remains to be seen if the amount of delivered photosensitizer will also be sufficient for an efficient PDT. On the other hand, a variety of experimental strategies are under investigation to improve the trafficking of adoptively transferred T lymphocytes to malignant tissues [268-270]. Thus, there is potential that the T cell-based targeted PDT approach may lead to a better photosensitizer biodistribution toward the tumor sites than systemically administered drug.

We have demonstrated that drug transfer is directly dependent on a proximity effect and/or cell-cell interaction. When non-redirectioned mTHPP-loaded human T lymphocytes were co-incubated with human allogenic cancer cells, the transferred dose of mTHPP was sufficient to kill a considerable amount of cancer cells upon exposure to light. In contrast, when loaded T lymphocytes were substituted for supernatants obtained from drug-loaded T cells, tumor cells were not affected after irradiation. We conclude that mTHPP transfer is primarily not mediated via the cell culture medium. After addition, loaded T cells, representing spots of high PS-concentration, will settle on top of or between cancer cells. All eukaryotic cells have constitutive exocytic pathways to the cell surface and for secretion of molecules like proteins [271]. Along these secretory routes complexed mTHPP could be released by loaded T cells and endocytosed by tumor cells located in close proximity. Besides, T cells are also able to migrate from tumor cell to tumor cell *in vitro* [272]. As a consequence, bsAb-independent contacts are presumably established between the two cell types and the photosensitizer can be passed from loaded T lymphocytes to tumor cells. These interactions are probably induced by adhesion molecules and mediated for instance via LFA-1/ICAM-1 or CD2/CD58-complexes [273]. Most notably, when carcinoma cells were co-cultivated with loaded T cells in combination with bsAb EpCAM \times CD3, even more photosensitizer was transferred, emphasizing the importance of cell-cell contacts for a more efficient drug transfer.

Salnikov and colleagues have demonstrated that the duration of contacts between T lymphocytes and pancreatic cancer cells mediated by EpCAM \times CD3 was substantially longer compared to a control antibody ¹⁹¹. It is conceivable that bsAb-mediated increase of drug transfer is caused by prolonged cell-cell interactions. In addition, bispecific antibodies bind to the ϵ -chain of the CD3 molecule ¹¹⁰, which is a component of the T cell receptor (TCR) complex. Upon restimulation of TCRs of activated T cells regulated exocytic processes occur, in which immunological mediators are secreted into the intercellular lumen. While CD4⁺ T cells mainly release different kinds of chemokines and cytokines, CD8⁺ T cells predominantly secrete cytokines and degranulate their lytic granules to exert their intrinsic cytotoxic function ¹²⁷⁴. Thus, additionally to constitutive exocytic pathways, PSS/mTHPP could be released by those regulated secretory processes as well. Therefore, the bsAb does not only provide tumor cell specificity but also indirectly enhances “drug selectivity”. This explains why in irradiated co-cultures and in the presence of bsAb, PSS/mTHPP-loaded carrier cells inhibited tumor cell growth more efficiently than unloaded T lymphocytes. Most importantly, the combination of freely applied drug and bsAb-retargeted immune cells was less effective in killing cancer cells than PS-loaded redirected T cells indicating that drug effect and T cell effect act together in a synergistic manner.

Assessment of the feasibility of lymphocyte-based drug delivery started 31 years ago, when it was shown that ricin carrying spleen cells could transfer the toxin to recipient spleen cells *in vitro* ¹⁹⁷. In following studies ricin-loaded T cells ¹⁸⁴ as well as lymphokine-activated killer (LAK) cells ¹⁸² were used to treat tumor bearing mice. Although these studies provided a proof of concept for the T cell-based drug delivery approach, the selection of ricin as payload for carrier cells had several drawbacks. The major one was that after ricin loading the cytolytic activity of lymphocytes was seriously impaired ^{182, 84, 99}. Due to high systemic toxicity in mice, Mandruzzato and colleagues substituted ricin for an anthracycline ¹⁶. The authors achieved a reduction of lung metastases. However, since loaded LAK cells had redistributed to liver and spleen, considerable and presumably harmful drug levels were found in these organs of mice. Above all, cytotoxic activity of carrier cells was gravely inhibited again. Obviously, active agents exerting immediate cytotoxicity prevent exploitation of the natural T cell cytotoxicity. To overcome this obstacle, we have encapsulated the chemotherapeutic agent idarubicin in polyester-based and gold-shell-coated polyester nanoparticles. The rationale was to protect T lymphocytes against drug toxicity upon loading. However, these drug encapsulations were not able to prevent premature death of carrier cells ¹²⁶⁰. As a consequence, we deem those respective active drugs not appropriate for

T cell-based drug delivery. Thus, by using a photosensitizer, the mode of action of which can be specifically triggered in a time-dependent manner at the diseased site, we provide a clear improvement to the cell-mediated drug delivery approach. Other investigators have also pursued similar strategies but did not yet demonstrate any therapeutic effects *in vitro* as well as *in vivo* [102-104]. To our best knowledge, only Stephan and colleagues were able to augment the therapeutic potential of T cells without impairing cell functions, so far. By covalent coupling of cytokine or small-molecule drug containing nanoparticles onto the plasma membrane surface, they provided a sustained “pseudoautocrine” stimulation to carrier cells, which caused an increased T cell expansion, longevity and an enhanced tumor elimination after *in vivo* transfer [90, 91]. However, the approach of Stephan and co-workers differs from ours in that the payload is attached to the outside of carrier cells. Furthermore, non-cytotoxic drugs were used, which acted on carrier cells and not directly on target cells.

Using drug-loaded cytotoxic T cells seems to be counterintuitive as the target cell to which mTHPP is transferred will already be killed by the attacking CTL. However, we have clearly demonstrated that using bsAb-retargeted loaded CD8⁺ T lymphocyte was the most effective approach in elimination target cancer cells (Fig. 4.6B). The reason for this *in vitro* efficiency could be the mentioned proximity effect. One CTL is attached to a target cell and kills it. In the meantime the same CTL releases drug molecules via exocytic pathways or degranulation of lytic granules is accompanied by drug “secretion”. The photosensitizer is then taken up by bystander cells. In case those cells are not immediately attacked by the same or other CTLs light irradiation will eradicate them. This could happen all over the cell monolayer. Furthermore, while receiving the “lethal hit” by loaded CTLs, target cells could internalize the drug. After cell death, drug containing remains of eliminated target cells could be endocytosed by neighboring cells. This could also destroy those cells after irradiation.

4.6 Conclusions

We have shown that PS-loaded *ex vivo* activated human T lymphocytes survive the drug payload and do not show impaired natural cytolytic function. When retargeted through a bispecific antibody, the resulting living drug delivery system is able to transfer the photosensitizer to carcinoma cells more efficiently. Redirected loaded T cells of all tested populations (CD3⁺, CD4⁺ or CD8⁺)

are superior to redirected unloaded T lymphocytes in killing tumor cells after irradiation. The T cell-drug effect is synergistic rather than additive supporting the selectivity of bsAb-mediated mTHPP transfer, which, to our knowledge, was not demonstrated yet. The combination of cell-mediated drug delivery, cellular immunotherapy and photodynamic therapy could significantly increase selectivity and effectiveness of PDT. In addition, “super-killer T cells” [84] with drug boosted cytotoxicity could be beneficial for adoptive cell therapies. Our *in vitro* proof of concept study is the first step to establish the T lymphocyte-based photosensitizer delivery approach for *in vivo* studies.

4.7 Supplementary Information

4.7.1 Purity of isolated, activated and expanded CD4+ or CD8+ T lymphocytes

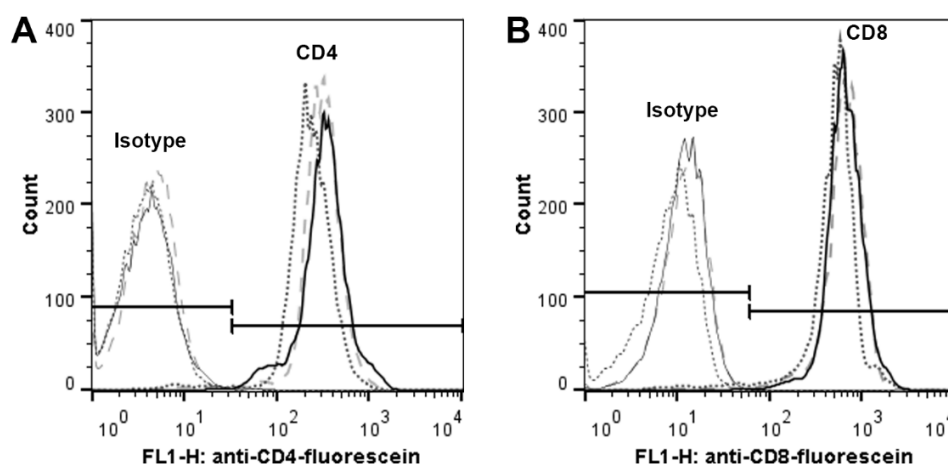


Fig. S4.1. Purity of isolated, activated and then expanded CD4+ (A) or CD8+ T cells (B) determined by flow cytometry. To assess the purity of T lymphocyte populations of healthy donors (3 per cell subset), cells were labeled in duplicate with either 5 $\mu\text{g}/\text{mL}$ of FITC-conjugated anti-human-CD4 or anti-human-CD8 monoclonal antibodies. As negative control, T cells were labeled with 5 $\mu\text{g}/\text{mL}$ of FITC-conjugated monoclonal antibodies of the same isotype as well (Bio-Rad AbD Serotec, Puchheim, Germany). One representative sample of each donor and subset is shown in the histograms. The illustrated markers within the overlays were used to calculate the purity of T cell populations: purity (CD4+ T cells) = 97.6 % \pm 1.3 %; purity (CD8+ T cells) = 97.5 % \pm 1.4 %; (mean \pm SD; n = 3 per cell subset).

4.7.2 Calibration of PSS/mTHPP preparations

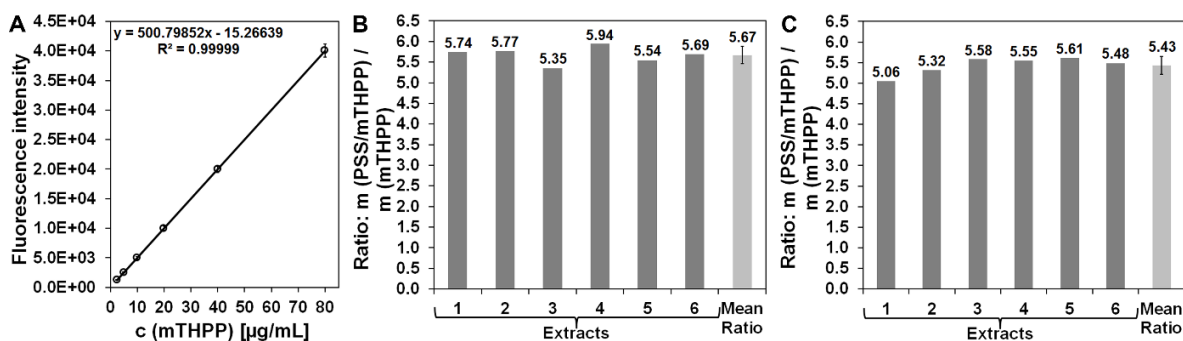


Fig. S4.2. Calibration of PSS/mTHPP by fluorescence spectrometry. (A) Calibration curve for pure mTHPP. Means \pm SD are shown (each data point is based on 12 measurements, $n = 3$, for fluorescence intensity arbitrary units were used). (B, C) Mass ratios of two PSS/mTHPP preparations are illustrated. The mass value of each extracted mTHPP is based on 9 fluorescence measurements. On average 5.67 mg and 5.43 mg of the first and the second complex preparation, respectively, contain 1 mg of pure mTHPP (Error bars represent \pm SD, $n = 6$ per preparation).

4.7.3 UV/Vis spectra of PSS/mTHPP

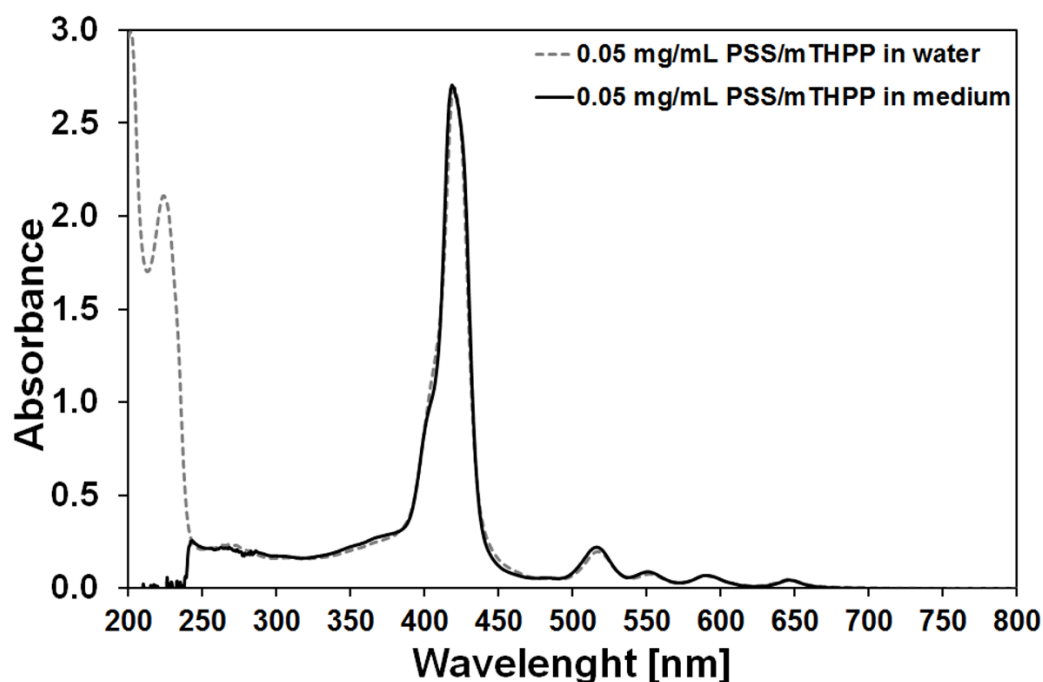


Fig. S4.3. UV/Vis spectra of complexed mTHPP dissolved in purified water or RPMI 1640 medium containing 10% (v/v) heat-inactivated FBS, 100 U/mL penicillin and 0.1 mg/mL streptomycin. As reference the respective solvent without PSS/mTHPP was used. The pH value of both solvents was adjusted to 7.4. Spectra were determined using an Ultrospec 3300 pro UV/Visible Spectrophotometer (Amersham pharmacia biotech, Cambridge, England).

4.7.4 Contribution of mTHPP to absorbance in WST-1 assays

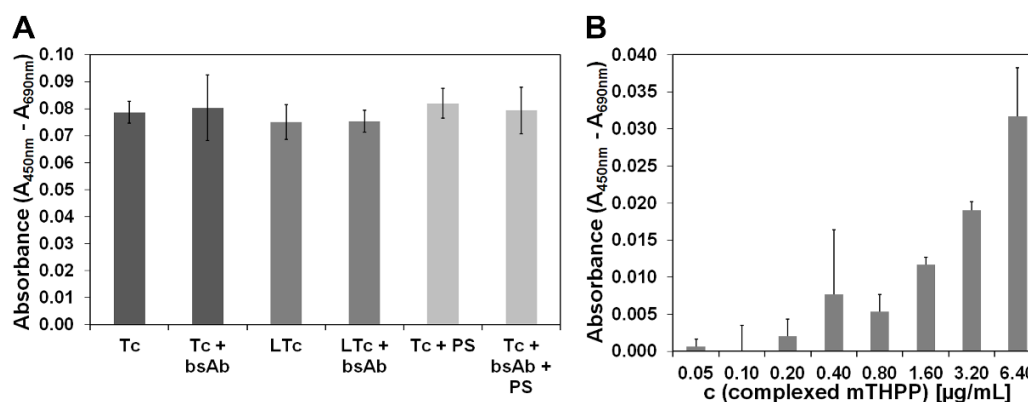


Fig. S4.4. Contribution of mTHPP to absorbance. In the present study, WST-1 assays were adjusted so that controls of untreated cancer cells would yield an absorbance of approximately $A = 1$. (A) Absorbance of non-irradiated blank controls of one of the experiments shown in Fig. 4B (Tc = T cells) after an incubation period of 1 h is illustrated. A contribution of mTHPP in loaded T cells (LTc) to the total absorbance is not detectable. The concentration of separately applied complexed mTHPP was $0.23 \mu\text{g/mL}$. Absorbance of PSS/mTHPP (PS) at this concentration is also negligible (A (bright grey bars), B). (A, B) Means and SD of triplicate samples are shown ($n = 1$).

4.7.5 Qualitative analysis of mTHPP uptake by fluorescence microscopy

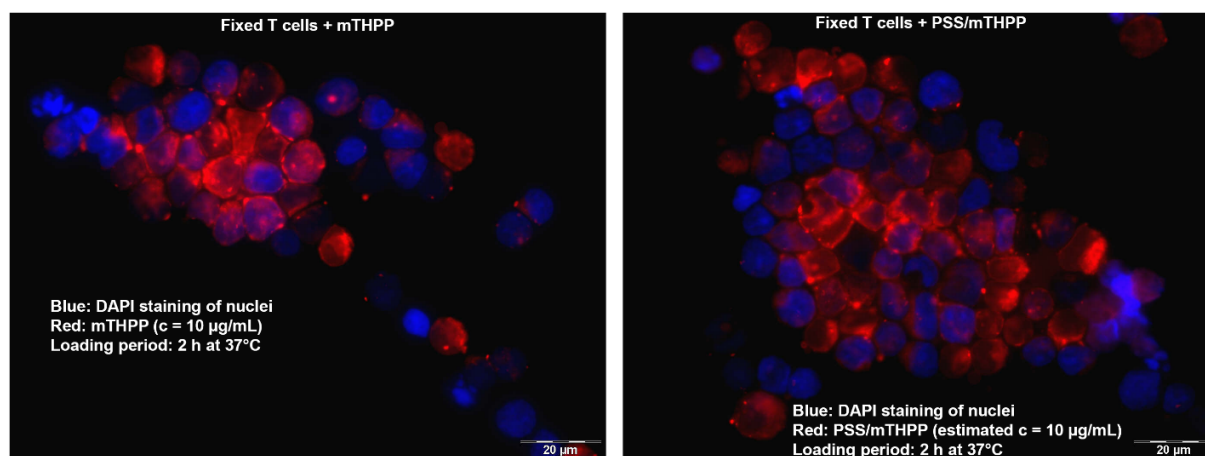


Fig. S4.5. Fluorescence images of formaldehyde-fixed and FluorSave (Merck Millipore, Darmstadt, Germany) mounting medium embedded T cells (principle of staining procedure is described in section 3.3.8).

4.7.6 Viability of T cells after loading with free or complexed mTHPP

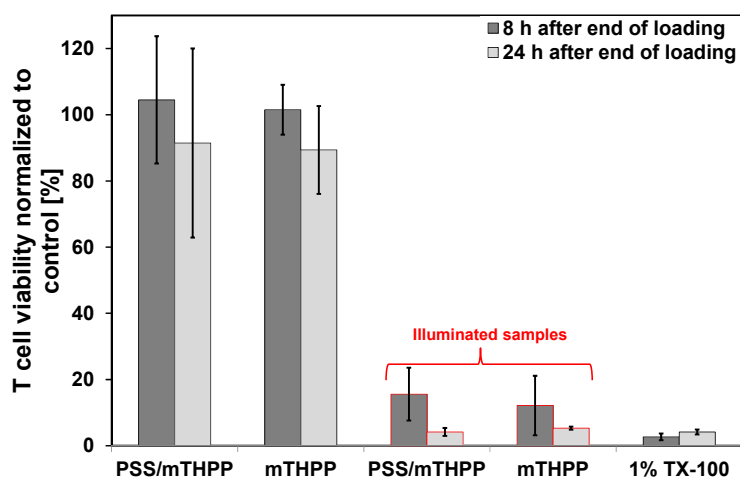


Fig. S4.6. Viability of T cells after loading with 10 $\mu\text{g}/\text{mL}$ of free mTHPP and approximately (see caption of Fig. S4.7) 10 $\mu\text{g}/\text{mL}$ of complexed mTHPP for 2 h. Cell survival was determined using a colorimetric XTT assay as described in section 3.3.9. After loading, cells were washed to remove non-internalized drug (mean values \pm SD of quadruplets, $n = 1$).

4.7.7 Qualitative analysis of mTHPP uptake by flow cytometry

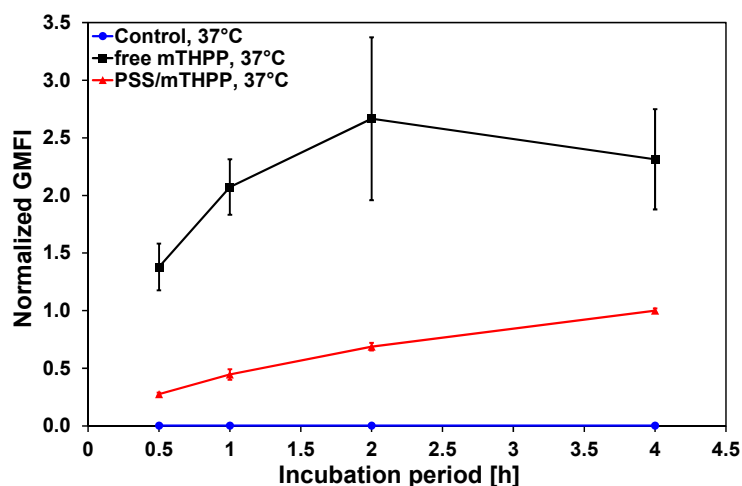


Fig. S4.7. T lymphocytes were loaded with 10 $\mu\text{g}/\text{mL}$ of free mTHPP and approximately (see below) 10 $\mu\text{g}/\text{mL}$ of complexed mTHPP for indicated incubation periods. After loading, cells were washed to remove non-internalized drug and fluorescence intensities of T cell populations were determined via flow cytometry (GMFI \pm SD values of 2 loadings of T cells obtained from the same donor, $n = 1$).

The data implies that the amount of internalized complexed mTHPP is smaller than the amount of free drug. However, at the time the experiments were conducted, PSS/mTHPP had not been calibrated so far. The concentration of complexed mTHPP was theoretically deduced based on the findings of Reum and colleagues ^[193]. In retrospect, it is likely that the actual concentration used for loading of T cells was well below 10 $\mu\text{g}/\text{mL}$.

5. Overall Conclusion and Outlook

Living T cells can be exploited as phagocytes to transport therapeutics to diseased sites as demonstrated in various pre-clinical studies. However, most of these studies showed that physiological and immunological functions such as migration, circulation, and cytolytic activity of human T lymphocytes were impaired after loading them with cytotoxic anticancer compounds. In addition, premature death of carrier cells has been a major drawback of cell-based approaches to transport cytotoxic payloads, probably hampering clinical trials up to now. One purpose of the presented work was to identify anticancer drug formulations that preserve drug loaded T lymphocytes from cell death and ideally do not reduce the cytolytic function of CTLs. The latter requirement is essential because the other main objective of this thesis was to combine the cytotoxicity of cell-delivered pharmaceuticals with cell-mediated cytotoxicity. Particularly, the question was addressed whether this combination acts in an additive or synergistic manner.

One strategy to overcome the aforementioned obstacles could be the encapsulation of cytotoxic therapeutics into protective nanoparticulate systems for cellular uptake. These materials for drug encapsulation must have some basic characteristics such as non-toxicity for carrier cells and biodegradability to ensure sustained release of enclosed pharmaceuticals inside the carrier cells as well as exocytosis of payload at the diseased site. Furthermore, ligands attached to the respective material that facilitate increased drug loading would be favorable.

In the first part of this thesis, interactions between lysine-based statistical glycosylated copolypeptides and human T lymphocytes were investigated for the first time. These biodegradable polymers, kindly provided by Thomas Stöhr (Organic Macromolecular Chemistry, Saarland University, Germany), could serve as an encapsulation material for pharmaceuticals. A standard XTT-based colorimetric viability assay confirmed that these glycopolypeptides were well tolerated by T cells, fulfilling a basic requirement. In addition, flow cytometric and fluorescence microscopic analysis demonstrated that galactosylated and mannosylated polymers were readily taken up by *ex vivo* activated T lymphocytes. This occurred in a temperature-dependent manner, suggesting an energy-dependent uptake mechanism such as endocytosis. In contrast, internalization of glucosylated polypeptides was significantly reduced and uptake of unsubstituted polypeptides was even lesser pronounced. This result indicates that attached galactose as well as attached mannose could indeed facilitate an increased cellular uptake of polylysine-based nanoscale particles. Preliminary experiments conducted by Thomas Stöhr demonstrated that the generation of these particles is feasible [224]. However, suboptimal size distribution of nanoparticles indicated that the

process for NP generation needs to be optimized. In addition, drug encapsulation was not realized. Nevertheless, these results highlights the potential use of statistical glycosylated copolypeptides in biomedical applications.

Instead of investigating polypeptide-based nanoscale systems, idarubicin (IDA) enclosing poly(lactic-*co*-glycolic-acid) (PLGA) nanoparticles and NPs based on newly synthesized poly(diethylene glycol-maleate-*co*-sebacate)ester (MPE) were tested in the second part of this thesis. The polyester-based NPs were kindly provided by Qiong Lian (Biopharmaceutics and Pharmaceutical Technology, Saarland University, Germany). Using flow cytometry and fluorescence microscopy the fluorescent drug was detected within cells. NPs devoid of IDA were non-toxic, thereby showing their biocompatibility. However, nanoparticulate drug formulations were not able to protect activated human T lymphocytes from the toxic effect of the active chemotherapeutic agent idarubicin as determined by XTT assay. Following, Qiong Lian coated MPE-IDA NPs with a gold layer to reduce premature drug release. However, this measure did not improve the viability of T cells either. On the contrary, gold-coated MPE-based NPs, even without drug content, already exhibited significant cytotoxicity in themselves. The observed decrease in T cell viability suggests that upon contact of IDA-NPs with T lymphocytes idarubicin was rapidly released. This could be due to the high lipophilicity of IDA, which could have facilitated immediate transfer from nanoparticles to hydrophobic areas such as lipid membranes of T cells. A “simple” solution to this problem could be the substitution of IDA for a less lipophilic anthracycline such as doxorubicin. However, this would probably require the development of a new nanoparticulate system including its characterization. The maleate part of MPE-NPs contains a double bond, which is accessible for cross-linking of polyesters within these NPs. Cross-linking could probably cause better entrapment of IDA within nanoparticles. Again, this approach would require more research, before cellular tests would be feasible. Another idea could be a replacement of the gold shell. Indeed, Lian and colleagues have already developed IDA-NPs coated with the polysaccharide chitosan. However, the development of these NPs was coincident with the pursuit of a new strategy for the T cell-mediated drug delivery approach.

This new strategy was the third part of this thesis and encompassed the replacement of the active anthracycline (IDA) by a stimulus-sensitive photosensitizer (mTHPP), the mode of action of which is only triggered by light irradiation in the presence of oxygen. The PS was kindly provided by Hagar Ibrahim Labouta (HIPS, Saarland University, Germany) in a water-soluble formulation (PSS/mTHPP). Cellular incorporation of the PS was confirmed by flow cytometry and fluo-

rescence microscopy. Uptake was temperature-dependent, suggesting an energy-dependent internalization by endocytosis. PS-loaded *ex vivo* activated human T lymphocytes survived the drug payload and did not show impaired natural cytolytic function when kept in the dark as assessed with WST-1 viability assay. When retargeted through a bispecific antibody, drug-loaded T cells were able to transfer the photosensitizer to carcinoma cells more efficiently. Redirected loaded T lymphocytes of all tested cell subsets were superior to redirected unloaded T lymphocytes in killing tumor cells after irradiation. The T cell-drug effect is synergistic rather than additive supporting the selectivity of bsAb-mediated mTHPP transfer, which was not demonstrated yet. These results are promising and justify testing the approach *in vivo*. However, the model photosensitizer mTHPP is not an ideal compound for the application in animal experiments and should be replaced by mTHPC. In contrast to mTHPP, its derivative is far more sensitive for activation with red light, which penetrates living tissue more deeply. Since both compounds have very similar chemical structures, results obtained in experiments with mTHPC are expected to be similar to those gained in this thesis. Furthermore, it was revealed that the uptake efficiency of PSS/mTHPP was rather poor. It remains to be seen whether ligands targeting receptors on the surface of T cells could achieve a greater drug uptake. A possible ligand, for instance, could be transferrin, which binds to the transferrin-receptor expressed by activated T cells.

In this thesis, all peripheral T cells were loaded with drugs. However, as noted in the introduction, while certain subsets of T lymphocytes can promote tumor regression other populations are responsible for tumor progression. It remains to be elucidated which composition of T cell subsets represents the best pharmaocyte mixture. On the other hand, this concern could be irrelevant, because T lymphocytes will die due to the drug effect. This poses a major drawback of the approach, because adoptive T cell therapies regularly rely on the generation of memory T lymphocytes to provide long-term tumor control. However, it does not necessarily mean that the drug delivery concept is not reasonable. Solid tumors often represent a major obstacle for successful ACT. It is imaginable that a first attack with pharmaocytes could render the cancer vulnerable for subsequent adoptive T cell therapy. For instance, although T lymphocytes can accumulate in the tumor stroma, the tumor vasculature can be a barrier that prevents deep tumor infiltration. The drug effect could damage this barrier and pave the way for later administered T cells. Generally, it is advantageous that carriers survive as long as possible to ensure maximal drug release and exploitation of the T cell effect. Engineering T lymphocytes with a resistance for the delivered drug could be the subject of further research. In the context of photosensitizers, this

resistance could be provided, to speculate, by scavengers of reactive oxygen species. These should remain within the carrier cells, while the PS is released and activated. Moreover, the concept is not restricted to bispecific antibody redirected polyclonal *ex vivo* activated T cells. In theory, it could be transferred to other types of ACT. For instance, tumor-infiltrating lymphocytes as well as tumor specific CAR T cells, both frequently used in clinical trials, could be loaded with pharmaceuticals.

To conclude, the work presented here provides substantial new insights indicating the feasibility of the envisioned T cell-mediated drug delivery approach, which have implications for three research areas: The use of “drug-enhanced super-killer” T lymphocytes could improve the clinical outcome of adoptive T cell therapies. Furthermore, the approach opens new perspectives in the area of cell-mediated drug delivery, since it prevents premature death of carrier cells that has been a major drawback of cell-based transport of anti-cancer drugs until now. Finally, the selectivity of photodynamic therapy could be significantly improved. Therefore, the combination of T lymphocyte-mediated drug delivery, adoptive T cell transfer and PDT could become a potent modality for the treatment of cancer. However, it is obvious that more research, particularly *in vivo*, is needed to further determine important parameters, which require optimization for maximal efficacy of this concept.

6. List of Abbreviations

ACT: Adoptive cell transfer/therapy
ADME: Absorption, distribution, metabolism, and excretion
Ag: Antigen
APC(s): Antigen-presenting cell(s)
AuSh: Gold shell-coated
BSA: Bovine serum albumin
BsAb(s): Bispecific antibody(ies)
CAR: Chimeric antigen receptor
CD: Cluster of differentiation
CFSE: 5-(and-6)-carboxyfluorescein diacetate, succinimidyl ester
CLSM: Confocal laser scanning microscopy
CTL(s): Cytotoxic T lymphocyte(s)
DABCO: 1,4-diazabicyclo-[2,2,2]-octane
DAMPs: Damage-associated molecular patterns
DAPI: 4',6-diamidino-2-phenylindole dihydrochloride
DAU: Daunorubicin
DC(s): Dendritic cells
DDS: Drug delivery systems
DiD: 1,1'-dioctadecyl-3,3,3',3'- tetramethylindodicarbocyanine, 4-chlorobenzenesulfonate salt
DiO: 3,3'-dioctadecyloxacarboyanine, perchlorate
DMSO: Dimethyl sulfoxide
DNA: Deoxyribonucleic acid
DOX: Doxorubicin
DSC: Differential scanning calorimetry
EA: Ethyl acetate
EDTA: Ethylenediaminetetraacetic acid
EE: Encapsulation efficiency
EpCAM: Epithelial cell adhesion molecule
EPI: Epirubicin
FACS: Fluorescence-activated cell sorting
FBS: Fetal bovine serum
FCM: Flow cytometry
FI: Fluorescence intensity
FITC: Fluorescein isothiocyanate
FM: Fluorescence microscopy
GA: Golgi apparatus
CG: Cytotoxic granules

GeoMean: Geometric mean
GMFI: Geometric mean of fluorescence intensity
GPC: Gel permeation chromatography
HOMO: Highest occupied molecular orbital
HpD: Hematoporphyrin derivatives
HPLC: High-performance liquid chromatography
IS: Immunological synapse
ICD: Immunogenic cell death
IDA: Idarubicin
IDA-NP(s): Idarubicin encapsulating nanoparticle(s)
IDOL: Idarubicinol
IDX: 4'-deoxy-4'-iododoxorubicin
IL: Interleukin
ISC: Intersystem crossing
LAK cell: Lymphokine-activated killer cell
LED: Light-emitting diode
LTc: Loaded T cell
LUMO: Lowest unoccupied molecular orbital
mAb: Monoclonal antibody
MAIT: Mucosa-associated invariant T cells
MHC: Major histocompatibility complex
MPE: Maleate-polyester
mTHPC: 5,10,15,20-tetrakis(3-hydroxyphenyl)chlorin
mTHPP: 5,10,15,20-tetrakis(3-hydroxyphenyl)porphyrin
MW: Molecular weight
MTOC: Microtubule-organizing center
NADPH: Nicotinamide adenine dinucleotide phosphate
NCA: *N*-carboxyanhydride
NIR: Near infrared
NK cell: Natural killer cell
NMR: Nuclear magnetic resonance
NP(s): Nanoparticle(s)
PBS: Phosphate buffered saline
PD: Polylysinderivate
PDI: Polydispersity index
PDT: Photodynamic therapy
PHA: Phytohaemagglutinin
PL: Polylysine

PLGA: Poly(lactic-*co*-glycolic-acid)
PL-Gal: Galactosylated polylysine
PL-Glu: Glucosylated polylysine
PL-Man: Mannosylated polylysine
PP: Polypropylene
PMS: Phenazine methosulfate
PR: Phenol red
PS: Photosensitizer/Photosensibilisator
PSS: Poly(styrene sulfonate) sodium salt
PVA: Polyvinyl alcohol
RES: Reticuloendothelial system
RNA: Ribonucleic acid
ROS: Reactive oxygen species
SMT: Somatic mutation theory
SD: Standard deviation
SPM: Scanning probe microscopy
TAA(s): Tumor-associated antigen(s)
TCR(s): T cells receptor(s)
TDL(s): Thoracic duct lymphocyte(s)
Th: T helper (cell)
Thf: T helper follicular (cell)
TIL: Tumor-infiltrating lymphocyte
Top: Topoisomerase
Treg: Regulatory T cell
TZ: T-Zellen
UV/Vis: Ultraviolet/Visible
WST-1: 5-(2,4-disulfophenyl)-2-(4-iodophenyl)-3-(4-nitrophenyl)-2H-tetrazolium
XTT: 2,3-bis(2-methoxy-4-nitro-5-sulfophenyl)-5-[(phenylamino)carbonyl]-2H-tetrazolium
ZS: Zytostatika

7. References

1. **Hinrichs, C.S., Rosenberg, S.A.**, (2014). Exploiting the curative potential of adoptive T-cell therapy for cancer, *Immunol. Rev.* 257, 56-71.
2. **Rosenberg, S.A., Yang, J.C., Sherry, R.M., Kammula, U.S., Hughes, M.S., Phan, G.Q., Citrin, D.E., Restifo, N.P., Robbins, P.F., Wunderlich, J.R., Morton, K.E., Laurencot, C.M., Steinberg, S.M., White, D.E., Dudley, M.E.**, (2011). Durable complete responses in heavily pretreated patients with metastatic melanoma using T-cell transfer immunotherapy, *Clin. Cancer Res.* 17, 4550-4557.
3. **Murphy, K., Janeway, C.A., Travers, P., Walport, M., Mowat, A., Weaver, C.T.**, (2012). *Janeway's immunobiology*, 8th ed., Garland Science. Taylor & Francis Group, London ; New York.
4. **Somerville, R.P., Devillier, L., Parkhurst, M.R., Rosenberg, S.A., Dudley, M.E.**, (2012). Clinical scale rapid expansion of lymphocytes for adoptive cell transfer therapy in the WAVE(R) bioreactor, *J. Transl. Med.* 10, 69.
5. **Kontermann, R.E., Brinkmann, U.**, (2015). Bispecific antibodies, *Drug Discov. Today* 20, 838-847.
6. **Mandruzzato, S., Rosato, A., Bronte, V., Zanovello, P., Amboldi, N., Ballinari, D., Collavo, D.**, (1994). Adoptive transfer of lymphokine-activated killer cells loaded with 4'-deoxy-4'-iododoxorubicin: therapeutic effect in mice bearing lung metastases, *Cancer Res.* 54, 1016-1020.
7. **Lum, L.G., Thakur, A.**, (2011). Targeting T cells with bispecific antibodies for cancer therapy, *BioDrugs* 25, 365-379.
8. **Marme, A., Strauss, G., Bastert, G., Grischke, E.M., Moldenhauer, G.**, (2002). Intraperitoneal bispecific antibody (HEA125xOKT3) therapy inhibits malignant ascites production in advanced ovarian carcinoma, *Int. J. Cancer* 101, 183-189.
9. **Salnikov, A.V., Groth, A., Apel, A., Kallifatidis, G., Beckermann, B.M., Khamidjanov, A., Ryschich, E., Buchler, M.W., Herr, I., Moldenhauer, G.**, (2009). Targeting of cancer stem cell marker EpCAM by bispecific antibody EpCAMxCD3 inhibits pancreatic carcinoma, *J. Cell. Mol. Med.* 13, 4023-4033.
10. **Strauss, G., Guckel, B., Wallwiener, D., Moldenhauer, G.**, (1999). Without prior stimulation, tumor-associated lymphocytes from malignant effusions lyse autologous tumor cells in the presence of bispecific antibody HEA125xOKT3, *Clin. Cancer Res.* 5, 171-180.
11. **Huang, B., Abraham, W.D., Zheng, Y., Bustamante Lopez, S.C., Luo, S.S., Irvine, D.J.**, (2015). Active targeting of chemotherapy to disseminated tumors using nanoparticle-carrying T cells, *Sci. Transl. Med.* 7, 291ra294.
12. **Batrakova, E.V., Gendelman, H.E., Kabanov, A.V.**, (2011). Cell-mediated drug delivery, *Expert Opin. Drug Deliv.* 8, 415-433.
13. **Pereboeva, L., Curiel, D.T.**, (2004). Cellular vehicles for cancer gene therapy: current status and future potential, *BioDrugs : clinical immunotherapeutics, biopharmaceuticals and gene therapy* 18, 361-385.
14. **Fridman, W.H., Pages, F., Sautes-Fridman, C., Galon, J.**, (2012). The immune contexture in human tumours: impact on clinical outcome, *Nat. Rev. Cancer* 12, 298-306.
15. **Motz, G.T., Coukos, G.**, (2013). Deciphering and reversing tumor immune suppression, *Immunity* 39, 61-73.

16. **Swann, J.B., Smyth, M.J.**, (2007). Immune surveillance of tumors, *The Journal of clinical investigation* 117, 1137-1146.
17. **Burnet, F.M.**, (1971). Immunological surveillance in neoplasia, *Transplant. Rev.* 7, 3-25.
18. **Vinay, D.S., Ryan, E.P., Pawelec, G., Talib, W.H., Stagg, J., Elkord, E., Lichtor, T., Decker, W.K., Whelan, R.L., Kumara, H.M., Signori, E., Honoki, K., Georgakilas, A.G., Amin, A., Helferich, W.G., Boosani, C.S., Guha, G., Ciriolo, M.R., Chen, S., Mohammed, S.I., Azmi, A.S., Keith, W.N., Bilsland, A., Bhakta, D., Halicka, D., Fujii, H., Aquilano, K., Ashraf, S.S., Nowsheen, S., Yang, X., Choi, B.K., Kwon, B.S.**, (2015). Immune evasion in cancer: Mechanistic basis and therapeutic strategies, *Semin. Cancer Biol.*
19. **Upadhyay, R., Hammerich, L., Peng, P., Brown, B., Merad, M., Brody, J.D.**, (2015). Lymphoma: immune evasion strategies, *Cancers* 7, 736-762.
20. **Pahl, J., Cerwenka, A.**, (2015). Tricking the balance: NK cells in anti-cancer immunity, *Immunobiology*
21. **Kalos, M., Levine, B.L., Porter, D.L., Katz, S., Grupp, S.A., Bagg, A., June, C.H.**, (2011). T cells with chimeric antigen receptors have potent antitumor effects and can establish memory in patients with advanced leukemia, *Sci. Transl. Med.* 3, 95ra73.
22. **Kochenderfer, J.N., Dudley, M.E., Feldman, S.A., Wilson, W.H., Spaner, D.E., Maric, I., Stetler-Stevenson, M., Phan, G.Q., Hughes, M.S., Sherry, R.M., Yang, J.C., Kammula, U.S., Devillier, L., Carpenter, R., Nathan, D.A., Morgan, R.A., Laurencot, C., Rosenberg, S.A.**, (2012). B-cell depletion and remissions of malignancy along with cytokine-associated toxicity in a clinical trial of anti-CD19 chimeric-antigen-receptor-transduced T cells, *Blood* 119, 2709-2720.
23. **Park, T.S., Rosenberg, S.A., Morgan, R.A.**, (2011). Treating cancer with genetically engineered T cells, *Trends Biotechnol.* 29, 550-557.
24. **Kershaw, M.H., Westwood, J.A., Darcy, P.K.**, (2013). Gene-engineered T cells for cancer therapy, *Nat. Rev. Cancer* 13, 525-541.
25. **Su, Y., Xie, Z., Kim, G.B., Dong, C., Yang, J.**, (2015). Design strategies and applications of circulating cell-mediated drug delivery systems, *ACS biomaterials science & engineering* 1, 201-217.
26. **Peters, C., Brown, S.**, (2015). Antibody-drug conjugates as novel anti-cancer chemotherapeutics, *Biosci. Rep.* 35,
27. **Hu, X., Liu, S., Zhou, G., Huang, Y., Xie, Z., Jing, X.**, (2014). Electrospinning of polymeric nanofibers for drug delivery applications, *Journal of controlled release : official journal of the Controlled Release Society* 185, 12-21.
28. **Zelikin, A.N.**, (2010). Drug releasing polymer thin films: new era of surface-mediated drug delivery, *ACS nano* 4, 2494-2509.
29. **Maya, S., Sarmiento, B., Nair, A., Rejinold, N.S., Nair, S.V., Jayakumar, R.**, (2013). Smart stimuli sensitive nanogels in cancer drug delivery and imaging: a review, *Curr. Pharm. Des.* 19, 7203-7218.
30. **Allen, T.M., Cullis, P.R.**, (2013). Liposomal drug delivery systems: from concept to clinical applications, *Advanced drug delivery reviews* 65, 36-48.
31. **Parveen, S., Misra, R., Sahoo, S.K.**, (2012). Nanoparticles: a boon to drug delivery, therapeutics, diagnostics and imaging, *Nanomedicine : nanotechnology, biology, and medicine* 8, 147-166.

32. **Nicolas, J., Mura, S., Brambilla, D., Mackiewicz, N., Couvreur, P.,** (2013). Design, functionalization strategies and biomedical applications of targeted biodegradable/biocompatible polymer-based nanocarriers for drug delivery, *Chem. Soc. Rev.* 42, 1147-1235.
33. **Kedar, U., Phutane, P., Shidhaye, S., Kadam, V.,** (2010). Advances in polymeric micelles for drug delivery and tumor targeting, *Nanomedicine : nanotechnology, biology, and medicine* 6, 714-729.
34. **Kopecek, J.,** (2013). Polymer-drug conjugates: origins, progress to date and future directions, *Advanced drug delivery reviews* 65, 49-59.
35. **Zhang, J., Ma, P.X.,** (2013). Cyclodextrin-based supramolecular systems for drug delivery: recent progress and future perspective, *Advanced drug delivery reviews* 65, 1215-1233.
36. **Hafner, A., Lovric, J., Lakos, G.P., Pepic, I.,** (2014). Nanotherapeutics in the EU: an overview on current state and future directions, *Int. J. Nanomedicine* 9, 1005-1023.
37. **McMillan, J., Batrakova, E., Gendelman, H.E.,** (2011). Cell delivery of therapeutic nanoparticles, *Progress in molecular biology and translational science* 104, 563-601.
38. **Anselmo, A.C., Mitragotri, S.,** (2014). An overview of clinical and commercial impact of drug delivery systems, *Journal of controlled release : official journal of the Controlled Release Society* 190, 15-28.
39. **Torchilin, V.P.,** (2007). Targeted pharmaceutical nanocarriers for cancer therapy and imaging, *The AAPS journal* 9, E128-147.
40. **Bae, Y.H., Park, K.,** (2011). Targeted drug delivery to tumors: myths, reality and possibility, *Journal of controlled release : official journal of the Controlled Release Society* 153, 198-205.
41. **Anselmo, A.C., Mitragotri, S.,** (2014). Cell-mediated delivery of nanoparticles: taking advantage of circulatory cells to target nanoparticles, *Journal of controlled release : official journal of the Controlled Release Society* 190, 531-541.
42. **Wang, Q., Cheng, H., Peng, H., Zhou, H., Li, P.Y., Langer, R.,** (2014). Non-genetic engineering of cells for drug delivery and cell-based therapy, *Advanced drug delivery reviews*
43. **Roth, J.C., Curiel, D.T., Pereboeva, L.,** (2008). Cell vehicle targeting strategies, *Gene Ther.* 15, 716-729.
44. **Kolb, H.C., Finn, M.G., Sharpless, K.B.,** (2001). Click Chemistry: Diverse Chemical Function from a Few Good Reactions, *Angewandte Chemie* 40, 2004-2021.
45. **Wang, G.P., Guan, Y.S., Jin, X.R., Jiang, S.S., Lu, Z.J., Wu, Y., Li, Y., Li, M., Luo, F.,** (2010). Development of novel 5-fluorouracil carrier erythrocyte with pharmacokinetics and potent antitumor activity in mice bearing malignant ascites, *J. Gastroenterol. Hepatol.* 25, 985-990.
46. **Zocchi, E., Tonetti, M., Polvani, C., Guida, L., Benatti, U., De Flora, A.,** (1989). Encapsulation of doxorubicin in liver-targeted erythrocytes increases the therapeutic index of the drug in a murine metastatic model, *Proc. Natl. Acad. Sci. U. S. A.* 86, 2040-2044.
47. **Flynn, G., McHale, L., McHale, A.P.,** (1994). Methotrexate-loaded, photosensitized erythrocytes: a photo-activatable carrier/delivery system for use in cancer therapy, *Cancer Lett.* 82, 225-229.
48. **Staedtke, V., Brahler, M., Muller, A., Georgieva, R., Bauer, S., Sternberg, N., Voigt, A., Lemke, A., Keck, C., Moschwitz, J., Baumler, H.,** (2010). In vitro inhibition of fungal activity by macrophage-

- mediated sequestration and release of encapsulated amphotericin B nanosuspension in red blood cells, *Small* 6, 96-103.
49. **Bossa, F., Latiano, A., Rossi, L., Magnani, M., Palmieri, O., Dallapiccola, B., Serafini, S., Damonte, G., De Santo, E., Andriulli, A., Annese, V.,** (2008). Erythrocyte-mediated delivery of dexamethasone in patients with mild-to-moderate ulcerative colitis, refractory to mesalamine: a randomized, controlled study, *The American journal of gastroenterology* 103, 2509-2516.
 50. **Biagiotti, S., Rossi, L., Bianchi, M., Giacomini, E., Pierige, F., Serafini, G., Conaldi, P.G., Magnani, M.,** (2011). Immunophilin-loaded erythrocytes as a new delivery strategy for immunosuppressive drugs, *Journal of controlled release : official journal of the Controlled Release Society* 154, 306-313.
 51. **Rossi, L., Brandi, G., Schiavano, G.F., Scarfi, S., Millo, E., Damonte, G., Benatti, U., De Flora, A., Magnani, M.,** (1999). Heterodimer-loaded erythrocytes as bioreactors for slow delivery of the antiviral drug azidothymidine and the antimycobacterial drug ethambutol, *AIDS Res. Hum. Retroviruses* 15, 345-353.
 52. **Dale, G.L., Kuhl, W., Beutler, E.,** (1979). Incorporation of glucocerebrosidase into Gaucher's disease monocytes in vitro, *Proc. Natl. Acad. Sci. U. S. A.* 76, 473-475.
 53. **Zaitsev, S., Danielyan, K., Murciano, J.C., Ganguly, K., Krasik, T., Taylor, R.P., Pincus, S., Jones, S., Cines, D.B., Muzykantov, V.R.,** (2006). Human complement receptor type 1-directed loading of tissue plasminogen activator on circulating erythrocytes for prophylactic fibrinolysis, *Blood* 108, 1895-1902.
 54. **Kontos, S., Kourtis, I.C., Dane, K.Y., Hubbell, J.A.,** (2013). Engineering antigens for in situ erythrocyte binding induces T-cell deletion, *Proc. Natl. Acad. Sci. U. S. A.* 110, E60-68.
 55. **Pizzo, D.P., Coufal, N.G., Lortie, M.J., Gage, F.H., Thal, L.J.,** (2006). Regulatable acetylcholine-producing fibroblasts enhance cognitive performance, *Molecular therapy : the journal of the American Society of Gene Therapy* 13, 175-182.
 56. **Yasuhara, T., Shingo, T., Muraoka, K., Kameda, M., Agari, T., Wen Ji, Y., Hayase, H., Hamada, H., Borlongan, C.V., Date, I.,** (2005). Neurorescue effects of VEGF on a rat model of Parkinson's disease, *Brain Res.* 1053, 10-18.
 57. **Shao, J., DeHaven, J., Lamm, D., Weissman, D.N., Malanga, C.J., Rojanasakul, Y., Ma, J.K.,** (2001). A cell-based drug delivery system for lung targeting: II. Therapeutic activities on B16-F10 melanoma in mouse lungs, *Drug delivery* 8, 71-76.
 58. **Kim, D., Hoory, T., Monie, A., Wu, A., Hsueh, W.T., Pai, S.I., Hung, C.F.,** (2010). Delivery of chemotherapeutic agents using drug-loaded irradiated tumor cells to treat murine ovarian tumors, *J. Biomed. Sci.* 17, 61.
 59. **Dubrot, J., Portero, A., Orive, G., Hernandez, R.M., Palazon, A., Rouzaut, A., Perez-Gracia, J.L., Hervas-Stubbs, S., Pedraz, J.L., Melero, I.,** (2010). Delivery of immunostimulatory monoclonal antibodies by encapsulated hybridoma cells, *Cancer Immunology Immunotherapy* 59, 1621-1631.
 60. **Menon, L.G., Kelly, K., Yang, H.W., Kim, S.K., Black, P.M., Carroll, R.S.,** (2009). Human bone marrow-derived mesenchymal stromal cells expressing S-TRAIL as a cellular delivery vehicle for human glioma therapy, *Stem Cells* 27, 2320-2330.

61. **Studený, M., Marini, F.C., Champlin, R.E., Zompetta, C., Fidler, I.J., Andreeff, M.,** (2002). Bone marrow-derived mesenchymal stem cells as vehicles for interferon-beta delivery into tumors, *Cancer Res.* 62, 3603-3608.
62. **Stoff-Khalili, M.A., Rivera, A.A., Mathis, J.M., Banerjee, N.S., Moon, A.S., Hess, A., Rocconi, R.P., Numnum, T.M., Everts, M., Chow, L.T., Douglas, J.T., Siegal, G.P., Zhu, Z.B., Bender, H.G., Dall, P., Stoff, A., Pereboeva, L., Curiel, D.T.,** (2007). Mesenchymal stem cells as a vehicle for targeted delivery of CRAds to lung metastases of breast carcinoma, *Breast Cancer Res. Treat.* 105, 157-167.
63. **Martinez-Serrano, A., Bjorklund, A.,** (1998). Ex vivo nerve growth factor gene transfer to the basal forebrain in presymptomatic middle-aged rats prevents the development of cholinergic neuron atrophy and cognitive impairment during aging, *Proc. Natl. Acad. Sci. U. S. A.* 95, 1858-1863.
64. **Martinez-Serrano, A., Hantzopoulos, P.A., Bjorklund, A.,** (1996). Ex vivo gene transfer of brain-derived neurotrophic factor to the intact rat forebrain: neurotrophic effects on cholinergic neurons, *The European journal of neuroscience* 8, 727-735.
65. **Blurton-Jones, M., Spencer, B., Michael, S., Castello, N.A., Agazaryan, A.A., Davis, J.L., Muller, F.J., Loring, J.F., Masliah, E., LaFerla, F.M.,** (2014). Neural stem cells genetically-modified to express neprilysin reduce pathology in Alzheimer transgenic models, *Stem cell research & therapy* 5, 46.
66. **Akerud, P., Canals, J.M., Snyder, E.Y., Arenas, E.,** (2001). Neuroprotection through delivery of glial cell line-derived neurotrophic factor by neural stem cells in a mouse model of Parkinson's disease, *The Journal of neuroscience : the official journal of the Society for Neuroscience* 21, 8108-8118.
67. **Casper, D., Engstrom, S.J., Mirchandani, G.R., Pidel, A., Palencia, D., Cho, P.H., Brownlee, M., Edelstein, D., Federoff, H.J., Sonstein, W.J.,** (2002). Enhanced vascularization and survival of neural transplants with ex vivo angiogenic gene transfer, *Cell Transplant.* 11, 331-349.
68. **Ahmed, A.U., Tyler, M.A., Thaci, B., Alexiades, N.G., Han, Y., Ulasov, I.V., Lesniak, M.S.,** (2011). A comparative study of neural and mesenchymal stem cell-based carriers for oncolytic adenovirus in a model of malignant glioma, *Mol. Pharm.* 8, 1559-1572.
69. **Garcia, P., Youssef, I., Utvik, J.K., Florent-Bechard, S., Barthelemy, V., Malaplate-Armand, C., Kriem, B., Stenger, C., Koziel, V., Olivier, J.L., Escanye, M.C., Hanse, M., Allouche, A., Desbene, C., Yen, F.T., Bjerkvig, R., Oster, T., Niclou, S.P., Pillot, T.,** (2010). Ciliary neurotrophic factor cell-based delivery prevents synaptic impairment and improves memory in mouse models of Alzheimer's disease, *The Journal of neuroscience : the official journal of the Society for Neuroscience* 30, 7516-7527.
70. **Kumar, A., Glaum, M., El-Badri, N., Mohapatra, S., Haller, E., Park, S., Patrick, L., Nattkemper, L., Vo, D., Cameron, D.F.,** (2011). Initial observations of cell-mediated drug delivery to the deep lung, *Cell Transplant.* 20, 609-618.
71. **Orange, D.E., Blachere, N.E., Fak, J., Parveen, S., Frank, M.O., Herre, M., Tian, S., Monette, S., Darnell, R.B.,** (2013). Dendritic cells loaded with FK506 kill T cells in an antigen-specific manner and prevent autoimmunity in vivo, *eLife* 2, e00105.

72. **Ikehara, Y., Niwa, T., Biao, L., Ikehara, S.K., Ohashi, N., Kobayashi, T., Shimizu, Y., Kojima, N., Nakanishi, H.**, (2006). A carbohydrate recognition-based drug delivery and controlled release system using intraperitoneal macrophages as a cellular vehicle, *Cancer Res.* 66, 8740-8748.
73. **Basel, M.T., Balivada, S., Wang, H., Shrestha, T.B., Seo, G.M., Pyle, M., Abayaweera, G., Dani, R., Koper, O.B., Tamura, M., Chikan, V., Bossmann, S.H., Troyer, D.L.**, (2012). Cell-delivered magnetic nanoparticles caused hyperthermia-mediated increased survival in a murine pancreatic cancer model, *Int. J. Nanomedicine* 7, 297-306.
74. **Choi, J., Kim, H.Y., Ju, E.J., Jung, J., Park, J., Chung, H.K., Lee, J.S., Park, H.J., Song, S.Y., Jeong, S.Y., Choi, E.K.**, (2012). Use of macrophages to deliver therapeutic and imaging contrast agents to tumors, *Biomaterials* 33, 4195-4203.
75. **Baek, S.K., Makkouk, A.R., Krasieva, T., Sun, C.H., Madsen, S.J., Hirschberg, H.**, (2011). Photothermal treatment of glioma; an in vitro study of macrophage-mediated delivery of gold nanoshells, *J. Neurooncol.* 104, 439-448.
76. **Fu, J., Wang, D., Mei, D., Zhang, H., Wang, Z., He, B., Dai, W., Wang, X., Zhang, Q.**, (2015). Macrophage mediated biomimetic delivery system for the treatment of lung metastasis of breast cancer, *Journal of controlled release : official journal of the Controlled Release Society* 204, 11-19.
77. **Klyachko, N.L., Haney, M.J., Zhao, Y., Manickam, D.S., Mahajan, V., Suresh, P., Hingtgen, S.D., Mosley, R.L., Gendelman, H.E., Kabanov, A.V., Batrakova, E.V.**, (2014). Macrophages offer a paradigm switch for CNS delivery of therapeutic proteins, *Nanomed.* 9, 1403-1422.
78. **Brynskikh, A.M., Zhao, Y., Mosley, R.L., Li, S., Boska, M.D., Klyachko, N.L., Kabanov, A.V., Gendelman, H.E., Batrakova, E.V.**, (2010). Macrophage delivery of therapeutic nanozymes in a murine model of Parkinson's disease, *Nanomed.* 5, 379-396.
79. **Dou, H., Grotetas, C.B., McMillan, J.M., Destache, C.J., Chaubal, M., Werling, J., Kipp, J., Rabinow, B., Gendelman, H.E.**, (2009). Macrophage delivery of nanoformulated antiretroviral drug to the brain in a murine model of neuroAIDS, *J. Immunol.* 183, 661-669.
80. **Birch, M., Sharma, H.L., Bell, E.B., Ford, W.L.**, (1986). The carriage and delivery of substances to lymphatic tissues by recirculating lymphocytes. II. Long-term selective irradiation of the spleen and lymph nodes by deposition of indium-114m, *Immunology* 58, 359-364.
81. **Mandrizzato, S., Rosato, A., Bronte, V., Pollis, F., Zambon, A., Zanovello, P., Collavo, D.**, (1992). Therapeutical effect of 4'-deoxy-4'-iododoxorubicin-loaded LAK cells in mice bearing lung metastases, *Pharmacol. Res.* 26 Suppl 2, 124-125.
82. **Zanovello, P., Rosato, A., Bronte, V., Mandrizzato, S., Cerundolo, V., Collavo, D.**, (1992). Antitumour efficacy of lymphokine-activated killer cells loaded with ricin against experimentally induced lung metastases, *Cancer Immunol. Immunother.* 35, 27-32.
83. **Quintieri, L., Rosato, A., Amboldi, N., Vizler, C., Ballinari, D., Zanovello, P., Collavo, D.**, (1999). Delivery of methoxymorpholinyl doxorubicin by interleukin 2-activated NK cells: effect in mice bearing hepatic metastases, *Br. J. Cancer* 79, 1067-1073.

84. **Cerundolo, V., Zanovello, P., McIntosh, D., Fabbris, R., Davies, A.J., Collavo, D.**, (1987). Temporary inhibition of Moloney-murine sarcoma virus (M-MSV) induced-tumours by adoptive transfer of ricin-treated T-lymphocytes, *Br. J. Cancer* 55, 413-419.
85. **Chen, S.Y., Yang, A.G., Chen, J.D., Kute, T., King, C.R., Collier, J., Cong, Y., Yao, C., Huang, X.F.**, (1997). Potent antitumour activity of a new class of tumour-specific killer cells, *Nature* 385, 78-80.
86. **Vallera, D.A., Jin, N., Baldrice, J.M., Panoskaltis-Mortari, A., Chen, S.Y., Blazar, B.R.**, (2000). Retroviral immunotoxin gene therapy of acute myelogenous leukemia in mice using cytotoxic T cells transduced with an interleukin 4/diphtheria toxin gene, *Cancer Res.* 60, 976-984.
87. **Jin, N., Chen, W., Blazar, B.R., Ramakrishnan, S., Vallera, D.A.**, (2002). Gene therapy of murine solid tumors with T cells transduced with a retroviral vascular endothelial growth factor--immunotoxin target gene, *Hum. Gene Ther.* 13, 497-508.
88. **Vallera, D.A., Jin, N., Shu, Y., Panoskaltis-Mortari, A., Kelekar, A., Chen, W.**, (2003). Retroviral immunotoxin gene therapy of leukemia in mice using leukemia-specific T cells transduced with an interleukin-3/Bax fusion protein gene, *Hum. Gene Ther.* 14, 1787-1798.
89. **Cole, C., Qiao, J., Kottke, T., Diaz, R.M., Ahmed, A., Sanchez-Perez, L., Brunn, G., Thompson, J., Chester, J., Vile, R.G.**, (2005). Tumor-targeted, systemic delivery of therapeutic viral vectors using hitchhiking on antigen-specific T cells, *Nat. Med.* 11, 1073-1081.
90. **Stephan, M.T., Moon, J.J., Um, S.H., Bershteyn, A., Irvine, D.J.**, (2010). Therapeutic cell engineering with surface-conjugated synthetic nanoparticles, *Nat. Med.* 16, 1035-1041.
91. **Stephan, M.T., Stephan, S.B., Bak, P., Chen, J., Irvine, D.J.**, (2012). Synapse-directed delivery of immunomodulators using T-cell-conjugated nanoparticles, *Biomaterials* 33, 5776-5787.
92. **Brambilla, D., Luciani, P., Leroux, J.C.**, (2014). Breakthrough discoveries in drug delivery technologies: the next 30 years, *Journal of controlled release : official journal of the Controlled Release Society* 190, 9-14.
93. **NCI**, (2015). <http://www.cancer.gov/about-cancer/what-is-cancer>, National Cancer Institute at the National Institutes of Health.
94. **Hanahan, D., Weinberg, R.A.**, (2011). Hallmarks of cancer: the next generation, *Cell* 144, 646-674.
95. **Bedessem, B., Ruphy, S.**, (2015). SMT or TOFT? How the Two Main Theories of Carcinogenesis are Made (Artificially) Incompatible, *Acta Biotheor.* 63, 257-267.
96. **Wild, C.P., Stewart, B.W., Denmark. International Agency for Research on Cancer, World Health Organization**, (2014). *World Cancer Report 2014*, World Health Organization : International Agency for Research on Cancer, Lyon.
97. **McIntosh, D.P., Edwards, D.C., Davies, A.J.**, (1984). Transfer of ricin toxicity by spleen cells, *Toxicol* 22, 293-299.
98. **Wimer, B.M.**, (1997). Therapeutic immunostimulating effects of plant mitogens exemplified by the L4 isolectin of PHA, *Cancer Biother. Radiopharm.* 12, 195-212.
99. **Sparshott, S.M., Forrester, J.A., McIntosh, D.P., Wood, C., Davies, A.J., Ford, W.L.**, (1985). The carriage and delivery of substances to lymphatic tissues by recirculating lymphocytes. I. The concentration of ricin in lymphocyte traffic areas, *Immunology* 54, 731-743.

100. **Phillips, J.H., Lanier, L.L.**, (1986). Dissection of the lymphokine-activated killer phenomenon. Relative contribution of peripheral blood natural killer cells and T lymphocytes to cytolysis, *The Journal of experimental medicine* 164, 814-825.
101. **Steinfeld, U., Pauli, C., Kaltz, N., Bergemann, C., Lee, H.H.**, (2006). T lymphocytes as potential therapeutic drug carrier for cancer treatment, *Int. J. Pharm.* 311, 229-236.
102. **Mortensen, M.W., Kahns, L., Hansen, T., Sorensen, P.G., Bjorkdahl, O., Jensen, M.R., Gundersen, H.J., Bjornholm, T.**, (2007). Next generation adoptive immunotherapy--human T cells as carriers of therapeutic nanoparticles, *J. Nanosci. Nanotechnol.* 7, 4575-4580.
103. **Iida, H., Takayanagi, K., Nakanishi, T., Kume, A., Muramatsu, K., Kiyohara, Y., Akiyama, Y., Osaka, T.**, (2008). Preparation of human immune effector T cells containing iron-oxide nanoparticles, *Biotechnol. Bioeng.* 101, 1123-1128.
104. **Kennedy, L.C., Bear, A.S., Young, J.K., Lewinski, N.A., Kim, J., Foster, A.E., Drezek, R.A.**, (2011). T cells enhance gold nanoparticle delivery to tumors in vivo, *Nanoscale Res Lett* 6, 283.
105. **Gutcher, I., Becher, B.**, (2007). APC-derived cytokines and T cell polarization in autoimmune inflammation, *The Journal of clinical investigation* 117, 1119-1127.
106. **den Haan, J.M., Arens, R., van Zelm, M.C.**, (2014). The activation of the adaptive immune system: cross-talk between antigen-presenting cells, T cells and B cells, *Immunol. Lett.* 162, 103-112.
107. **Curtsinger, J.M., Mescher, M.F.**, (2010). Inflammatory cytokines as a third signal for T cell activation, *Curr. Opin. Immunol.* 22, 333-340.
108. **Bevan, M.J.**, (2004). Helping the CD8(+) T-cell response, *Nat. Rev. Immunol.* 4, 595-602.
109. **Geginat, J., Paroni, M., Facciotti, F., Gruarin, P., Kastirr, I., Caprioli, F., Pagani, M., Abrignani, S.**, (2013). The CD4-centered universe of human T cell subsets, *Semin. Immunol.* 25, 252-262.
110. **Cosmi, L., Maggi, L., Santarlasci, V., Liotta, F., Annunziato, F.**, (2014). T helper cells plasticity in inflammation, *Cytometry. Part A : the journal of the International Society for Analytical Cytology* 85, 36-42.
111. **Wan, Y.Y., Flavell, R.A.**, (2009). How diverse--CD4 effector T cells and their functions, *J. Mol. Cell Biol.* 1, 20-36.
112. **Jiang, S., Dong, C.**, (2013). A complex issue on CD4(+) T-cell subsets, *Immunol. Rev.* 252, 5-11.
113. **Cheroutre, H., Husain, M.M.**, (2013). CD4 CTL: living up to the challenge, *Semin. Immunol.* 25, 273-281.
114. **Chavez-Galan, L., Arenas-Del Angel, M.C., Zenteno, E., Chavez, R., Lascurain, R.**, (2009). Cell death mechanisms induced by cytotoxic lymphocytes, *Cell. Mol. Immunol.* 6, 15-25.
115. **Mittrucker, H.W., Visekruna, A., Huber, M.**, (2014). Heterogeneity in the differentiation and function of CD8(+) T cells, *Arch. Immunol. Ther. Exp. (Warsz.)* 62, 449-458.
116. **Mahnke, Y.D., Brodie, T.M., Sallusto, F., Roederer, M., Lugli, E.**, (2013). The who's who of T-cell differentiation: human memory T-cell subsets, *Eur. J. Immunol.* 43, 2797-2809.
117. **Berard, M., Tough, D.F.**, (2002). Qualitative differences between naive and memory T cells, *Immunology* 106, 127-138.
118. **Chien, Y.H., Meyer, C., Bonneville, M.**, (2014). gammadelta T cells: first line of defense and beyond, *Annu. Rev. Immunol.* 32, 121-155.

119. **Cowley, S.C.**, (2014). MAIT cells and pathogen defense, *Cellular and molecular life sciences* : CMLS 71, 4831-4840.
120. **Jerud, E.S., Bricard, G., Porcelli, S.A.**, (2006). CD1d-restricted natural killer T cells: Roles in tumor immunosurveillance and tolerance, *Transfusion Medicine and Hemotherapy* 33, 18-36.
121. **Chen, D.S., Mellman, I.**, (2013). Oncology meets immunology: the cancer-immunity cycle, *Immunity* 39, 1-10.
122. **Muranski, P., Restifo, N.P.**, (2009). Adoptive immunotherapy of cancer using CD4(+) T cells, *Curr. Opin. Immunol.* 21, 200-208.
123. **June, C.H.**, (2007). Principles of adoptive T cell cancer therapy, *The Journal of clinical investigation* 117, 1204-1212.
124. **Vegran, F., Apetoh, L., Ghiringhelli, F.**, (2015). Th9 cells: a novel CD4 T-cell subset in the immune war against cancer, *Cancer Res.* 75, 475-479.
125. **Minotti, G., Menna, P., Salvatorelli, E., Cairo, G., Gianni, L.**, (2004). Anthracyclines: molecular advances and pharmacologic developments in antitumor activity and cardiotoxicity, *Pharmacol. Rev.* 56, 185-229.
126. **Cutts, S.M., Swift, L.P., Pillay, V., Forrest, R.A., Nudelman, A., Rephaeli, A., Phillips, D.R.**, (2007). Activation of clinically used anthracyclines by the formaldehyde-releasing prodrug pivaloyloxymethyl butyrate, *Mol. Cancer Ther.* 6, 1450-1459.
127. **Grein, A., Spalla, C., Canevazz, G., Di Marco, A.**, (1963). Descrizione e classificazione di un attinomicete (*Streptomyces peucetius* sp. nova) produttore di una sostanza ad attivita antitumorale - la daunomicina, *G. Microbiol.* 11, 109-115.
128. **Di Marco, A., Gaetani, M., Orezzi, P., Scarpinato, B.M., Silvestrini, R., Soldati, M., Dasdia, T., Valentini, L.**, (1964). 'Daunomycin', a New Antibiotic of the Rhodomycin Group, *Nature* 201, 706-707.
129. **Arcamone, F., Cassinelli, G., Fantini, G., Grein, A., Orezzi, P., Pol, C., Spalla, C.**, (1969). Adriamycin, 14-hydroxydaunomycin, a new antitumor antibiotic from *S. peucetius* var. *caesius*, *Biotechnol. Bioeng.* 11, 1101-1110.
130. **Seiter, K.**, (2005). Toxicity of the topoisomerase II inhibitors, *Expert Opin. Drug Saf.* 4, 219-234.
131. **Gewirtz, D.A.**, (1999). A critical evaluation of the mechanisms of action proposed for the antitumor effects of the anthracycline antibiotics adriamycin and daunorubicin, *Biochem. Pharmacol.* 57, 727-741.
132. **Kizek, R., Adam, V., Hrabeta, J., Eckschlager, T., Smutny, S., Burda, J.V., Frei, E., Stiborova, M.**, (2012). Anthracyclines and ellipticines as DNA-damaging anticancer drugs: recent advances, *Pharmacol. Ther.* 133, 26-39.
133. **Sobek, S., Boege, F.**, (2014). DNA topoisomerases in mtDNA maintenance and ageing, *Exp. Gerontol.* 56, 135-141.
134. **Pommier, Y., Leo, E., Zhang, H., Marchand, C.**, (2010). DNA topoisomerases and their poisoning by anticancer and antibacterial drugs, *Chem. Biol.* 17, 421-433.
135. **Chen, S.H., Chan, N.L., Hsieh, T.S.**, (2013). New mechanistic and functional insights into DNA topoisomerases, *Annu. Rev. Biochem.* 82, 139-170.

136. **Dal Ben, D., Palumbo, M., Zagotto, G., Capranico, G., Moro, S.,** (2007). DNA topoisomerase II structures and anthracycline activity: insights into ternary complex formation, *Curr. Pharm. Des.* 13, 2766-2780.
137. **Moro, S., Beretta, G.L., Dal Ben, D., Nitiss, J., Palumbo, M., Capranico, G.,** (2004). Interaction model for anthracycline activity against DNA topoisomerase II, *Biochemistry (Mosc.)* 43, 7503-7513.
138. **Wu, C.C., Li, Y.C., Wang, Y.R., Li, T.K., Chan, N.L.,** (2013). On the structural basis and design guidelines for type II topoisomerase-targeting anticancer drugs, *Nucleic Acids Res.* 41, 10630-10640.
139. **Garg, A.D., Agostinis, P.,** (2014). ER stress, autophagy and immunogenic cell death in photodynamic therapy-induced anti-cancer immune responses, *Photochemical & photobiological sciences : Official journal of the European Photochemistry Association and the European Society for Photobiology* 13, 474-487.
140. **Dudek, A.M., Garg, A.D., Krysko, D.V., De Ruyscher, D., Agostinis, P.,** (2013). Inducers of immunogenic cancer cell death, *Cytokine Growth Factor Rev.* 24, 319-333.
141. **Kepp, O., Menger, L., Vacchelli, E., Locher, C., Adjemian, S., Yamazaki, T., Martins, I., Sukkurwala, A.Q., Michaud, M., Senovilla, L., Galluzzi, L., Kroemer, G., Zitvogel, L.,** (2013). Crosstalk between ER stress and immunogenic cell death, *Cytokine Growth Factor Rev.* 24, 311-318.
142. **Zhang, S., Liu, X., Bawa-Khalfe, T., Lu, L.S., Lyu, Y.L., Liu, L.F., Yeh, E.T.,** (2012). Identification of the molecular basis of doxorubicin-induced cardiotoxicity, *Nat. Med.* 18, 1639-1642.
143. **Arcamone, F., Bernardi, L., Giardino, P., Patelli, B., Marco, A., Casazza, A.M., Pratesi, G., Reggiani, P.,** (1976). Synthesis and antitumor activity of 4-demethoxydaunorubicin, 4-demethoxy-7,9-diepidaurubicin, and their beta anomers, *Cancer Treat. Rep.* 60, 829-834.
144. **Mulder, H.S., Dekker, H., Pinedo, H.M., Lankelma, J.,** (1995). The P-glycoprotein-mediated relative decrease in cytosolic free drug concentration is similar for several anthracyclines with varying lipophilicity, *Biochem. Pharmacol.* 50, 967-974.
145. **Borchmann, P., Hubel, K., Schnell, R., Engert, A.,** (1997). Idarubicin: a brief overview on pharmacology and clinical use, *Int. J. Clin. Pharmacol. Ther.* 35, 80-83.
146. **Kuffel, M.J., Reid, J.M., Ames, M.M.,** (1992). Anthracyclines and their C-13 alcohol metabolites: growth inhibition and DNA damage following incubation with human tumor cells in culture, *Cancer Chemother. Pharmacol.* 30, 51-57.
147. **Roovers, D.J., van Vliet, M., Bloem, A.C., Lokhorst, H.M.,** (1999). Idarubicin overcomes P-glycoprotein-related multidrug resistance: comparison with doxorubicin and daunorubicin in human multiple myeloma cell lines, *Leuk. Res.* 23, 539-548.
148. **Yamashita, T., Fukushima, T., Ueda, T.,** (2008). Pharmacokinetic self-potential of idarubicin by induction of anthracycline carbonyl reducing enzymes, *Leuk. Lymphoma* 49, 809-814.
149. **Hohloch, K., Zwick, C., Ziepert, M., Hasenclever, D., Kaiser, U., Engert, A., Hoffkes, H.G., Kroschinsky, F., Mesters, R., Feller, A.C., Loffler, M., Trumper, L., Pfreundschuh, M.,** (2014). Significant dose Escalation of Idarubicin in the treatment of aggressive Non- Hodgkin Lymphoma leads to increased hematotoxicity without improvement in efficacy in comparison to standard CHOEP-14: 9-year follow up results of the CIVEP trial of the DSHNHL, *SpringerPlus* 3, 5.

150. **Vejpongsa, P., Yeh, E.T.**, (2014). Prevention of anthracycline-induced cardiotoxicity: challenges and opportunities, *J. Am. Coll. Cardiol.* 64, 938-945.
151. **Safra, T.**, (2003). Cardiac safety of liposomal anthracyclines, *The oncologist* 8 Suppl 2, 17-24.
152. **Allison, R.R., Moghissi, K.**, (2013). Photodynamic Therapy (PDT): PDT Mechanisms, *Clinical endoscopy* 46, 24-29.
153. **Senge, M.O., Brandt, J.C.**, (2011). Temoporfin (Foscan(R), 5,10,15,20-tetra(m-hydroxyphenyl)chlorin)--a second-generation photosensitizer, *Photochem. Photobiol.* 87, 1240-1296.
154. **Dolmans, D.E., Fukumura, D., Jain, R.K.**, (2003). Photodynamic therapy for cancer, *Nat. Rev. Cancer* 3, 380-387.
155. **Juarranz, A., Jaen, P., Sanz-Rodriguez, F., Cuevas, J., Gonzalez, S.**, (2008). Photodynamic therapy of cancer. Basic principles and applications, *Clinical & translational oncology : official publication of the Federation of Spanish Oncology Societies and of the National Cancer Institute of Mexico* 10, 148-154.
156. **Raab, O.**, (1900). Über die Wirkung fluoreszierender Stoffe auf Infusorien, *Zeitung Biol.* 39, 524-526.
157. **Waksman, R., McEwan, P.E., Moore, T.I., Pakala, R., Kolodgie, F.D., Hellinga, D.G., Seabron, R.C., Rychnovsky, S.J., Vasek, J., Scott, R.W., Virmani, R.**, (2008). PhotoPoint photodynamic therapy promotes stabilization of atherosclerotic plaques and inhibits plaque progression, *J. Am. Coll. Cardiol.* 52, 1024-1032.
158. **Kereiakes, D.J., Szyniszewski, A.M., Wahr, D., Herrmann, H.C., Simon, D.I., Rogers, C., Kramer, P., Shear, W., Yeung, A.C., Shunk, K.A., Chou, T.M., Popma, J., Fitzgerald, P., Carroll, T.E., Forer, D., Adelman, D.C.**, (2003). Phase I drug and light dose-escalation trial of motexafin lutetium and far red light activation (phototherapy) in subjects with coronary artery disease undergoing percutaneous coronary intervention and stent deployment: procedural and long-term results, *Circulation* 108, 1310-1315.
159. **Szeimies, R.M., Lischner, S., Philipp-Dormston, W., Walker, T., Hiepe-Wegener, D., Feise, K., Podda, M., Prager, W., Kohl, E., Karrer, S.**, (2013). Photodynamic therapy for skin rejuvenation: treatment options - results of a consensus conference of an expert group for aesthetic photodynamic therapy, *Journal der Deutschen Dermatologischen Gesellschaft = Journal of the German Society of Dermatology : JDDG* 11, 632-636.
160. **Gursoy, H., Ozcakir-Tomruk, C., Tanalp, J., Yilmaz, S.**, (2013). Photodynamic therapy in dentistry: a literature review, *Clin. Oral Investig.* 17, 1113-1125.
161. **Wan, M.T., Lin, J.Y.**, (2014). Current evidence and applications of photodynamic therapy in dermatology, *Clinical, cosmetic and investigational dermatology* 7, 145-163.
162. **Mennel, S., Barbazetto, I., Meyer, C.H., Peter, S., Stur, M.**, (2007). Ocular photodynamic therapy--standard applications and new indications (part 1). Review of the literature and personal experience, *Ophthalmologica. Journal international d'ophtalmologie. International journal of ophthalmology. Zeitschrift fur Augenheilkunde* 221, 216-226.
163. **Mennel, S., Barbazetto, I., Meyer, C.H., Peter, S., Stur, M.**, (2007). Ocular photodynamic therapy--standard applications and new indications. Part 2. Review of the literature and personal experience, *Ophthalmologica. Journal international d'ophtalmologie. International journal of ophthalmology. Zeitschrift fur Augenheilkunde* 221, 282-291.

164. **Yin, R., Dai, T., Avci, P., Jorge, A.E., de Melo, W.C., Vecchio, D., Huang, Y.Y., Gupta, A., Hamblin, M.R.,** (2013). Light based anti-infectives: ultraviolet C irradiation, photodynamic therapy, blue light, and beyond, *Curr. Opin. Pharmacol.* 13, 731-762.
165. **Agostinis, P., Berg, K., Cengel, K.A., Foster, T.H., Girotti, A.W., Gollnick, S.O., Hahn, S.M., Hamblin, M.R., Juzeniene, A., Kessel, D., Korbelik, M., Moan, J., Mroz, P., Nowis, D., Piette, J., Wilson, B.C., Golab, J.,** (2011). Photodynamic therapy of cancer: an update, *CA. Cancer J. Clin.* 61, 250-281.
166. **Dougherty, T.J., Gomer, C.J., Henderson, B.W., Jori, G., Kessel, D., Korbelik, M., Moan, J., Peng, Q.,** (1998). Photodynamic therapy, *J. Natl. Cancer Inst.* 90, 889-905.
167. **Spring, B.Q., Rizvi, I., Xu, N., Hasan, T.,** (2015). The role of photodynamic therapy in overcoming cancer drug resistance, *Photochemical & photobiological sciences : Official journal of the European Photochemistry Association and the European Society for Photobiology*
168. **Castano, A.P., Demidova, T.N., Hamblin, M.R.,** (2005). Mechanisms in photodynamic therapy: part two-cellular signaling, cell metabolism and modes of cell death, *Photodiagnosis and photodynamic therapy* 2, 1-23.
169. **Ronn, A.M., Batti, J., Lee, C.J., Yoo, D., Siegel, M.E., Nouri, M., Lofgren, L.A., Steinberg, B.M.,** (1997). Comparative biodistribution of meta-Tetra(Hydroxyphenyl) chlorin in multiple species: clinical implications for photodynamic therapy, *Lasers Surg. Med.* 20, 437-442.
170. **Bugaj, A.M.,** (2011). Targeted photodynamic therapy--a promising strategy of tumor treatment, *Photochem. Photobiol. Sci.* 10, 1097-1109.
171. **Schouwink, H., Ruevekamp, M., Oppelaar, H., van Veen, R., Baas, P., Stewart, F.A.,** (2001). Photodynamic therapy for malignant mesothelioma: preclinical studies for optimization of treatment protocols, *Photochem. Photobiol.* 73, 410-417.
172. **Douglas, P., Burrow, H.D., Evans, R.C.,** (2013). Foundations of Photochemistry: A Background on the Interaction Between Light and Molecules, in: *Applied Photochemistry*, Springer Netherlands, 1-88.
173. **Benov, L.,** (2015). Photodynamic therapy: current status and future directions, *Medical principles and practice : international journal of the Kuwait University, Health Science Centre* 24 Suppl 1, 14-28.
174. **Ogilby, P.R.,** (2010). Singlet oxygen: there is indeed something new under the sun, *Chem. Soc. Rev.* 39, 3181-3209.
175. **Vatanever, F., de Melo, W.C., Avci, P., Vecchio, D., Sadasivam, M., Gupta, A., Chandran, R., Karimi, M., Parizotto, N.A., Yin, R., Tegos, G.P., Hamblin, M.R.,** (2013). Antimicrobial strategies centered around reactive oxygen species--bactericidal antibiotics, photodynamic therapy, and beyond, *FEMS Microbiol. Rev.* 37, 955-989.
176. **Girotti, A.W., Kriska, T.,** (2004). Role of lipid hydroperoxides in photo-oxidative stress signaling, *Antioxidants & redox signaling* 6, 301-310.
177. **Pattison, D.I., Rahmanto, A.S., Davies, M.J.,** (2012). Photo-oxidation of proteins, *Photochemical & photobiological sciences : Official journal of the European Photochemistry Association and the European Society for Photobiology* 11, 38-53.
178. **Cadet, J., Loft, S., Olinski, R., Evans, M.D., Bialkowski, K., Richard Wagner, J., Dedon, P.C., Moller, P., Greenberg, M.M., Cooke, M.S.,** (2012). Biologically relevant oxidants and terminology, classification and

- nomenclature of oxidatively generated damage to nucleobases and 2-deoxyribose in nucleic acids, *Free Radic. Res.* 46, 367-381.
179. **Hatz, S., Lambert, J.D., Ogilby, P.R.**, (2007). Measuring the lifetime of singlet oxygen in a single cell: addressing the issue of cell viability, *Photochemical & photobiological sciences : Official journal of the European Photochemistry Association and the European Society for Photobiology* 6, 1106-1116.
 180. **Hatz, S., Poulsen, L., Ogilby, P.R.**, (2008). Time-resolved singlet oxygen phosphorescence measurements from photosensitized experiments in single cells: effects of oxygen diffusion and oxygen concentration, *Photochem. Photobiol.* 84, 1284-1290.
 181. **Nowis, D., Makowski, M., Stoklosa, T., Legat, M., Issat, T., Golab, J.**, (2005). Direct tumor damage mechanisms of photodynamic therapy, *Acta Biochim. Pol.* 52, 339-352.
 182. **Kessel, D., Oleinick, N.L.**, (2009). Initiation of autophagy by photodynamic therapy, *Methods Enzymol.* 453, 1-16.
 183. **Reiners, J.J., Jr., Agostinis, P., Berg, K., Oleinick, N.L., Kessel, D.**, (2010). Assessing autophagy in the context of photodynamic therapy, *Autophagy* 6, 7-18.
 184. **Robertson, C.A., Evans, D.H., Abrahamse, H.**, (2009). Photodynamic therapy (PDT): a short review on cellular mechanisms and cancer research applications for PDT, *J. Photochem. Photobiol. B* 96, 1-8.
 185. **Castano, A.P., Demidova, T.N., Hamblin, M.R.**, (2005). Mechanisms in photodynamic therapy: Part three- Photosensitizer pharmacokinetics, biodistribution, tumor localization and modes of tumor destruction, *Photodiagnosis and photodynamic therapy* 2, 91-106.
 186. **Panzarini, E., Inguscio, V., Dini, L.**, (2013). Immunogenic cell death: can it be exploited in PhotoDynamic Therapy for cancer?, *BioMed research international* 2013, 482160.
 187. **Castano, A.P., Mroz, P., Hamblin, M.R.**, (2006). Photodynamic therapy and anti-tumour immunity, *Nat. Rev. Cancer* 6, 535-545.
 188. **O'Connor, A.E., Gallagher, W.M., Byrne, A.T.**, (2009). Porphyrin and nonporphyrin photosensitizers in oncology: preclinical and clinical advances in photodynamic therapy, *Photochem. Photobiol.* 85, 1053-1074.
 189. **Ackroyd, R., Kelty, C., Brown, N., Reed, M.**, (2001). The history of photodetection and photodynamic therapy, *Photochem. Photobiol.* 74, 656-669.
 190. **Bonnett, R., Charlesworth, P., Djelal, B.D., Foley, S., McGarvey, D.J., Truscott, T.G.**, (1999). Photophysical properties of 5,10,15,20-tetrakis(m-hydroxyphenyl)porphyrin-(m-THPP), 5,10,15,20-tetrakis(m-hydroxyphenyl)chlorin (m-THPC) and 5,10,15,20-tetrakis(m-hydroxyphenyl)bacteriochlorin (m-THPBC): a comparative study, *Journal of the Chemical Society-Perkin Transactions 2* 325-328.
 191. **Ma, L., Moan, J., Berg, K.**, (1994). Evaluation of a new photosensitizer, meso-tetra-hydroxyphenyl-chlorin, for use in photodynamic therapy: a comparison of its photobiological properties with those of two other photosensitizers, *International journal of cancer. Journal international du cancer* 57, 883-888.
 192. **Ma, L., Moan, J., Berg, K.**, (1994). Evaluation of a new photosensitizer, meso-tetra-hydroxyphenyl-chlorin, for use in photodynamic therapy: a comparison of its photobiological properties with those of two other photosensitizers, *Int. J. Cancer* 57, 883-888.

193. **Reum, N., Fink-Straube, C., Klein, T., Hartmann, R.W., Lehr, C.M., Schneider, M.,** (2010). Multilayer coating of gold nanoparticles with drug-polymer coadsorbates, *Langmuir* 26, 16901-16908.
194. **Chatterjee, D.K., Fong, L.S., Zhang, Y.,** (2008). Nanoparticles in photodynamic therapy: an emerging paradigm, *Advanced drug delivery reviews* 60, 1627-1637.
195. **Hughes, G.A.,** (2005). Nanostructure-mediated drug delivery, *Nanomedicine : nanotechnology, biology, and medicine* 1, 22-30.
196. **Cho, K., Wang, X., Nie, S., Chen, Z.G., Shin, D.M.,** (2008). Therapeutic nanoparticles for drug delivery in cancer, *Clinical cancer research : an official journal of the American Association for Cancer Research* 14, 1310-1316.
197. **Springer, T.A.,** (1994). Traffic signals for lymphocyte recirculation and leukocyte emigration: the multistep paradigm, *Cell* 76, 301-314.
198. **Baaten, B.J., Cooper, A.M., Swain, S.L., Bradley, L.M.,** (2013). Location, location, location: the impact of migratory heterogeneity on T cell function, *Frontiers in immunology* 4, 311.
199. **Russell, J.H., Ley, T.J.,** (2002). Lymphocyte-mediated cytotoxicity, *Annu. Rev. Immunol.* 20, 323-370.
200. **Silva, M.T.,** (2010). When two is better than one: macrophages and neutrophils work in concert in innate immunity as complementary and cooperative partners of a myeloid phagocyte system, *J. Leukoc. Biol.* 87, 93-106.
201. **Danhier, F., Ansorena, E., Silva, J.M., Coco, R., Le Breton, A., Preat, V.,** (2012). PLGA-based nanoparticles: an overview of biomedical applications, *J. Control. Release* 161, 505-522.
202. **Kumari, A., Yadav, S.K., Yadav, S.C.,** (2010). Biodegradable polymeric nanoparticles based drug delivery systems, *Colloids Surf. B Biointerfaces* 75, 1-18.
203. **Fischer, S., Uetz-von Allmen, E., Waeckerle-Men, Y., Groettrup, M., Merkle, H.P., Gander, B.,** (2007). The preservation of phenotype and functionality of dendritic cells upon phagocytosis of polyelectrolyte-coated PLGA microparticles, *Biomaterials* 28, 994-1004.
204. **Zupke, O., Distler, E., Baumann, D., Strand, D., Meyer, R.G., Landfester, K., Herr, W., Mailander, V.,** (2010). Preservation of dendritic cell function upon labeling with amino functionalized polymeric nanoparticles, *Biomaterials* 31, 7086-7095.
205. **Gabius, H.J., Siebert, H.C., Andre, S., Jimenez-Barbero, J., Rudiger, H.,** (2004). Chemical biology of the sugar code, *ChemBiochem* 5, 741-764.
206. **Bertozzi, C.R., Kiessling, L.L.,** (2001). Chemical Glycobiology, *Science* 291, 2357-2364.
207. **Houk, K.N., Leach, A.G., Kim, S.P., Zhang, X.Y.,** (2003). Binding affinities of host-guest, protein-ligand, and protein-transition-state complexes, *Angew. Chem., Int. Ed.* 42, 4872-4897.
208. **Mammen, M., Chio, S.-K., Whitesides, G.M.,** (1998). Polyvalent interactions in biological systems: implications for design and use of multivalent ligands and inhibitors, *Angew. Chem., Int. Ed.* 37, 2755-2794.
209. **Rabuka, D., Parthasarathy, R., Lee, G.S., Chen, X., Groves, J.T., Bertozzi, C.R.,** (2007). Hierarchical Assembly of Model Cell Surfaces: Synthesis of Mucin Mimetic Polymers and Their Display on Supported Bilayers, *J. Am. Chem. Soc.* 129, 5462-5471.

210. **Rabuka, D., Forstner, M.B., Groves, J.T., Bertozzi, C.R.,** (2008). Noncovalent Cell Surface Engineering: Incorporation of Bioactive Synthetic Glycopolymers into Cellular Membranes, *J. Am. Chem. Soc.* 130, 5947-5953.
211. **Chen, X., Tam, U.C., Czapinski, J.L., Lee, G.S., Rabuka, D., Zettl, A., Bertozzi, C.R.,** (2006). Interfacing Carbon Nanotubes with Living Cells, *J. Am. Chem. Soc.* 128, 6292-6293.
212. **Andre, S., Kaltner, H., Furuike, T., Nishimura, S.I., Gabius, H.J.,** (2004). Persubstituted cyclodextrin-based glycoclusters as inhibitors of protein-carbohydrate recognition using purified plant and mammalian lectins and wild-type and lectin-gene-transfected tumor cells as targets, *Bioconjugate Chem.* 15, 87-98.
213. **Gómez-García, M., Benito, J.M., Rodríguez-Lucena, D., Yu, J.-X., Chmurski, K., Ortiz- Mellet, C., Gallego, R.G., Maestre, A., Defaye, J., Fernández, J.M.G.,** (2005). Probing Secondary Carbohydrate-Protein Interactions with Highly Dense Cyclodextrin-Centered Heteroglycoclusters: The Heterocluster Effect, *J. Am. Chem. Soc.* 7970-7971.
214. **Ortega-Caballero, F., Gimenez-Martinez, J.J., Garcia-Fuentes, L., Ortiz-Salmeron, E., Santoyo-Gonzalez, F., Vargas-Berenguel, A.,** (2001). Binding affinity properties of dendritic glycosides based on a beta-cyclodextrin core toward guest molecules and concanavalin A, *J. Org. Chem.* 66, 7786-7795.
215. **Ashton, P.R., Boyd, S.E., Brown, C.L., Nepogodiev, S.A., Meijer, E.W., Peerlings, H.W.I., Stoddart, J.F.,** (1997). Synthesis of Glycodendrimers by Modification of Poly(propylene imine) Dendrimers, *Chem. Eur. J.* 3, 974-984.
216. **Lehr, C.M.,** (2000). Lectin-mediated drug delivery: The second generation of bioadhesives, *J. Controlled Release* 65, 19-29.
217. **Bies, C., Lehr, C.M., Woodley, J.F.,** (2004). Lectin-mediated drug targeting: history and applications, *Adv. Drug Deliv. Rev.* 56, 425-435.
218. **Neumann, D., Lehr, C.M., Lenhof, H.P., Kohlbacher, O.,** (2004). Computational modeling of the sugar-lectin interaction, *Advanced drug delivery reviews* 56, 437-457.
219. **Gomez-Garcia, M., Benito, J.M., Gutierrez-Gallego, R., Maestre, A., Mellet, C.O., Fernandez, J.M.G., Blanco, J.L.J.,** (2010). Comparative studies on lectin-carbohydrate interactions in low and high density homo- and heteroglycoclusters, *Org. Biomol. Chem.* 8, 1849-1860.
220. **Vargas-Berenguel, A., Ortega-Caballero, F., Casas-Solvas, J.M.,** (2007). Supramolecular chemistry of carbohydrate clusters with cores having guest binding abilities, *Mini-Reviews in Organic Chemistry* 4, 1-14.
221. **Oda, Y., Kobayashi, N., Yamanoi, T., Katsuraya, K., Takahashi, K., Hattori, K.,** (2008). beta-cyclodextrin conjugates with glucose moieties designed as drug carriers: Their syntheses, evaluations using concanavalin A and doxorubicin, and structural analyses by NMR spectroscopy, *Medicinal Chemistry* 4, 244-255.
222. **Fan, X., Lin, L., Messersmith, P.B.,** (2006). Cell fouling resistance of polymer brushes grafted from ti substrates by surface-initiated polymerization: effect of ethylene glycol side chain length, *Biomacromolecules* 7, 2443-2448.
223. **Zheng, M., Davidson, F., Huang, X.,** (2003). Ethylene glycol monolayer protected nanoparticles for eliminating nonspecific binding with biological molecules, *J. Am. Chem. Soc.* 125, 7790-7791.

-
224. **Stöhr, T.**, (2010). Kohlenhydrat-funktionalisierte Polypeptide: Synthese und molekulare Erkennung von Zellen, Dissertation, Saarland University, 225.
225. **Rainer, T.H.**, (2002). L-selectin in health and disease, *Resuscitation* 52, 127-141.
226. **Liu, F.T., Rabinovich, G.A.**, (2010). Galectins: regulators of acute and chronic inflammation, *Ann. N. Y. Acad. Sci.* 1183, 158-182.
227. **Ikushima, H., Munakata, Y., Ishii, T., Iwata, S., Terashima, M., Tanaka, H., Schlossman, S.F., Morimoto, C.**, (2000). Internalization of CD26 by mannose 6-phosphate/insulin-like growth factor II receptor contributes to T cell activation, *Proc. Natl. Acad. Sci. U. S. A.* 97, 8439-8444.
228. **Kim, J.J., Olson, L.J., Dahms, N.M.**, (2009). Carbohydrate recognition by the mannose-6-phosphate receptors, *Curr. Opin. Struct. Biol.* 19, 534-542.
229. **Jacobs, S.R., Herman, C.E., Maciver, N.J., Wofford, J.A., Wieman, H.L., Hammen, J.J., Rathmell, J.C.**, (2008). Glucose uptake is limiting in T cell activation and requires CD28-mediated Akt-dependent and independent pathways, *J. Immunol.* 180, 4476-4486.
230. **Mueckler, M., Thorens, B.**, (2013). The SLC2 (GLUT) family of membrane transporters, *Mol. Aspects Med.* 34, 121-138.
231. **Stöhr, T., Blaudszun, A.R., Steinfeld, U., Wenz, G.**, (2011). Synthesis of glycosylated peptides by NCA polymerization for recognition of human T-cells, *Polymer Chemistry* 2, 2239-2248.
232. **Scudiero, D., Shoemaker, R., Paull, K., Monks, A., Tierney, S., Nofziger, T., Currens, M., Seniff, D., Boyd, M.**, (1988). Evaluation of a soluble tetrazolium/formazan assay for cell growth and drug sensitivity in culture using human and other tumor cell lines, *Cancer Res.* 48, 4827-4833.
233. **Brenchley, J.M., Douek, D.C., Ambrozak, D.R., Chatterji, M., Betts, M.R., Davis, L.S., Koup, R.A.**, (2002). Expansion of activated human naive T-cells precedes effector function, *Clin. Exp. Immunol.* 130, 432-440.
234. **Wang, R., Green, D.R.**, (2012). Metabolic checkpoints in activated T cells, *Nat. Immunol.* 13, 907-915.
235. **Palmer, C.S., Ostrowski, M., Balderson, B., Christian, N., Crowe, S.M.**, (2015). Glucose metabolism regulates T cell activation, differentiation, and functions, *Frontiers in immunology* 6, 1.
236. **Finlay, D.K.**, (2012). Regulation of glucose metabolism in T cells: new insight into the role of Phosphoinositide 3-kinases, *Frontiers in immunology* 3, 247.
237. **Silverstein, S.C., Steinman, R.M., Cohn, Z.A.**, (1977). Endocytosis, *Annu. Rev. Biochem.* 46, 669-722.
238. **Berridge, M.V., Herst, P.M., Tan, A.S.**, (2005). Tetrazolium dyes as tools in cell biology: new insights into their cellular reduction, *Biotechnol. Annu. Rev.* 11, 127-152.
239. **Somers, W.S., Tang, J., Shaw, G.D., Camphausen, R.T.**, (2000). Insights into the molecular basis of leukocyte tethering and rolling revealed by structures of P- and E-selectin bound to SLe(X) and PSGL-1, *Cell* 103, 467-479.
240. **Papp, I., Dervedde, J., Enders, S., Haag, R.**, (2008). Modular synthesis of multivalent glycoarchitectures and their unique selectin binding behavior, *Chem. Commun.* 5851-5853.
241. **Springer, T.A.**, (1994). Traffic signals for lymphocyte recirculation and leukocyte emigration: The multistep paradigm, *Cell* 76, 301-314.

-
242. **Chao, C.C., Jensen, R., Dailey, M.O.**, (1997). Mechanisms of L-selectin regulation by activated T cells, *J. Immunol.* 159, 1686-1694.
243. **Barondes, S.H., Castronovo, V., Cooper, D.N.W., Cummings, R.D., Drickamer, K., Feizi, T., Gitt, M.A., Hirabayashi, J., Hughes, C., Kasai, K., Leffler, H., Liu, F.T., Lotan, R., Mercurio, A.M., Monsigny, M., Pillai, S., Poirer, F., Raz, A., Rigby, P.W.J., Rini, J.M., Wang, J.L.**, (1994). Galectins: a family of animal beta-galactoside-binding lectins, *Cell* 76, 597-598.
244. **Garner, O.B., Baum, L.G.**, (2008). Galectin-glycan lattices regulate cell-surface glycoprotein organization and signalling, *Biochem. Soc. Trans.* 36, 1472-1477.
245. **Fuertes, M.B., Molinero, L.L., Toscano, M.A., Ilarregui, J.M., Rubinstein, N., Fainboim, L., Zwirner, N.W., Rabinovich, G.A.**, (2004). Regulated expression of galectin-1 during T-cell activation involves Lck and Fyn kinases and signaling through MEK1/ERK, p38 MAP kinase and p70S6 kinase, *Mol. Cell. Biochem.* 267, 177-185.
246. **Joo, H.G., Goedegebuure, P.S., Sadanaga, N., Nagoshi, M., von Bernstorff, W., Eberlein, T.J.**, (2001). Expression and function of galectin-3, a beta-galactoside-binding protein in activated T lymphocytes, *J. Leukocyte Biol.* 69, 555-564.
247. **Burkhardt, O., Merker, H.J.**, (2002). Immunoelectron microscopic investigations of patching, capping, endocytotic and shedding processes in T and B lymphocytes, *Annals of anatomy = Anatomischer Anzeiger : official organ of the Anatomische Gesellschaft* 184, 45-53.
248. **Marsh, E.W., Leopold, P.L., Jones, N.L., Maxfield, F.R.**, (1995). Oligomerized transferrin receptors are selectively retained by a luminal sorting signal in a long-lived endocytic recycling compartment, *The Journal of cell biology* 129, 1509-1522.
249. **Liu, B., Huang, P.J., Zhang, X., Wang, F., Pautler, R., Ip, A.C., Liu, J.**, (2013). Parts-per-million of polyethylene glycol as a non-interfering blocking agent for homogeneous biosensor development, *Anal. Chem.* 85, 10045-10050.
250. **Barnett, J.E., Holman, G.D., Munday, K.A.**, (1973). Structural requirements for binding to the sugar-transport system of the human erythrocyte, *The Biochemical journal* 131, 211-221.
251. **Barnett, J.E., Holman, G.D., Chalkley, R.A., Munday, K.A.**, (1975). Evidence for two asymmetric conformational states in the human erythrocyte sugar-transport system, *The Biochemical journal* 145, 417-429.
252. **Batrakova, E.V., Li, S., Reynolds, A.D., Mosley, R.L., Bronich, T.K., Kabanov, A.V., Gendelman, H.E.**, (2007). A macrophage-nanozyme delivery system for Parkinson's disease, *Bioconjug. Chem.* 18, 1498-1506.
253. **Park, H., Yang, J., Lee, J., Haam, S., Choi, I.H., Yoo, K.H.**, (2009). Multifunctional Nanoparticles for Combined Doxorubicin and Photothermal Treatments, *Acs Nano* 3, 2919-2926.
254. **Yang, J., Lee, J., Kang, J., Oh, S.J., Ko, H.-J., Son, J.-H., Lee, K., Suh, J.-S., Huh, Y.-M., Haam, S.**, (2009). Smart Drug-Loaded Polymer Gold Nanoshells for Systemic and Localized Therapy of Human Epithelial Cancer, *Adv. Mater.* 21, 4339-4342.
255. **Teiten, M.H., Bezdetnaya, L., Morliere, P., Santus, R., Guillemin, F.**, (2003). Endoplasmic reticulum and Golgi apparatus are the preferential sites of Foscan localisation in cultured tumour cells, *Br. J. Cancer* 88, 146-152.

-
256. **Kochenderfer, J.N., Rosenberg, S.A.**, (2013). Treating B-cell cancer with T cells expressing anti-CD19 chimeric antigen receptors, *Nat. Rev. Clin. Oncol.* 10, 267-276.
257. **Anand, S., Ortel, B.J., Pereira, S.P., Hasan, T., Maytin, E.V.**, (2012). Biomodulatory approaches to photodynamic therapy for solid tumors, *Cancer Lett.* 326, 8-16.
258. **Dougherty, T.J., Kaufman, J.E., Goldfarb, A., Weishaupt, K.R., Boyle, D., Mittleman, A.**, (1978). Photoradiation therapy for the treatment of malignant tumors, *Cancer Res.* 38, 2628-2635.
259. **Yang, J.C.**, (2013). The adoptive transfer of cultured T cells for patients with metastatic melanoma, *Clin. Dermatol.* 31, 209-219.
260. **Blaudszun, A.R., Lian, Q., Schnabel, M., Loretz, B., Steinfeld, U., Lee, H.H., Wenz, G., Lehr, C.M., Schneider, M., Philippi, A.**, (2014). Polyester-idarubicin nanoparticles and a polymer-photosensitizer complex as potential drug formulations for cell-mediated drug delivery, *Int. J. Pharm.* 474, 70-79.
261. **Nociari, M.M., Shalev, A., Benias, P., Russo, C.**, (1998). A novel one-step, highly sensitive fluorometric assay to evaluate cell-mediated cytotoxicity, *J. Immunol. Methods* 213, 157-167.
262. **Meidenbauer, N., Marienhagen, J., Laumer, M., Vogl, S., Heymann, J., Andreesen, R., Mackensen, A.**, (2003). Survival and tumor localization of adoptively transferred Melan-A-specific T cells in melanoma patients, *J. Immunol.* 170, 2161-2169.
263. **Yee, C., Thompson, J.A., Byrd, D., Riddell, S.R., Roche, P., Celis, E., Greenberg, P.D.**, (2002). Adoptive T cell therapy using antigen-specific CD8⁺ T cell clones for the treatment of patients with metastatic melanoma: in vivo persistence, migration, and antitumor effect of transferred T cells, *Proc. Natl. Acad. Sci. U. S. A.* 99, 16168-16173.
264. **Kershaw, M.H., Westwood, J.A., Parker, L.L., Wang, G., Eshhar, Z., Mavroukakis, S.A., White, D.E., Wunderlich, J.R., Canevari, S., Rogers-Freezer, L., Chen, C.C., Yang, J.C., Rosenberg, S.A., Hwu, P.**, (2006). A phase I study on adoptive immunotherapy using gene-modified T cells for ovarian cancer, *Clin. Cancer Res.* 12, 6106-6115.
265. **Parente-Pereira, A.C., Burnet, J., Ellison, D., Foster, J., Davies, D.M., van der Stegen, S., Burbidge, S., Chiaperro-Stanke, L., Wilkie, S., Mather, S., Maher, J.**, (2011). Trafficking of CAR-engineered human T cells following regional or systemic adoptive transfer in SCID beige mice, *J. Clin. Immunol.* 31, 710-718.
266. **Palmer, D.C., Balasubramaniam, S., Hanada, K., Wrzesinski, C., Yu, Z., Farid, S., Theoret, M.R., Hwang, L.N., Klebanoff, C.A., Gattinoni, L., Goldstein, A.L., Yang, J.C., Restifo, N.P.**, (2004). Vaccine-stimulated, adoptively transferred CD8⁺ T cells traffic indiscriminately and ubiquitously while mediating specific tumor destruction, *J. Immunol.* 173, 7209-7216.
267. **Fisher, D.T., Chen, Q., Appenheimer, M.M., Skitzki, J., Wang, W.C., Odunsi, K., Evans, S.S.**, (2006). Hurdles to lymphocyte trafficking in the tumor microenvironment: implications for effective immunotherapy, *Immunol. Invest.* 35, 251-277.
268. **Lo, A.S., Taylor, J.R., Farzaneh, F., Kemeny, D.M., Dibb, N.J., Maher, J.**, (2008). Harnessing the tumour-derived cytokine, CSF-1, to co-stimulate T-cell growth and activation, *Mol. Immunol.* 45, 1276-1287.
269. **Di Stasi, A., De Angelis, B., Rooney, C.M., Zhang, L., Mahendravada, A., Foster, A.E., Heslop, H.E., Brenner, M.K., Dotti, G., Savoldo, B.**, (2009). T lymphocytes coexpressing CCR4 and a chimeric antigen

- receptor targeting CD30 have improved homing and antitumor activity in a Hodgkin tumor model, *Blood* 113, 6392-6402.
270. **Moon, E.K., Carpenito, C., Sun, J., Wang, L.C., Kapoor, V., Predina, J., Powell, D.J., Jr., Riley, J.L., June, C.H., Albelda, S.M.**, (2011). Expression of a functional CCR2 receptor enhances tumor localization and tumor eradication by retargeted human T cells expressing a mesothelin-specific chimeric antibody receptor, *Clin. Cancer Res.* 17, 4719-4730.
271. **Stow, J.L., Murray, R.Z.**, (2013). Intracellular trafficking and secretion of inflammatory cytokines, *Cytokine Growth Factor Rev.* 24, 227-239.
272. **Rothstein, T.L., Mage, M., Jones, G., McHugh, L.L.**, (1978). Cytotoxic T lymphocyte sequential killing of immobilized allogeneic tumor target cells measured by time-lapse microcinematography, *J. Immunol.* 121, 1652-1656.
273. **Lee, G., Zhu, M., Ge, B., Potzold, S.**, (2012). Widespread expressions of immunoglobulin superfamily proteins in cancer cells, *Cancer Immunol. Immunother.* 61, 89-99.
274. **Huse, M., Quann, E.J., Davis, M.M.**, (2008). Shouts, whispers and the kiss of death: directional secretion in T cells, *Nat. Immunol.* 9, 1105-1111.

8. Publication List

Scientific Publications

Papers

Blaudszun A.-R., Moldenhauer G., Schneider M., Philippi A. (2015)

A photosensitizer delivered by bispecific antibody retargeted human T lymphocytes enhances cytotoxicity against carcinoma cells upon light irradiation

Journal of Controlled Release; 197: 58-68

Blaudszun A.-R., Lian Q., Schnabel M., Loretz B., Steinfeld U., Lee H.-H., Wenz G., Lehr C.-M., Schneider M., Philippi A. (2014)

Polyester-idarubicin nanoparticles and a polymer-photosensitizer complex as potential drug formulations for cell-mediated drug delivery.

International Journal of Pharmaceutics; 474: 70-79

Stöhr T., **Blaudszun A.-R.**, Steinfeld U. and Wenz G. (2011)

Synthesis of glycosylated peptides by NCA polymerization for recognition of human T-cells.

Polymer Chemistry; 2: 2239-48

Scientific Essay and Journal Issue Cover Page

Cover contest winners: Philippi A. and **Blaudszun A.-R.** (2014)

Living immune cells as drug carriers in cancer therapy.

European Journal of Nanomedicine; 6(1): 9-10

Patent

Philippi A., **Blaudszun A.-R.** and Schneider M. (2012)

Transport von photosensibilisierenden Substanzen mit Hilfe lebender Immunzellen zur Tumorbehandlung.

Patent Number DE102012107166, granted April 2015

Contribution to Scientific Conferences

Award

Reviewer Choice Award awarded to those posters deemed of the highest quality (top 1% of 2050 posters) by the reviewers at the annual meeting of the Biomedical Engineering Society (BMES 2015, October 7-10, Tampa, USA).

Posters

Blaudszun A.-R., Moldenhauer G., Schneider M., Philippi A. (2015)

Bispecific antibody retargeted human CD4+ and CD8+ T cells as living delivery vehicles for photosensitizers

The Biomedical Engineering Society (BMES), Annual Meeting, October 7-10, Tampa, USA.

Blaudszun A.-R., Moldenhauer G., Schneider M., Philippi A. (2014)

A photosensitizer delivered by bispecific antibody retargeted human T lymphocytes boosts cytotoxicity against carcinoma cells upon light irradiation

The European Summit for Clinical Nanomedicine and Targeted Medicine (CLINAM), 7th Conference and Exhibition, June 23-25, Basel, Switzerland.

Blaudszun A.-R., Moldenhauer G., Schneider M., Philippi A. (2014)

A photosensitizer delivered by bispecific antibody retargeted human T lymphocytes boosts cytotoxicity against carcinoma cells upon light irradiation

Cancer Immunotherapy (CIMT), 12th Annual Meeting, May 6-8, Mainz, Germany.

Blaudszun A.-R., Borth A., Eggers R., Beckhove P., Moldenhauer G., Philippi A. (2011)

Anti-neoplastic drug targeting to EpCAM-expressing tumors by redirected, ex vivo activated T lymphocytes

6th International Symposium on the Clinical use of Cellular Products, March 24-25, Erlangen, Germany.

Blaudszun A.-R., Philippi A., Borth A., Moldenhauer G., Beckhove P., Lee H.-H., Steinfeld U. (2010)

Adoptive transfer of ex vivo activated and antineoplastic drug loaded T lymphocytes retargeted to EpCAM expressing tumours

Cancer Immunotherapy (CIMT), 8th Annual Meeting, May 26-28, Mainz, Germany.

Philippi A., **Blaudszun A.-R.**, Borth A., Moldenhauer G., Beckhove P., Lee H.-H., Steinfeld U. **(2010)**

Redirected, ex vivo activated T lymphocytes as target site-specific delivery system for the anti-neoplastic drug idarubicin.

8th International Conference and Workshop on Biological Barriers - in vitro tools, nanotoxicology, and nanomedicine, March 21 - April 1, Saarland University, Saarbruecken, Germany.

Talk

Blaudszun A.-R., Moldenhauer G., Schneider M., Philippi A. **(2014)**

A photosensitizer delivered by bispecific antibody retargeted human T lymphocytes boosts cytotoxicity against carcinoma cells upon light irradiation

Cancer Immunotherapy (CIMT), 12th Annual Meeting, 6-8 May, Mainz, Germany.

Danksagungen/Acknowledgements

Diese Doktorarbeit wurde im Rahmen des Saarbridge-Projektes, „Polymere für die zeitkontrollierte Medikamentenfreisetzung in der Immuntherapie“, durch das Saarland Ministerium für Wirtschaft und Wissenschaft (D/2-14.2.1.1 LFFP 08/32) sowie durch Basismittel der Korea Institute of Science and Technology Europe (KIST Europe) Forschungsgesellschaft mbH finanziert.

Zuallererst möchte ich mich ganz herzlich bei Herrn Prof. Dr. Gerhard Wenz (Arbeitskreis Organische Makromolekulare Chemie, UdS) für die Übernahme der Betreuung meiner Doktorarbeit bedanken. Zudem danke ich ihm für die lehrreichen Erfahrungen, die ich Rahmen unserer gemeinsamen wissenschaftlichen Arbeit und Publikation machen durfte.

Mein besonderer Dank gilt meiner ehemaligen Teamleiterin Frau Dr. Anja Philippi (KIST Europe), die mir jederzeit bei Fragen und Problemen mit hilfreichem Rat zur Seite stand. Auch für ihre humorvolle Art und Weise der Betreuung bin ich sehr dankbar. Zudem hat sie mir die Möglichkeit und Freiheit gegeben hat, meinen eigenen wissenschaftlichen Weg zu finden. Ihrem Engagement ist es zu verdanken, daß mein Projekt erfolgreich beendet werden konnte.

Tiefen Dank möchte ich auch Herrn Prof. Dr. Marc Schneider (Arbeitskreis Biopharmazie und Pharmazeutische Technologie, UdS) aussprechen, der mir stets ein Ansprechpartner war. Durch seine Ideen, Anregungen und konstruktive Kritik hat er fortwährend meine Arbeit unterstützt. Aufgrund seines Vorschlags einen Photosensibilisator zu testen, konnten nach vielen Rückschlägen die wesentlichen Ziele, die für diese Arbeit definiert worden waren, schließlich erreicht werden.

Bei Herrn Dr. Hyeck-Hee Lee und Frau Dr. Ute Steinfeld, meinen ehemaligen Gruppenleiter am KIST Europe, möchte ich mich für das initiieren des Saarbridge-Projektes bedanken, durch das ich wertvolle Erfahrungen für meine Doktorarbeit gewinnen konnte.

Herrn Prof. Dr. Claus-Michael Lehr (Abteilung Wirkstoff-Transport, HIPS) sowie Frau Dr. Brigitta Loretz danke ich für die hilfreiche Diskussionen im Rahmen des Saarbridge-Projektes.

Bei Herrn Dr. Gerhard Moldenhauer (Abteilung Translationale Immunologie, DKFZ) bedanke ich mich für die Überlassung des bispezifischen Antikörpers. Bei Herrn Dr. Thomas Stöhr möchte ich mich für die Zurverfügungstellung der glykosylierten Polymere bedanken. Zudem bedanke ich mich bei Frau Qiong Lian für die Herstellung und Charakterisierung der Nanopartikel. Frau Dr. Hagar Ibrahim Labouta danke ich für die Herstellung des Photosensibilisator-Komplexes. In

diesem Zusammenhang möchte ich mich auch bei der Biolitec AG bedanken, die den Photosensibilisator zur Verfügung stellte.

Unserer ehemaligen technischen Assistentin Frau Birgit Wiegand sowie Frau Daniela Vanni-Strassner danke ich für die tatkräftige Unterstützung im Laboralltag. Zudem möchte ich mich bei Leon Muijs für die Hilfe bei der Arbeit am konfokalen Laser-Scanning-Mikroskop bedanken. Herrn Dr. Oliver Lischtschenko (Ocean Optics, Inc.) danke ich für die Anleitung zur Messung von Bestrahlungsgrößen bei der PDT.

Recht herzlich möchte ich mich auch bei Dr. Eric R. Castro und Michael F. Müller für die sorgfältige Durchsicht meiner Arbeit bedanken. Beiden möchte ich zudem für ihre kollegiale Freundschaft danken.

Schließlich möchte ich mich bei allen hier nicht explizit genannten „Postdocs“, Doktoranden, Praktikanten und koreanischen „Interns“, denen ich im Verlauf meiner Arbeit begegnet bin, für die wissenschaftlichen Diskussionen bedanken.